Calibrations of ROSINA-COPS and Observations at Comet 67P/Churyumov-Gerasimenko

Inauguraldissertation
der Philosophisch-naturwissenschaftlichen Fakultät
der Universität Bern

vorgelegt von

Chia-Yu Tzou

von Taiwan

Leiterin der Arbeit:
Prof. Dr. Kathrin Altwegg
Physikalisches Institut der Universität Bern

Von der Philosophisch-naturwissenschaftlichen Fakultät angenommen.

Calibrations of ROSINA-COPS and Observations at Comet 67P/Churyumov-Gerasimenko

Inauguraldissertation
der Philosophisch-naturwissenschaftlichen Fakultät
der Universität Bern

vorgelegt von

Chia-Yu Tzou

von Taiwan

Leiterin der Arbeit:
Prof. Dr. Kathrin Altwegg
Physikalisches Institut der Universität Bern

Von der Philosophisch-naturwissenschaftlichen Fakultät angenommen.

Bern, den 28.02.2017

Der Dekan:
Prof. Dr. G. Colangelo

Abstract

Comets are thought to be the most pristine objects in the Solar System. Investigating comets will therefore shed light on the origin and formation of the Solar System. For this purpose the European Space Agency selected the Rosetta mission to carry out a study of the Jupiter family comet 67P/Churyumov-Gerasimenko at a close distance continuously for a period of more than two years around its closest approach to the Sun.

This work presents laboratory calibration and neutral gas coma measurements of the COmet Pressure Sensor (COPS) of the Rosetta Orbiter Spectrometer for Ion and Neutral Analysis (ROSINA). Following a brief introduction to the mission and the instrument, the data treatment principles are illustrated. Next, the laboratory calibrations to characterize COPS long term stability and to verify the data analysis methods are demonstrated. Finally, the results of COPS observations in the coma of comet 67P are shown and discussed in detail.

A few highlights are as follows: the peak total neutral gas production rate is slightly shifted from perihelion passage and estimated to be approximately $4 \cdot 10^{28}$ molecules/s; neutral gas expansion velocities in October 2014 have been derived to be around 300 to 1200 m/s depending on illumination conditions on the surface and Rosetta's location above the comet; though built to measure neutral gas, COPS surprisingly observed as well dust and plasma signatures.

All in all, COPS was working well throughout the Rosetta mission and has assisted to unravel a small section of the extensive puzzle about the formation of our Solar System.

Contents

List of Figures

List of Tables

1. Introduction

Comets are believed to be the most pristine bodies in the Solar System and offer clues to the origin and formation of the Solar System (Balsiger et al., 2007). Therefore, the Rosetta space mission was designed to carry out a close study of comet 67P/Churyumov-Gerasimenko (67P). Onboard of Rosetta, the Rosetta Orbiter Spectrometer for Ion and Neutral Analysis (ROSINA) observed in situ the abundances of the volatiles in 67P's atmosphere and ionosphere and characterize the dynamics of the comet's near nucleus environment by measuring the bulk velocity and temperature of the gas. ROSINA consists of two mass spectrometers and a pressure sensor. Each ROSINA sensor has an identical twin in the lab that can be used for calibration and testing purposes. Calibration measurements and analysis of space observations of the COmet Pressure Sensor (COPS) have been performed over the course of this study and are reported in this thesis.

Out of the three sensors of ROSINA, COPS is best suited to measure the total neutral gas density/pressure required to derive the absolute abundances in the coma, together with the ram pressure the bulk gas velocity can be obtained, and eventually the gas temperature. Thus it is important to verify the calibration methods and characteristics of COPS through lab based measurements. Results of these calibration measurements are then used to analyze data obtained by ROSINA COPS in space.

This chapter is dedicated to introduce the comet, the mission, and the instruments; COPS will be described in further detail in the following chapter. The data treatment principles will be outlined in the third chapter. Afterwards, the conducted experiments to calibrate or to verify the behavior of COPS will be presented. In the end, observation results of comet 67P achieved by COPS during the mission will be discussed.

1.1 Comets

Comets are known as "dirty snowballs" composed of ices and meteoritic materials (Whipple, 1950). They are thought to be the remaining objects that escaped the incorporation into planets and ejection from the Solar System during Solar System formation. Comets were formed in the cold regions of the solar nebula. Some formed in the comparatively "warm" nebular regions near Jupiter where the temperature may have been > 120 K and others formed beyond Neptune where temperatures may have been < 30 K (Bell et al., 1997).

Traditionally, comets can be classified into two groups based on their orbital period. Those with orbital periods shorter than 200 yr are called short-period comets and as opposed long-period comets. Short-period comets with periods between 30 to 200 yr are considered to be Halley-type comets. Moreover, most of the short-period comets with periods less than 30 yr have aphelia near Jupiter, and were captured into the short-period orbits as a result of close encounters with Jupiter, therefore they are named Jupiter-family comets.

There are two common comet reservoirs – the Oort cloud and the Kuiper Belt. An illustration of the two reservoirs is shown in Figure 1.1. The Oort cloud is a distribution of comets orbiting the Sun in arbitrarily inclined orbits. Weissman (1996) estimated by the size of long-period comet orbits that the Oort cloud extends to around 50000 AU from the Sun. It is generally believed that they are bodies that were scattered outwards by the giant planets. The Kuiper belt is a disk-like distribution of comets beyond Neptune's orbit that can explain the observed amount of short period comets (Fernandez, 1980). The Kuiper belt objects (KBOs; also known as trans-Neptunian objects (TNOs)) usually have inclinations less than 30°and are distributed on a disk 30 to 400 AU from the Sun.

It seems that comets with orbital periods less than 30 yr originate from the Kuiper Belt while the others are from the Oort cloud (Brownlee, 2014). Comet 1P/Halley is thought to originate from the Oort cloud, whereas 67P/Churyumov-Gerasimenko the comet of this study from the Kuiper belt. Nevertheless, latest Rosetta results indicate that a comet's dynamical history does not necessarily reflect its origin of formation as indicated by the strong variation in D/H among the different populations (Altwegg et al., 2015; Biver et al., 2016).

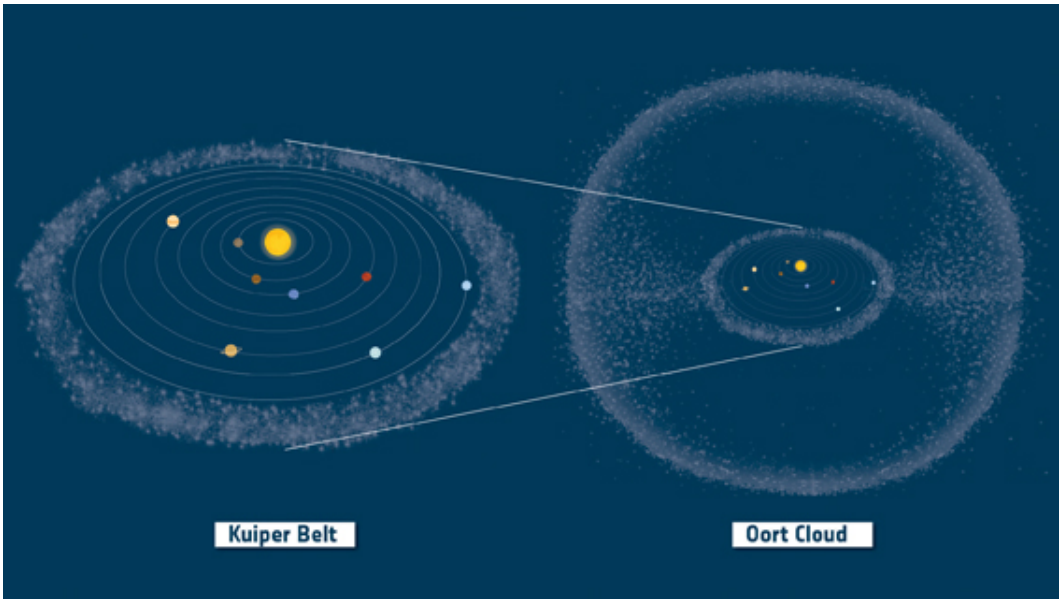

Figure 1.1: Illustration of Kuiper belt and Oort cloud (not to scale). Credit: ESA.

As comets approach the Sun, the increasing solar illumination leads to an enhanced cometary activity by sublimation and release of gas and solids into space. The nucleus of the comet is hard to observe, it has a low albedo and its size is typically smaller than 15 km in diameter. Gas and dust that escapes from the nucleus form a coma that can reach several 10^6 km in size. While the comet moves along its orbit, small dust particles pushed away by solar radiation forms the dust tail; at the same time, gas is ionized and forms the ion tail which is always pointing away from the Sun as it is strongly affected by the solar wind.

Figure 1.2 shows a schematic of a comet approaching the Sun and a picture of the ion and dust tail of comet Hale-Bopp (C/1995 O1). Furthermore, solid desiccated comet debris left on the comet's orbit forms cometary meteor streams, seen as meteor showers

when the Earth passes through them. A photo of comet McNaught (C/2006 P1) with its spectacular dust tail is shown in Figure 1.3. The Ulysses spacecraft encountered the ion tail of comet McNaught at a distance of more than 10^8 km to the nucleus; it has been identified to be the largest comet observed from Earth to date.

The active life of a comet can cease by either of the three major fates (Keller and Jorda, 2002): 1. it sublimes if it is dominated by ice, then shrinks and becomes invisible; 2. it disintegrates by splitting and shedding of subnuclei and chunks ending up as dust within the planetary system; a prominent example is comet Shoemaker-Levy 9 that broke apart to more than 10 pieces in 1992 and collided with Jupiter in 1994; 3. it becomes dormant when its surface becomes inert and may remain as a body close to its original size.

The cold temperatures at their reservoirs allowed comets to preserve the volatile species since the formation of the Solar System. Hence, studying comets would give hints about the composition of the early Solar System, transportation of material to the inner planets like Earth, etc. Therefore, several cometary missions were executed started with The International Cometary Explorer (ICE) in 1978. The missions are listed in Table 1.1 with Rosetta in 2014 to be this first one to orbit and study a comet closely for more than two years.

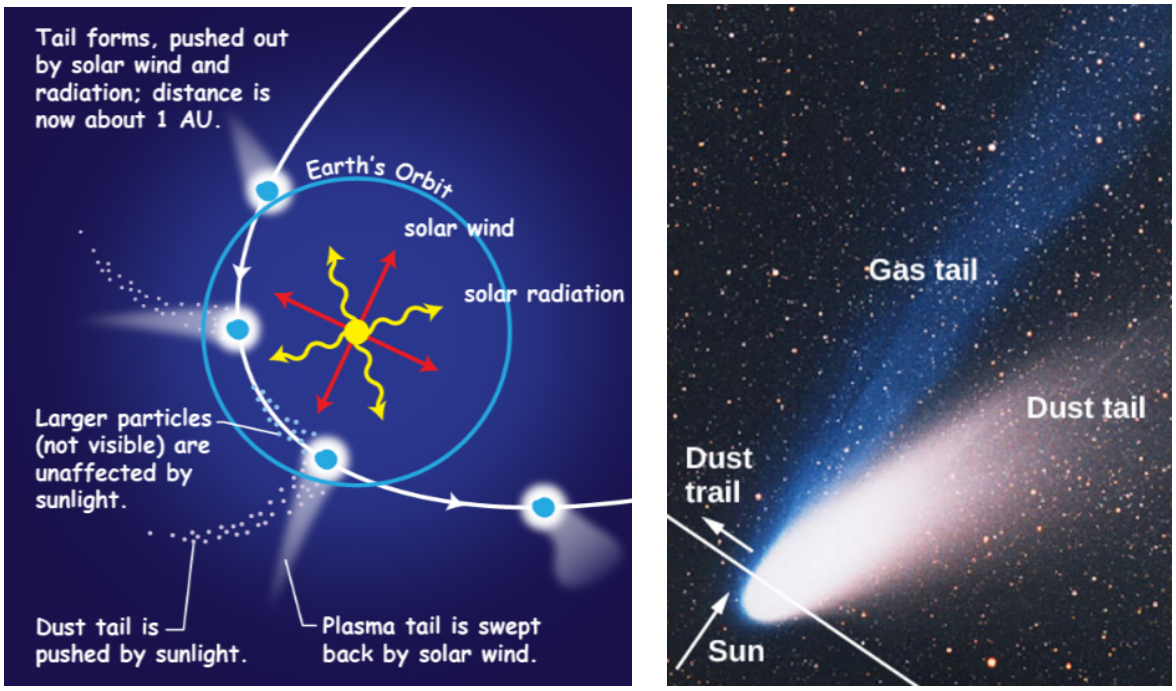

Figure 1.2: Left: Schematic of a comet approaching the Sun (not to scale); This picture is based on http://spaceplace.nasa.gov/comet-quest/en/. Right: illustration showing the dust and ion tail of comet Hale-Bopp (C/1995 O1); Credit: NASA. The ion tail is pointing away from the Sun; the dust tail is curved and pushed out on the orbit of the comet due the solar radiation pressure.

Figure 1.3: Comet McNaught (C/2006 P1) over the Pacific Ocean with its spectacular dust tail. Image taken from Paranal Obaservatory in January 2007. Credit: S. Deiries/ESO.

Table 1.1: List of cometary space missions.

Launch Date	**Comet Mission**	**Target Comet**
1978 Aug 12	ICE	21P/Giacobini-Zinner
1984 Dec 15	Vega-1 and Vega-2	1P/Halley
1985 Aug 19	Suisei	1P/Halley
1985 Jan 07	Sakigake	1P/Halley
1985 Jul 02	Giotto	1P/Halley, 26P/Grigg-Skjellerup
1998 Oct 24	Deep Space 1	19P/Borrelly
1999 Feb 07	Stardust	81P/Wild, 9P/Tempel
2005 Jan 12	Deep Impact/EPOXI	9P/Tempel, 103P/Hartley
2004 Mar 02	Rosetta	67P/Churymov-Gerasimenko

1.2 Rosetta

Rosetta was an international space mission led by the European Space Agency (ESA). It was the first space mission to orbit and also land on a comet. The spacecraft was launched on 2 March 2004 on a 10 year journey through the Solar System towards 67P. Rosetta underwent three gravity assists at Earth and one at Mars, flew by asteroids 2867 Šteins and 21 Lutetia, and went through a deep space hibernation of two and a half years before arriving at the comet.

On 6 August 2014 Rosetta rendezvoused with 67P at a distance of less than 100 km from the nucleus. It deployed its lander Philae to the comet on 12 November 2014 to focus on the composition and structure of the comet nucleus material. The orbiter

Rosetta then continued to accompany 67P through perihelion measuring the increase and decrease in coma activity throughout the comet's apparition until 30 September 2016 when the mission ended with a soft landing on the comet. A timeline with the key events of the Rosetta mission can be found in Table 1.2.

Table 1.2: Timeline of Rosetta.

Date	**Events**
2004 Mar 02	Launch
2005 Mar 04	1st Earth gravity assist
2007 Feb 25	Mars gravity assist
2007 Nov 13	2nd Earth gravity assist
2008 Sep 05	Flyby - asteroid 2867 Šteins
2009 Nov 13	3rd Earth gravity assist
2010 Jul 10	Flyby - asteroid 21 Lutetia
2011 Jun 08	Start of deep space hibernation
2014 Jan 20	Wake up from deep space hibernation
2014 Aug 06	Arrival at <100 km from comet 67P
2014 Nov 12	Release and landing of Philae on 67P
2015 Aug 13	Perihelion passage
2015 Dec 12	End of nominal mission
2016 Sep 30	End of extended mission

To investigate the origin of the Solar System by studying the origin of comets, and to study the relationship between cometary and interstellar material with its implications to the origin of the Solar System, the scientific measurement goals of Rosetta are (Schwehm and Schulz, 1999):

1. Global characterization of the nucleus, determination of dynamic properties, surface morphology and composition.
2. Determination of chemical, mineralogical and isotopic compositions of volatiles and refractories in a cometary nucleus.
3. Determination of the physical properties and interrelation of volatiles and refractories in a cometary nucleus.
4. Study of the development of cometary activity and the processes in the surface layer of the nucleus and inner coma (dust/gas interaction).
5. Global characterisation of asteroids, including determination of dynamic properties, surface morphology and composition.

To achieve these goals Rosetta consisted of an 11-instrument orbiter and a 10-experiment lander. The Rosetta orbiter was used to study the volatile and refractory material in the coma and composition and physical properties of the nucleus; the lander Philae performed the first in situ analysis of the comet nucleus, including the composition and physical properties. A short description of the orbiter instruments are given below. Further information may be found in Schulz (2010).

The remote sensing instruments are designed to characterize the nucleus surface and the gas and dust abundances in the coma. OSIRIS is a camera system designed to

determine the size, shape, rotational state, and the surface topography, sublimation, and erosion processes of the nucleus; MIRO is a microwave spectroscope to detect the surface and subsurface temperatures of the nuclues, and also the outgassing rates and isotopic ratios of certain volatile species; VIRTIS is an infrared imaging spectrometer focused on the detection and characterization of minerals and molecules to identify and quantify different constituents of cometary material; Alice is an ultraviolet imaging spectrograph to determine the production rates of atoms and gas molecules, and characterizes the nucleus surface at UV wavelengths.

The in-situ instruments collect and analyze gas and dust from the inner coma. ROSINA is a mass spectrometer suite that measures the composition and physical properties of neutral gas and ions; COSIMA performs dust composition measurements; GIADA and MIDAS obtain dust fluxes and physical properties of the grains.

CONSERT (with its counterpart on the lander Philae) and RSI are radio instruments that are designed to investigate the interior nucleus properties such as mass, bulk density, and mass distribution. RPC monitors in-situ the comet plasma environment and its interaction with the solar wind. The radiation environment was measured by SREM.

The lander Philae was designed to be dropped onto the cometary surface to obtain the first in situ measurements of a comet nucleus (Glassmeier et al., 2007). The CIVA and ROLIS camera systems take images of the nucleus surface. SESAME performs electric and acoustic sounding of the surface and monitors dust impacts from the nucleus outgassing activity. CONSERT works with its counterpart on the Rosetta orbiter to explore the interior of the nucleus. ROMAP monitors the magnetic and plasma environment. APXS and MUPUS are to be deployed to the surface to measure elemental composition of the surface materials and subsurface physical properties. Mass spectrometers and gas chromatographs PTOLEMY and COSAC analyze the surface and subsurface samples from the drill and sampling acquisition system SD-2 for isotopic and molecular composition.

The results in this study were performed by ROSINA. Therefore it will be introduced in more detail in the following section.

1.3 ROSINA

The main objective of the Rosetta Orbiter Spectrometer for Ion and Neutral Analysis (ROSINA) is to determine the major atmospheric and ionospheric compositions in the coma and to investigate the gas dynamics around the comet. It is capable of measuring the neutral coma composition, composition of cold thermal ions, total neutral gas density, and ram pressure. ROSINA consists of a pressure sensor and two mass spectrometers: the COmet Pressure Sensor (COPS), the Reflectron-type Time-Of-Flight mass spectrometer (RTOF), and the Double Focusing Mass Spectrometer (DFMS). All three sensors are controlled by the Data Processing Unit (DPU).

1.3.1 DPU

The Data Processing Unit (DPU) is in charge of the operating of all three ROSINA sensors and the communication with the spacecraft. The operation modes are stored in the DPU and can be modified via software update or direct commanding. A picture of the DPU is shown in Figure 1.4.

Figure 1.4: Picture of the ROSINA DPU extracted from Balsiger et al. (2007).

1.3.2 RTOF

RTOF is a time-of-flight mass spectrometer designed to reach a mass range of up to 3000 mass to charge ratio. It has the advantage that the entire mass spectra is recorded at once and has a high time resolution of around 200 seconds. RTOF is designed to be capable of measuring both ions and neutrals. RTOF has a mass resolution better than 400 at 50% peak height for mass 28.

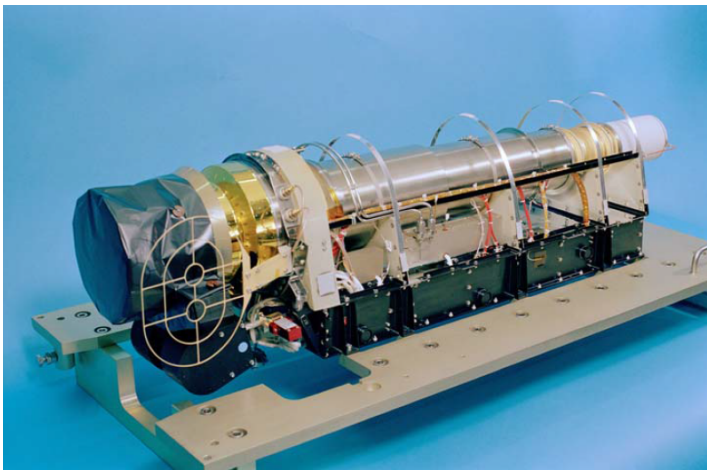

Figure 1.5: Picture of the ROSINA RTOF.

1.3.3 DFMS

DFMS is a double focusing mass spectrometer with a mass range of 12 to 150 mass to charge ratio. It has an ion mode for measuring cometary ions and also a gas mode for

measuring neutrals being ionized with electron impact ionization. The mass resolution at 1% peak height is 3000 and 9000 at 50% peak height for mass 28. DFMS measures one mass spectra after another, thus a typical time interval between the same mass is around 50 minutes. Therefore, DFMS with high mass resolution complements well with RTOF which has a lower mass resolution but a much higher time resolution and a higher mass range.

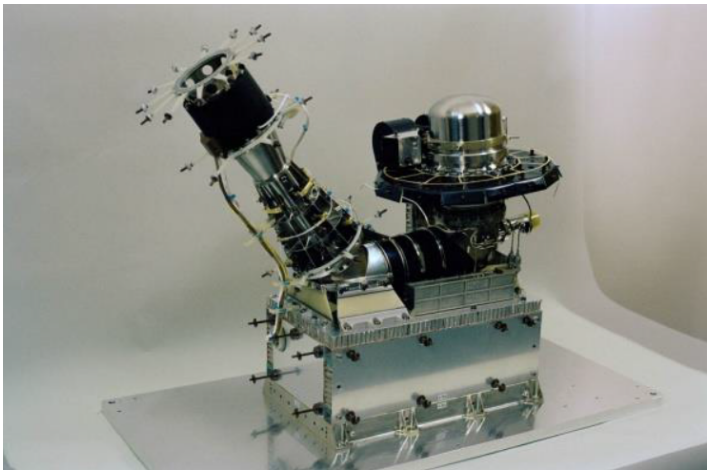

Figure 1.6: Picture of the ROSINA DFMS.

1.3.4 COPS

COPS has two pressure/density gauges; one is the nude gauge with an almost 4π field of view to measure total neutral pressure; the other is the ram gauge to measure the ram pressure. Figure 1.7 shows a picture of the Rosetta spacecraft with the location of COPS highlighted with a red circle; the ram gauge was pointing in the spacecraft +z direction which is most of the time nadir to the comet and the nude gauge was pointing to the solar panel -y direction. It is worth mentioning that in flight COPS was running continuously most of the time throughout the two-year orbiting phase, except during orbit control maneuvers and when the density was below the detection limit. A detailed description of COPS will be given in Chapter 2.

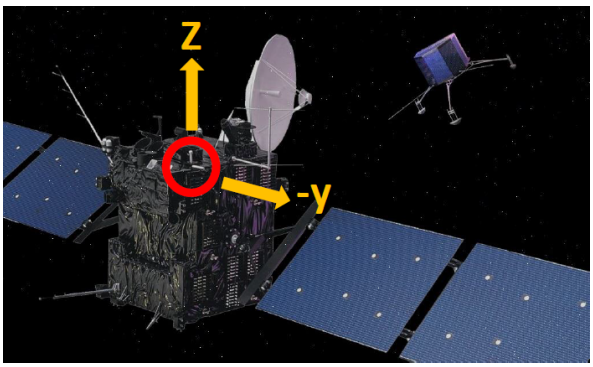

Figure 1.7: COPS on Rosetta spacecraft is highlighted with the red circle. The arrows show the COPS ram gauge pointing in +z direction and the nude gauge pointing in -y direction of the spacecraft. Modified from ESA spacecraft image (NSSDCA/COSPAR ID: 2004-006A).

1.4 67P/Churyumov-Gerasimenko

Comet 67P/Churyumov-Gerasimenko (67P) is a Jupiter-family comet discovered by Klim Churyumov on a photograph taken by Svetlana Gerasimenko in 1969. It has an orbital period of around 6.45 years and has now been observed from Earth during eight approaches to the Sun. Before Rosetta approached 67P, very little of the physical properties were known. Scientists tried to characterize the comet to be well prepared for the encounter of the Rosetta spacecraft.

One of the attempts was to reconstruct the nucleus of 67P based on Hubble Space Telescope observations of the light curve as shown on the left in Figure 1.8. These observations suggested that the nucleus of 67P is a football-shaped object with a diameter of nearly 6 km. When Rosetta rendezvoused with 67P, one of the first surprises was that the actual shape is quite different from expected. It appears rather like a rubber duck with a bi-lobed shape as shown in the right figure of Figure 1.8.

A shape model of 67P reconstructed by the Rosetta-OSIRIS camera team is shown in Figure 1.9 overlaid with the longitudes and latitudes. Furthermore, some of the key physical properties of 67P are shown in Figure 1.10.

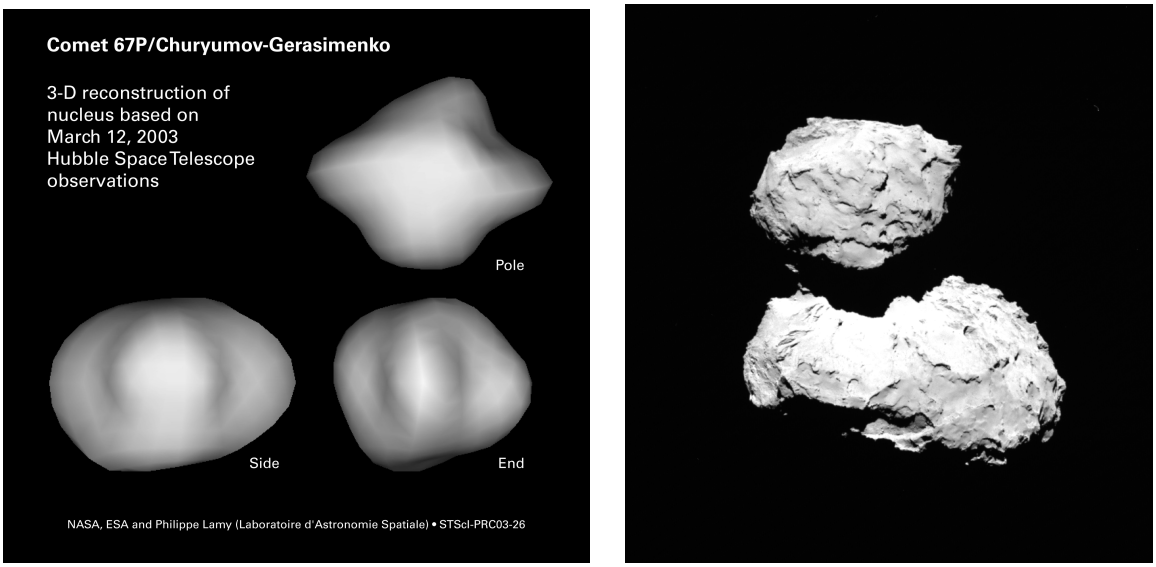

Figure 1.8: Left: Shape of 67P reconstructed from Hubble Space Telescope observations of the light curve in 2003; credit: NASA, ESA and Philippe Lamy (Laboratoire d'Astronomie Spatiale). Right: Image of 67P taken by the Rosetta-OSIRIS camera in August 2014; credit: ESA/Rosetta/MPS for OSIRIS Team, MPS/UPD/LAM/IAA/SSO/INTA/UPM/DASP/IDA

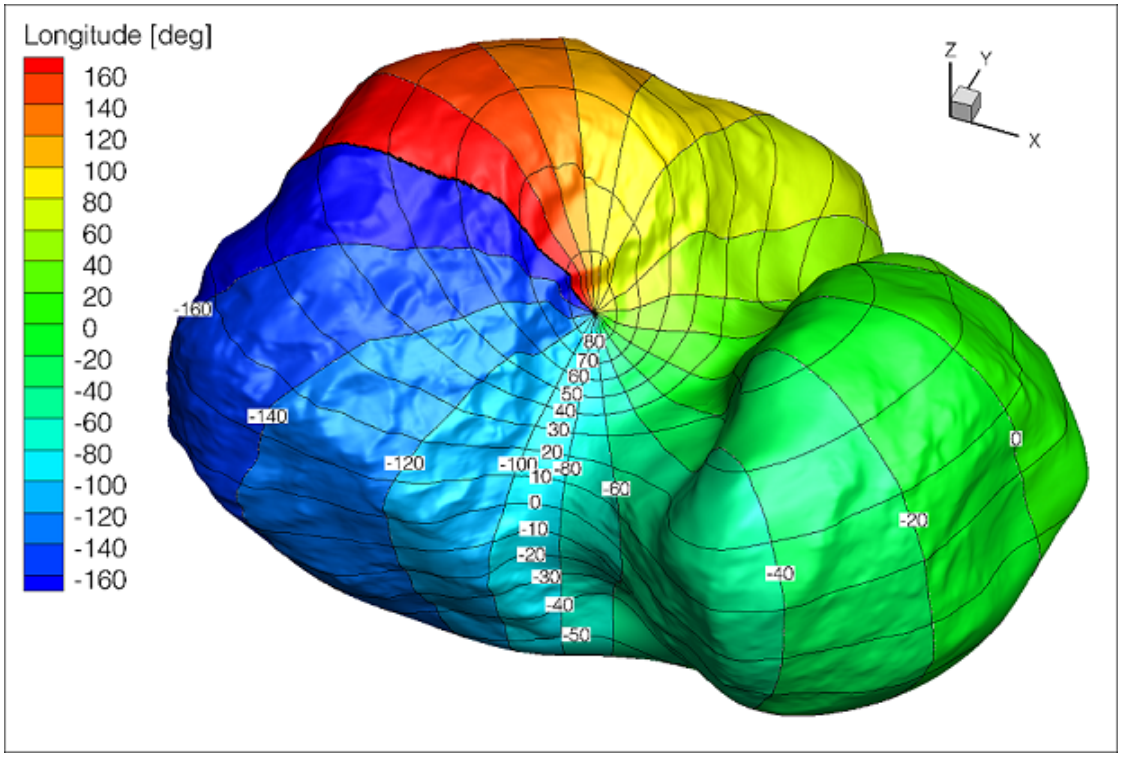

Figure 1.9: The Rosetta-OSIRIS SHAP2 model of 67P with the longitudes and latitudes. Credit: ESA/Rosetta/MPS for OSIRIS Team, MPS/UPD/LAM/IAA/SSO /INTA/UPM/DASP/IDA.

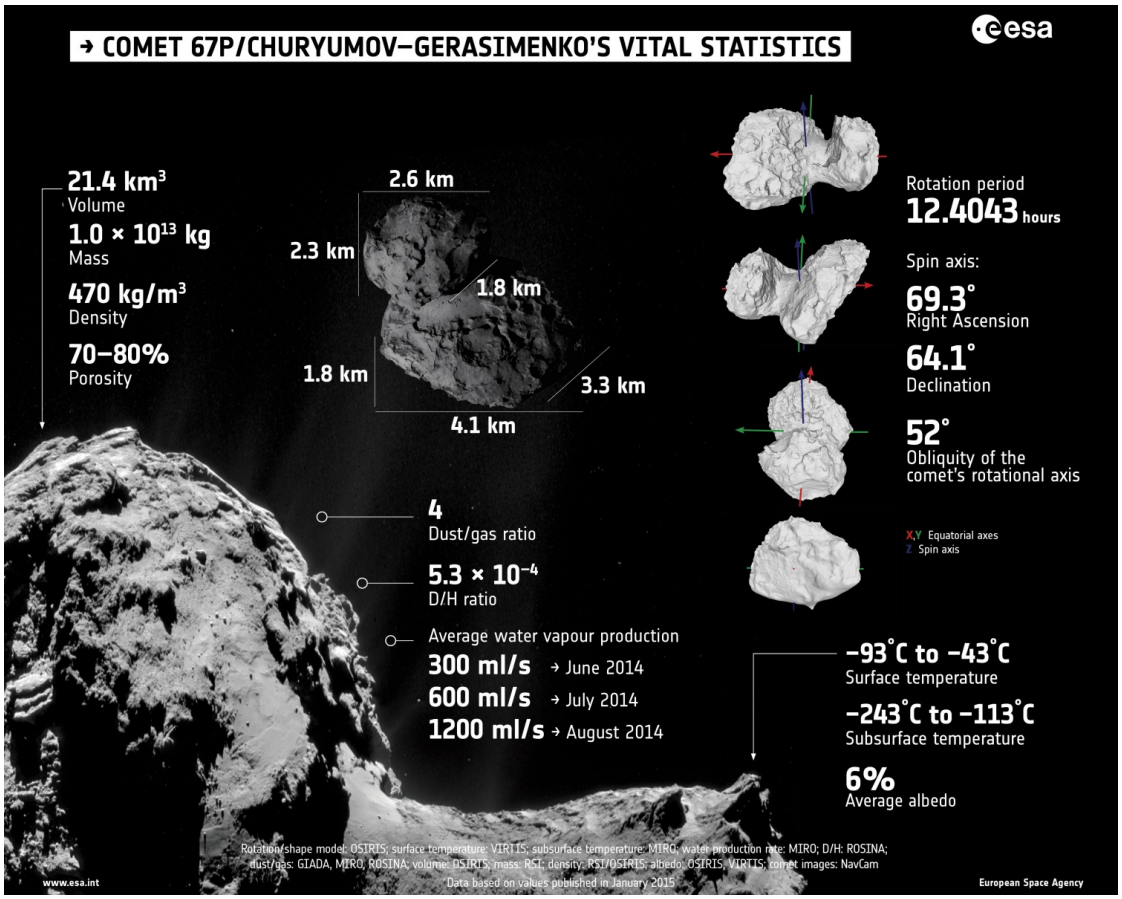

Figure 1.10: Infographic summarising key properties of comet 67P. Copyright: ESA.

1.4.1 Scientific Results

Since the encounter of Rosetta with 67P, many scientific results were pulished in rapid succession. Some of the results are listed as follows:

- Altwegg et al. (2015) reported a D/H ratio of $(5.3 \pm 0.7) \cdot 10^{-4}$ in 67P by ROSINA direct in situ measurement which is around three times the D/H terrestrial value. The detected value and previous cometary measurements suggest a wide range of D/H within Jupiter-family objects and precludes the idea that this reservoir is solely composed of Earth ocean-like water.

- Thomas et al. (2015) showed the variety of texture and structure of the nucleus surface observed with OSIRIS, and the importance of airfall, surface dust transport, mass wasting, insolation weathering for cometary surface evolution.

- Hässig et al. (2015) presented ROSINA measurements of the main volatile species H_2O, CO_2, CO in a heterogeneous coma showing diurnal and possibly seasonal variations.

- Rotundi et al. (2015) reported a dust to gas ratio of 4 ± 2 on the sunlit side of the comet based on GIADA, MIRO, and ROSINA observations.

- Le Roy et al. (2015) presented an inventory of the volatiles showing a CO_2 and ethane rich coma measured by ROSINA. The presence of heavy oxygenated compounds proves that Kuiper belt comets also contain complex organic molecules.

- Rubin et al. (2015) reported ROSINA measurements on molecular nitrogen with a N_2/CO ratio of $(5.70 \pm 0.66) \cdot 10^{-3}$ which is strongly depleted compared to protosolar value. This suggests that cometary grains formed at low temperature conditions < 30 K.

- Davidsson et al. (2015) showed orbital grains observed with OSIRIS having diameters in the range of 0.14 to 0.50 m. The results have possible implications for the understanding of the cloud debris around cometary nuclei and the ejection of large grains far from the Sun.

- Bieler et al. (2015a) presented the detection of molecular oxygen in cometary coma with a O_2/H_2O ratio of 3.8 ± 0.85 per cent from ROSINA measurements. O_2 seems to be isotropic in the coma and doesn't change systematically with heliocentric distance.

- Bertaux (2015) reported the erosion rate per orbit from SWAN/SOHO (Solar Wind Anisotropies/Solar and Heliospheric Observatory) measurements in previous perihelions estimating a layer of 1.0 ± 0.5 m thickness lost at each orbit. It supports the idea that the composition of the material that is measured in the coma is representative of the bulk material of the nucleus.

- Balsiger et al. (2015) presented the ROSINA in situ determination of argon. The range of the relative abundance of argon to water confirms that 67P-type comets cannot be the major source of Earth's major volatiles.

- Feaga et al. (2015) showed an average geometric albedo of 0.054 ± 0.008 at 1475 Å estimated with Alice spectral data and that the material on the nucleus surface are not very spectrally distinct from location to location.
- Altwegg et al. (2016) presented the detection of volatile glycine, phosphorous, and a multitude of organic molecules. This demonstrated that comets could have played a crucial role in the emergence of life on Earth.
- Hansen et al. (2016) reported evolution of water production based on in situ and remote sensing measurements made by Rosetta instruments. An empirical model is developed giving a peak water production 18 to 22 days after perihelion at $(3.5 \pm 0.5) \cdot 10^{28}$ molecules/s as measured by ROSINA.

1.5 Neutral Gas in Cometary Coma

The atmosphere formation applicable for a typical comet observed in the range of a few tenths to about 2 AU from the Sun is described by Combi et al. (2004). Dust and gas are released from the nucleus and forms an outflowing coma when heated up near to the Sun.

The expansion of gas and dust into vacuum and the week gravity of the nucleus forms a transient stationary thermal layer of a few meters thick near the surface. The start of a regular flow converts this thermal layer to a fast transonic dusty-gas flow. The flow expands and cools nearly adiabatically out to about 100 km. There the dust and gas becomes decoupled collisionally with a gas flow speed of around 700 m/s and a temperature of less than 30 K. Outwards of 100 km the UV photodissociation then starts to heat the gas faster than it is cooled by adiabatic expansion or infrared radiation. Photoionization and charge impact ionization then forms a cometary ionosphere that extends out to $10^3 - 10^4$ km which eventually forms an ion tail on scales of $10^5 - 10^7$ km resulting from the interaction with solar wind.

Observations often gives a snapshot of the the observed target, thus models constrained by in situ or remote observations are needed for a better understanding of the whole picture. Therefore, coma neutral gas properties, such as density, production rates, velocity, and temperature, are important inputs for developing coma models to gain better knowledge of the the physics behind.

1.5.1 Production Rates

Haser Model

A still widely used quantitative description of the molecule spatial distribution in the coma was mentioned by Haser (1957). The Haser model assumes that the coma is a spherically symmetric point source of constantly sublimating parent molecules from the surface of the nucleus and the gas expands radially outward with an exponential

lifetime describing the destruction of molecules (Combi et al., 2004). The density of the parent molecules n_p and daughter molecules n_d is described as

$$n_p(r) = \frac{Q}{4\pi r^2 v}(e^{-\frac{r}{\gamma_p}}) \tag{1.1}$$

$$n_d(r) = \frac{Q}{4\pi r^2 v}\frac{\gamma_d}{\gamma_p - \gamma_d}(e^{-\frac{r}{\gamma_p}} - e^{-\frac{r}{\gamma_d}}) \tag{1.2}$$

where r is the radial distance from the comet, v is the gas velocity, Q is the production rate of the parent species, γ_p and γ_d are the parent and daughter scale lengths, respectively. The formulation assumes that all dissociated parents go into exactly one daughter. The scale lengths of the parent and daughter molecules are typically much more than a thousand km away from the comet compared to Rosetta, which spent most of the time within a few hundred km from the nucleus. Thus the destruction of molecules can be ignored in most cases and the local neutral density n in the coma is simply given by

$$n(r) = \frac{Q}{4\pi r^2 v} \tag{1.3}$$

Water Production Rate at 67P

In situ or remote observations, local densities and column densities derived from spectral lines of molecules can be converted to molecular production rates to estimate the relative abundances of the different species in the nucleus. Water is known to be the most abundant component of cometary ices, therefore water production/outgassing rates are commonly used for quantifying the activity of comets. In addition, in situ information quite often provides only a snapshot of the observed body. Hence, models constrained with observations are needed to get the full picture of the comet.

In the study of Hansen et al. (2016) the water production rate of comet 67P estimated with various Rosetta instrument measurements and ground-based observations is summarized in Figure 1.11. Models are used to compute the total water production rate from ROSINA water density measurements (Fougere et al., 2016a), VIRTIS column density observations (Fougere et al., 2016a; Bockelée-Morvan et al., 2015; Fink et al., 2016), MIRO microwave spectral lines (Gulkis et al., 2015; Lee et al., 2015; Biver et al., 2015), and RPC/ICA plasma flux (Simon Wedlund et al., 2016). Ground-based dust brightness observations by Snodgrass et al. (2016) are scaled and showed high correlation with the water production rate. With the empirical model in Hansen et al. (2016) it is found that the peak water production rate is around $3.5 \cdot 10^{28}$ molecules/s.

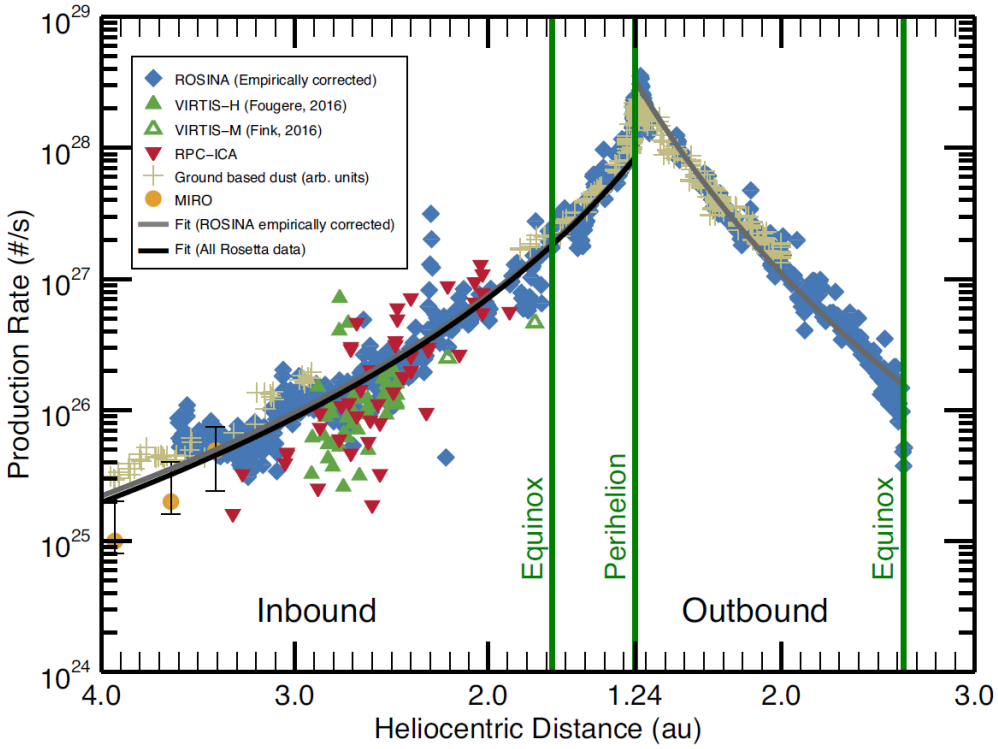

Figure 1.11: Water production rate as a function of heliocentric distance estimated with Rosetta instruments and ground-based observations: ROSINA in blue diamonds, VIRTIS in green triangles, RPC/ICA in red triangles, MIRO in yellow circles. The tan crosses are ground-based represent dust brightnesses scaled by an arbitrary factor for comparison with Rosetta instruments. The gray line is a fit to ROSINA data, and the black line is a fit to all inbound Rosetta data. Extracted from Hansen et al. (2016).

1.5.2 Gas Expansion Velocity and Temperature

At Comet 1P/Halley

The radial gas expansion velocity of water from Giotto Neutral Mass Spectrometer in situ observations at comet 1P/Halley was derived to be around 800 m/s at distances from the nucleus between 1000 and 4000 km; the expansion speed increases to at least 30000 km where around 1080 m/s was observed (Lammerzahl et al., 1987). Spectral observations of 1P/Halley (Larson et al., 1986; Schloerb et al., 1986; Krasnopolsky et al., 1986) show an outflow velocity in the range around 800 m/s to 1400 m/s.

Lammerzahl et al. (1987) derived the upper limit of water temperature to be around 300 K at 1000 km from comet 1P/Halley; the increase of gas temperature from 1000 to 15000 km is about 200 K.

At 67P/Churyumov-Gerasimenko

Gas velocities in the coma of 67P are estimated with numerical models restricted by observation data of several instruments on board of Rosetta. Total gas velocities and

the ones of water and CO_2 are mentioned in various studies.

Simulation outputs of DSMC models (Fougere et al., 2016a) constrained by ROSINA-DFMS data show a maximum water velocity around 680 m/s for end of year 2014. The MIRO instrument water velocities are derived from models of the observed H_2O spectral lines: presented by (Gulkis et al., 2015) and (Lee et al., 2015) water velocities observed near the subsolar point is roughly 0.68 km/s for June to September, 2014. Shown by Biver et al. (2015) water velocities near the terminator are about 0.52 km/s for measurements obtained in September 2014. In addition, Fink et al. (2016) estimated the H_2O outflow velocity to be 580 m/s for February and April 2015 from VIRTIS observations.

Fougere et al. (2016b) derive CO_2 outflow velocities reaching up to 600 m/s for December 2014 from a DSMC model constrained by ROSINA data. Furthermore, Fink et al. (2016) estimated the CO_2 outflow velocity to be 380 m/s for February and April in 2015 from VIRTIS observations.

The gas expansion velocity of the total neutrals has been derived by 3D kinetic and hydrodynamic models and ranges from 0.4 to 0.8 km/s for August-December 2014 (Bieler et al., 2015b).

Prior to the arrival of Rosetta at 67P, Tenishev et al. (2008) showed pre-encounter estimations of the kinetic temperature in 67P's coma to be lower than 100 K within 100 km from the nucleus surface. Analysis of MIRO water spectral data at 67P showed terminal gas temperatures varying from 47 K to 74 K (Lee et al., 2015). In addition, Bockelée-Morvan et al. (2015) derived rotational temperatures of H_2O and CO_2 with VIRTIS measurements from 2.9 to 2.5 AU from the Sun, which are close to model predicted values for 67P at 2.5 AU (Davidsson et al., 2010).

2. COPS - COmet Pressure Sensor

The main goal of COPS, the COmet Pressure Sensor of ROSINA, is to determine the cometary gas densities, velocities, and eventually temperature in the coma of comet 67P. COPS has a very wide dynamic range of 10^6 to accommodate large differences and changes in the neutral gas density and flux as the comet activity changes towards and away from perihelion. COPS as well plays the role of a safety instrument of Rosetta to monitor the ambient gas density and alert other instruments on board of the spacecraft when the neutral gas density is too high or density increase is too fast.

Calibration measurements with the COPS flight spare model (COPS-FS) in the lab is important for validating the calibration factors/procedures of the COPS flight model (COPS-FM) in space as well for cross-calibrations with the two ROSINA mass spectrometers DFMS and RTOF. COPS consists of two pressure gauges: the nude gauge and the ram gauge (Figure 2.1) are each located on a boom to prevent from measuring gas reflected by the spacecraft or nearby instruments. The nude gauge (NG) measures the total neutral particle density; the ram gauge (RG) is capable of measuring the gas flux/ram pressure.

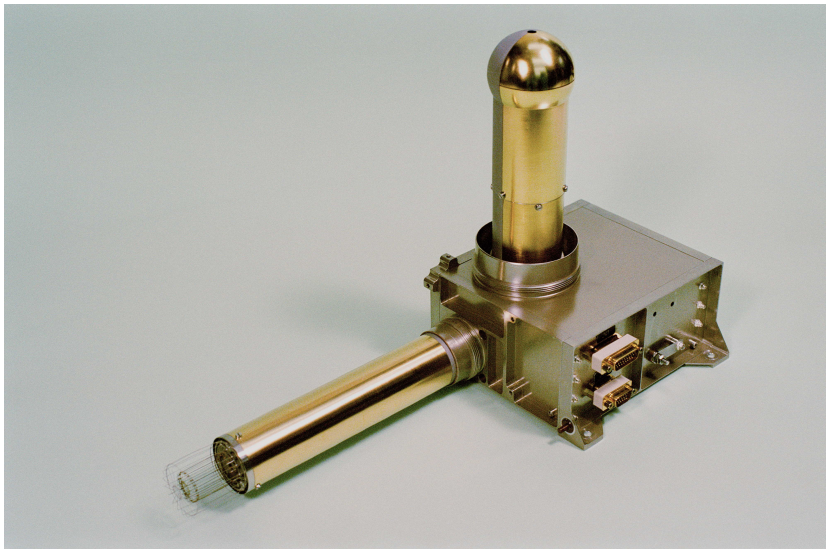

Figure 2.1: COPS with both gauges and the electronic box. The nude gauge is pointing to the left, the ram gauge to the top. The electronic box has a length of about 17 cm. From Balsiger et al. (2007).

2.1 Measurement Principle

Both of the gauges are based on the extractor-type ionization gauge principle (Redhead, 1966). In brief, the neutral gas is ionized by electrons. Then these ion signals are collected by the detector (electrometers) and can be translated back to the neutral gas density using the above mentioned calibration factors. A drawing showing the important electronic components of the nude gauge is shown in Fig. 2.2 and for the ram gauge in Fig. 2.3.

2.1.1 Nude Gauge

The cylindrical outer grid is at -12 V, and the cylindrical inner grid at +180 V (Balsiger et al., 2007). The inner and outer grids keep the cometary plasma away from entering the ionization region and therefore only the neutral particles have access to the ionization volume defined by the inner grid. The nude gauge has two filaments. Each time only one of them is used during operation; the other one is a spare. In this work for lab and space measurements the left filament is used.

The electrons emitted from the hot filament at +30 V are accelerated to the inner grid to ionize the neutrals in the ionization volume. The electron energy is therefore 150 eV. Next, the ions created from the neutrals are accelerated to the collection area below the base plate where they are focused by a hemispherical reflector at +110 V and then collected by the cathode ion collector. The collected ion current is proportional to the particle density in the ionization volume. The pressure range of the nude gauge is around $10^{-11} - 10^{-5}$ mbar which corresponds to the range $10^{5} - 10^{11}$ cm^{-3}. The field of view of the nude gauge is almost 4π sr.

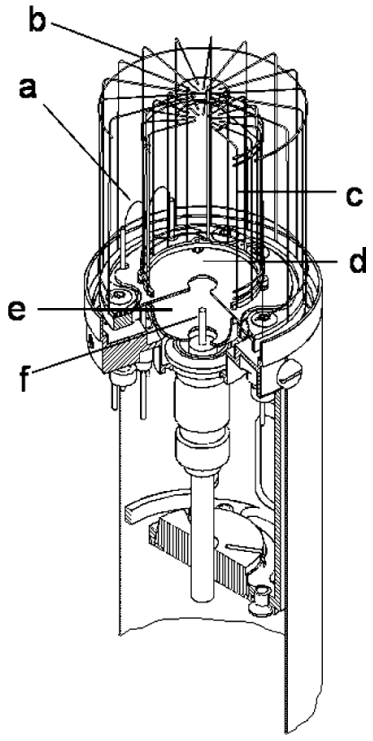

Figure 2.2: COPS nude gauge drawing with main electrodes labelled. a) the two filaments, +30 V, b) outer grid, -12 V, c) inner grid, +180 V, d) base plate, 0 V, e) reflector, +110 V, f) ion collector. From Balsiger et al. (2007).

2.1.2 Ram Gauge

The COPS ram gauge is most of the time pointing towards the comet. It has a spherical equilibrium cavity with a 6 mm opening on a hollow boom and an inner shield to allow impinging neutral gas to be isotropized and thermalized before entering the ionization

volume. The equilibrium time of neutral gas, e.g. water, at 200 K is less than 200 ms for the system (Balsiger et al., 2007); however, the real time resolution depends on the electrometer that measures the ion current (Section 2.2).

Similar to the nude gauge, the cylindrical anode grid is the ionization volume at +180 V. Additionally, the equilibrium sphere and hollow boom wall temperature should be the same as the surrounding gas, thus a cold electron source has to be used. So a microtip field-emitter device is used instead of a usual hot filament. The ram gauge microtip field-emitter device is arranged to have eight independent arrays of electron emitters that can be controlled separately. In ram gauge operation modes, a group of 3 microtip arrays is always used. The emitted electrons then ionize the thermalized neutral gas in the ionization volume. Then the ion signals are collected by the collector just like the nude gauge and can then be translated to ram pressure or number density of the gas flux when applying the suitable calibration factors. The pressure range of the ram gauge is $10^{-9} - 10^{-5}$ mbar. More details can be found in Balsiger et al. (2007).

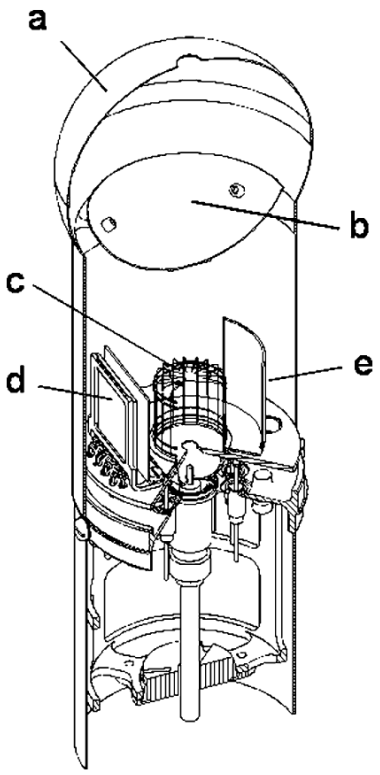

Figure 2.3: COPS ram gauge drawing with main components labelled. a) equilibrium sphere, b) inner shield, c) anode grid, +180 V, d) microtips, e) electron repeller. The lower part with the base plate, ion reflector, and collector basically functions the same as for the nude gauge. From Balsiger et al. (2007).

2.2 Data Output

At the electrometers of COPS the internal integration time is approximately 10 s. So what is read out by the electrometers is approximately a running average over the

last 10 s. Additionally, the DPU builds a running average over the last 5 electrometer measurements, providing a COPS neutral density measurement every 2 s at maximum frequency. This leads to COPS having a maximum time resolution of 10 s. Therefore, the time stamp of this read out has to be corrected by -5 seconds to obtain the mean time. During lab experiments, the DPU 2-second read out is mostly used, whereas for observations in space this value is transmitted by the DPU once every minute for normal monitoring measurement modes.

Besides the normal one-minute monitoring modes, COPS also has a scientific mode which can be commanded separately. In scientific mode, a file block is created every 5 minutes containing 150 of the 2-second data points for each operating gauge. However, the time resolution given by the running average at the DPU and the internal integration time of the electrometers is still approximately 10 s.

2.3 Offset Measurements

As the gas densities are detected with electrometers, it is important to consider the offsets of the electrometers during measurements as well. So COPS is designed to do offset measurements periodically during measurement/monitoring modes. To do the electrometer offset measurements the electron emission from the filament or microtips are switched off. Each offset measurement takes roughly 5 min to switch through all three ranges with different sensitivity; after the offset measurements it takes around 23 min to ramp up and switch the electron emission of the filament/microtips on again for the nude gauge or the ram gauge mode operation.

Offset measurements are done at the beginning of the first commanded mode after a DPU switch on and as well roughly every 24 hours after the end of the previous one for each gauge. Offset measurements of the nude gauge and the ram gauge are timed to be around 12 hours apart in order not to have COPS totally inactive during offset measurements (COPS-Manual, 2011).

2.4 Measurement Modes

Each gauge of COPS can be operated separately or together. Most of the time both gauges run together or only the nude gauge is operated. There are three different types of immission: 15 µA, 50 µA, and 100 µA; lower immissions are used when the neutral gas density is high and higher immissions are used when the density is low, respectively. There are also 3 different ion-ranges: low, medium, high; the lowest ion-range has the highest gas sensitivity so is suitable for measuring low gas density, and the highest ion-range has the lowest gas sensitivity suitable for measuring higher gas density. The different combinations of gauges, immission currents, and ion-ranges are collected in a suite of measurement modes.

In space when the pressure/density is varying a lot, automatic modes are used; the automatic modes switch automatically to suitable immission and ion-range combinations. In addition, for the COPS flight model in space the ram gauge modes with

high immission are always 100 µA; for safety reasons in the laboratory for the COPS flight spare, high immission modes are always set to around 30 µA only to have less aging/damage of the microtips. See Table 2.1 for the list of modes. COPS measurements in the laboratory on ground can be found in Chapter 4 and observations in flight can be found in Chapter 5.

Table 2.1: COPS operation modes.

		Nude Gauge		**Ram Gauge**	
Mode		**Immission [µA]**	**Ion-Range**	**Immission [µA]**	**Ion-Range**
BG [a]	326	Auto [d]	Auto	Auto	Auto
	316	15	Medium	15	Low
	396	100	Low	15	Low
	336	100	Low	30/100 [f]	Low
NG [b]	322	Auto	Auto	-	-
	352	15	Low	-	-
	312	15	Medium	-	-
	342	15	High	-	-
	332	100	Low	-	-
	362	100	Medium	-	-
RG [c]	314	-	-	15	Low
	324	-	-	Auto? [e]	Auto? [e]
	344	-	-	50	Low
	334	-	-	30/100 [f]	Low
Offset	51	NG offsets. To be commanded during a NG mode.			
	53	RG offsets. To be commanded during a RG mode.			
	55	BG offsets. To be commanded during a BG mode.			
Switch off	0	NG, RG, or BG off. Always command with offset off.			
Switch on	2	NG on with filament to standby, no emission.			
	4	RG on with microtips to standby, no emission.			
	6	Filament and microtips to standby, no emission.			

[a] BG ≡ both gauges.
[b] NG ≡ nude gauge only.
[c] RG ≡ ram gauge only.
[d] Auto ≡ automatic mode. Gauges automatically switches to the best Immission or Ion-Range for measuring the ambient gas.
[e] During tests of mode 324 in the laboratory it is behaving like mode 314 always with 15 µA immission. Probably the chamber pressure was never low enough that mode 314 switched automatically to higher immissions.
[f] For the COPS flight model in space the ram gauge modes with high immission are always 100 µA; for safety reasons in the laboratory for the COPS flight spare high immission modes are always set to around 30 µA only to have less aging/damage of the microtips.

3. Data Treatment Principles

3.1 Gas Density Correction

During the development phase of ROSINA, COPS was designed to have similar gas sensitivity to the Granville-Phillips Stabil-Ion Gauge (G.P.) which is a Bayard-Alpert gauge calibrated for N_2 with a typical error of 4% - 6% (Granville-Phillips, 2007). Same as G.P., at COPS different types of gas have different sensitivities due to the different individual electron-impact ionization cross-sections. Therefore, correction factors are needed for pressure/density readouts when measuring gas species different from N_2.

One thing to note is that gas density and gas pressure are interchangeable. For the case of COPS, pressure values are given directly in the housekeepings as if measuring only N_2 at 20 °C for which the calibration values were obtained in lab. The conversion between density and pressure follows the ideal gas law $P = nkT$ with P the pressure in pascal, n the number density in m^{-3}, the temperature $T = 293\,K$, and the Boltzmann constant $k = 1.38 \cdot 10^{-23}\ J \cdot K^{-1}$.

As shown in Equation (3.1) when measuring a non-N_2 gas with COPS, the pressure readouts $P_{C,i}$ are to be multiplied by a correction factor β_i for a single gas species i to retrieve the real pressure of an individual species. The correction/scale factors for individual species used in this study can be found in Table 3.1.

$$P_i = \beta_i \cdot P_{C,i} \tag{3.1}$$

In space COPS always measures the total pressure/density from the gas mixture in the coma of 67P but not single gas species. Here we introduce how to derive a species-dependent correction factor $\beta_{C,total}$ for gas mixtures measured with COPS as in Equation (3.2). P_{total} is assumed to be the real pressure for the total gas mixture, and $P_{C,total}$ the total gas mixture pressure readout from COPS.

$$P_{total} = \beta_{C,total} \cdot P_{C,total} \tag{3.2}$$

In Equation (3.3a) $P_{C,total}$ is represented as the sum of the individual species pressures as seen by COPS; then using the relation of single species between COPS and real pressure in Equation (3.1) $P_{C,total}$ can be shown with P_i the partial pressure of individual species i. Partial pressure P_i is expressed with R_i the volume mixing ratio of species i in Equation (3.3b).

$$P_{C,total} = \sum_i P_{C,i} = \sum_i \frac{P_i}{\beta_i} \tag{3.3a}$$

$$= \sum_i \frac{P_{total} \cdot R_i}{\beta_i} = P_{total} \sum_i \frac{R_i}{\beta_i} \tag{3.3b}$$

From Equations (3.2), (3.3a), and (3.3b) we can conclude that the correction factor for mixed gas is as Equation (3.4) where r_i is the density ratio of species i to water ($r_i = n_i / n_{H_2O}$) and the relation of volume mixing ratio to the density ratio of individual

species to water is as Equation (3.5). For COPS density measurements in flight the volume mixing ratio or the density ratio of main species relative to water are obtained with ROSINA-DFMS and ROSINA-RTOF.

$$\beta_{C,total} = \frac{1}{\sum_i \frac{R_i}{\beta_i}} = \frac{\sum_i r_i}{\sum_i \frac{r_i}{\beta_i}} \tag{3.4}$$

$$R_i = \frac{r_i}{\sum_i r_i} \tag{3.5}$$

One thing to be noted is that for measurements made with either the COPS-FS on ground or the COPS-FM in flight, background has to be subtracted before applying this species dependent β-factor correction. In flight the background is contributed by the spacecraft contamination (Graf et al., 2008; Schläppi et al., 2010) or the electrometer noise of the instrument itself. For COPS-FM the nude gauge subtracted background is $1.2 \cdot 10^6\,\mathrm{cm}^{-3}$ ($5 \cdot 10^{-11}\,\mathrm{mbar}$) and for the ram gauge it is $2.5 \cdot 10^7\,\mathrm{cm}^{-3}$ ($1 \cdot 10^{-9}\,\mathrm{mbar}$); for COPS-FS on ground the density of the residual gas in the vacuum chamber or the detection lower limit is taken as the background.

Table 3.1: Correction factors for the pressure measurements of COPS and the Granville-Phillips Stabil-Ion Gauge, extracted from Granville-Phillips (2007).

Gas Species		**Scale factor**
Helium	He	5.56
Neon	Ne	3.33
Nitrogen	N_2	1.00
Oxygen	O_2	$9.90 \cdot 10^{-1}$
Carbon monoxide	CO	$9.52 \cdot 10^{-1}$
Water	H_2O	$8.93 \cdot 10^{-1}$
Argon	Ar	$7.75 \cdot 10^{-1}$
Carbon dioxide	CO_2	$7.04 \cdot 10^{-1}$
Krypton	Kr	$5.15 \cdot 10^{-1}$
Xenon	Xe	$3.48 \cdot 10^{-1}$

3.2 Gas Velocity Calculation

Ram gauge densities are obtained when the total flux entering ($F_{in} = n_n v_z A$) and exiting ($F_{out} = n_r v_{r,z} A$) the equilibrium sphere reach a balance ($F_{in} = F_{out}$). Figure 3.1 illustrates the gas flow entering the ram gauge equilibrium sphere where on the instrument platform the ram gauge points to positive z-axis of the spacecraft (see Figure 1.7 in Section 1.3.4).

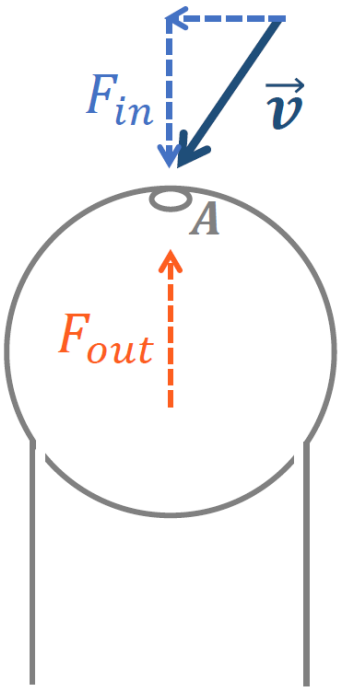

Figure 3.1: Illustration of coma gas flow with velocity $\vec{v}$ entering the ram gauge.

The variables n_n and n_r are the densities in the free gas flow measured by the nude gauge and the density in the ram gauge, respectively, A is the cross section of the aperture on the equilibrium sphere, v_z the z-component of the gas flow velocity $\vec{v}$, and $v_{r,z}$ the speed of the gas exiting the ram gauge. The flux entering the ram gauge in the z-direction is $F_{in} = n_n v_z A$; the flux exiting in the z-direction is $F_{out} = n_r v_{r,z} A$. Thus the flux balance $F_{in} = F_{out}$ leads to:

$$v_z = \frac{n_r}{n_n} v_{r,z} \tag{3.6}$$

Assumming a Maxwell-Boltzmann distribution at ram gauge temperature T_r the velocity probability density of the z-component of the outward flux is described as $f(v_{r,z})$ where m_g is the mean mass of the gas molecules and k the Boltzmann constant:

$$f(v_{r,z}) = \sqrt{\frac{m_g}{2\pi k T_r}} \exp\left(-\frac{m_g v_{r,z}^2}{2kT_r}\right) \tag{3.7}$$

The outward velocity $v_{r,z}$ can be written as the integral for velocities in the positive z-direction normalized to the whole distribution along the z-component as in Equation (3.8a). Substituting the distribution function (Equation (3.7)) yields Equation (3.8b) where the integral is equal to one-fourth of the mean thermal speed $\bar{v}_{th}$ (Equation (3.8c)). The interpretation is that on average half the molecules are moving in the positive z-direction and the bulk velocity of a half-sphere Maxwellian distribution

corresponds to half of the mean thermal speed.

$$v_{r,z} = \frac{\int_0^\infty v_{r,z} f(v_{r,z}) \mathrm{d}v_z}{\int_{-\infty}^\infty f(v_{r,z}) \mathrm{d}v_z} \tag{3.8a}$$

$$= \int_0^\infty v_{r,z} \sqrt{\frac{m_g}{2\pi k T_r}} \exp\left(\frac{m_g v_{r,z}^2}{2kT_r}\right) \mathrm{d}v_z \tag{3.8b}$$

$$= \frac{1}{4}\bar{v}_{th} \tag{3.8c}$$

Following the speed probability density function in spherical coordinates

$$f(v) = \left(\frac{m_g}{2\pi k T_r}\right)^{\frac{3}{2}} 4\pi v^2 \exp\left(-\frac{m_g v_{r,z}^2}{2kT_r}\right) \tag{3.9}$$

the mean thermal speed is written as

$$\bar{v}_{th} = \int_0^\infty v f(v) \mathrm{d}v = \sqrt{\frac{8kT_r}{\pi m_g}} \tag{3.10}$$

Then with Equations (3.8c), (3.10), and (3.6) the bulk gas flow velocity along the negative z-axis of the spacecraft is shown in Equation (3.11) and can be derived from the density ratio of both gauges, the ram gauge temperature, and the mean gas mass that can be obtained from DFMS or RTOF measurements as

$$v_{n,z} = \frac{n_r}{n_n}\sqrt{\frac{kT_r}{2\pi m_g}} \tag{3.11}$$

assuming that the thermal motion of the cometary gas entering the ram gauge is small compared to its bulk motion.

3.3 Gas Temperature Estimation

The main idea of deriving the gas temperature with COPS is that the derived velocity is actually composed of the bulk gas velocity and the thermal gas velocity. When the ram gauge is pointing to larger angles with respect to the gas flow, such as around 90 deg, gas enters the COPS ram gauge due to the thermal motion/velocity of the gas particles perpendicular to the bulk motion of the gas flow.

This means when the spacecraft changes its attitude with respect to the cometary gas flow and slews to larger angles gradually, the derived gas velocity will decrease from a large bulk velocity dominated to a small thermal dominated velocity.

Assume that the spacecraft is at rest and the cometary gas flow z-component v_z is along the spacecraft negative z-direction where the other two perpendicular gas flow components are v_x and v_y; the cometary gas bulk velocity $\vec{v}_0$ is represented by the vector (v_{0x}, v_{0y}, v_{0z}); the mass of the gas molecules is m_g, the gas temperature is T_g,

and the Boltzmann constant is k. Therefore, the Maxwell-Boltzmann distribution of the gas molecule/atom velocity vector can be written as

$$f(v_x, v_y, v_z) = \left(\frac{\xi}{\sqrt{\pi}}\right)^3 \exp\left(-\xi^2\left[(v_x - v_{x0})^2 + (v_y - v_{y0})^2 + (v_z - v_{z0})^2\right]\right) \tag{3.12}$$

with

$$\xi = \sqrt{\frac{m_g}{2kT_g}} \tag{3.13}$$

Only gas molecules/atoms with negative v_z velocity components enter the COPS ram gauge; velocities in the perpendicular directions, x and y, are not limited. The first moment of v_z can be calculated integrating the distribution function over all velocities entering the ram gauge giving

$$\bar{v}_z = \int_0^\infty \int_\infty^\infty \int_{-\infty}^\infty v_z \; f(v_x, v_y, v_z) \; dv_x \; dv_y \; dv_z \tag{3.14a}$$

$$= \int_0^\infty \int_\infty^\infty \int_{-\infty}^\infty v_z \left(\frac{\xi}{\sqrt{\pi}}\right)^3 \exp\Big(- \xi^2 \Big[(v_x - v_{x0})^2 + (v_y - v_{y0})^2 + (v_z - v_{z0})^2 \Big] \Big) \; dv_x \; dv_y \; dv_z \tag{3.14b}$$

If it is assumed that the coordinate system is rotated so that the bulk velocity of the cometary gas is in the x-z plane, then $v_{y0} = 0$. For an inflowing gas at an angle α with respect to the z-axis, the cometary gas flow bulk velocity can be rewritten as $(v_0 \sin(\alpha), 0, v_0 \cos(\alpha))$ with v_0 the absolute speed. Substituting the new bulk vector in Equation (3.14b) yields

$$\bar{v}_z = \int_0^\infty \int_\infty^\infty \int_{-\infty}^\infty v_z \left(\frac{\xi}{\sqrt{\pi}}\right)^3 \exp\Big(- \xi^2 \Big[(v_x - v_0 \sin(\alpha))^2 + (v_y)^2 + (v_z - v_0 \cos(\alpha))^2 \Big] \Big) dv_x \; dv_y \; dv_z \tag{3.15a}$$

In the x and y direction the integral boundaries are infinity and only positive v_z components for the velocity should be taken into account. The integral then becomes as the following containing the error function

$$\bar{v}_z = \frac{\exp(-\xi^2 v_0^2 \cos^2(\alpha)) + \sqrt{\pi}\xi v_0 \cos(\alpha)[1 + \mathrm{erf}(\xi v_0 \cos(\alpha))]}{2\sqrt{\pi}\xi} \tag{3.16}$$

The angle α between the spacecraft z-direction and the gas bulk flow can be technically viewed as two parts: $\alpha = \theta - \theta_0$; θ is the angle of the spacecraft z-axis with respect to the nadir direction which can be retrieved from the NASA developed observation geometry information system named SPICE; θ_0 is the angle of the bulk flow with respect to the

anti-nadir direction which one can get an idea of from a COPS dynamic slew covering angle ranges close to nadir, where the ram gauge density or gas velocity is the highest, since the gas flow direction is most probably almost parallel to nadir. By replacing α with $\theta - \theta_0$ yields Equation (3.17a) from Equation (3.13) and Equation (3.16), with the bulk flow speed v_0 and gas temperature T_g which may be obtained by fitting the curve to the actual COPS observations.

$$\bar{v}_z = \sqrt{\frac{kT_g}{2m_g\pi}}\left[\exp\left(-\frac{m_g}{2kT_g}v_0^2\cos^2(\theta-\theta_0)\right)\right.$$
$$\left.+\sqrt{-\frac{m_g\pi}{2kT_g}}v_0\cos(\theta-\theta_0)\left(1+\operatorname{erf}\left(\sqrt{\frac{m_g}{2kT_g}}v_0\cos(\theta-\theta_0)\right)\right)\right] \tag{3.17a}$$

Plotting Equation (3.16) for α from $0-140°$ gives Figure 3.2 demonstrating the feature that for gas (with a fixed mass of the water molecule) of the same bulk velocity (900 m/s) with different temperatures show the largest variation at around $\alpha = 80$ - 110 ° from the inflow direction. This suggests that it is possible to derive the coma gas temperature (perpendicular to the gas bulk motion) by observing and fitting the velocity-angle curve of COPS during a spacecraft dynamic slew.

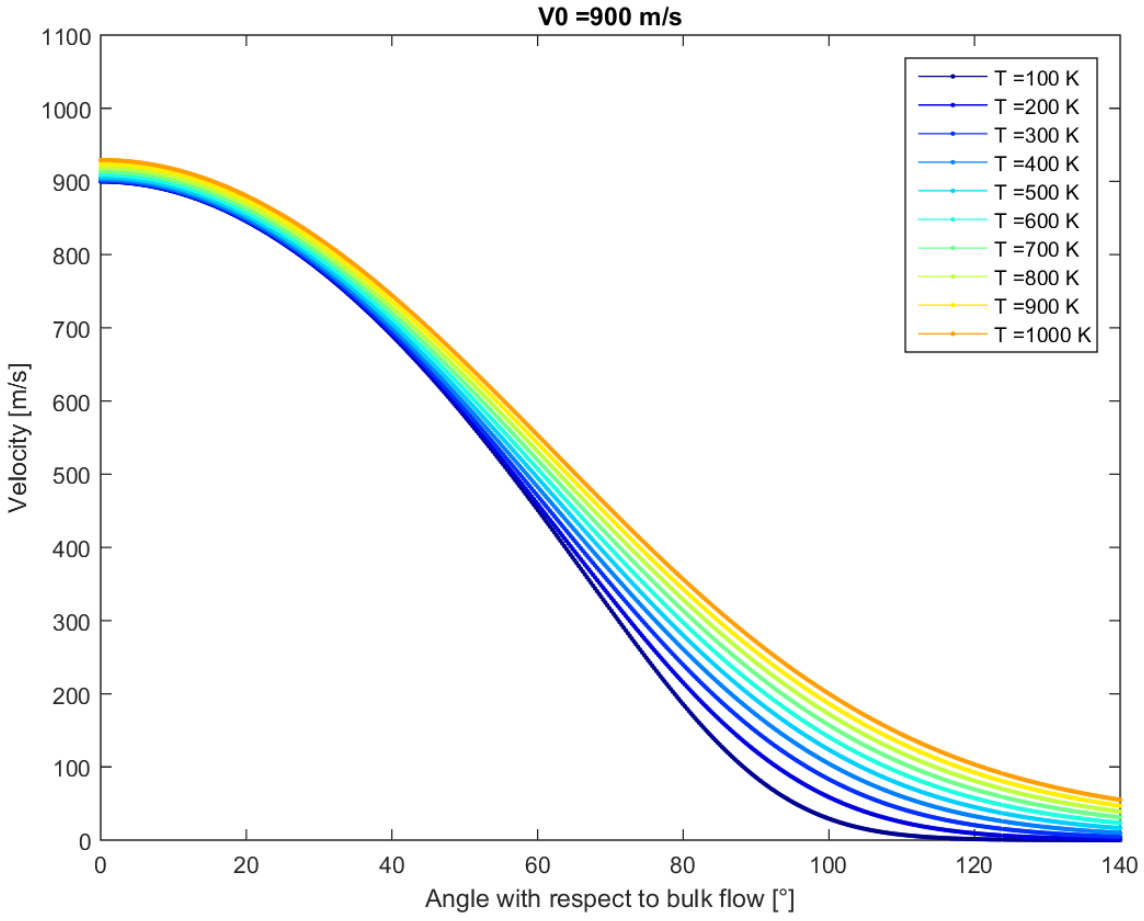

Figure 3.2: Theoretical velocity-angle curve of spacecraft dynamic slews of gas with same bulk velocity but different thermal temperatures.

In Figure 3.2 the bulk velocities ($\alpha = 0$) seem to be > 900 m/s for high temperatures. The reason is that with higher gas temperature there are more gas particles with higher thermal velocities in the distribution, so there are more high velocity particles moving away from COPS.

For clarification, we consider the case of gas with a relatively low bulk motion v_{z0} of -200 m/s and a relatively high gas temperature of 100 K compared to the gas conditions at the Rosetta distance to the nucleus which is most of the time within 100 km as shown by Tenishev et al. (2008) with the 67P coma model. Figure 3.3 shows the 1-dimension Maxwell-Boltzmann distribution function of the z-component of the velocity as in Equation (3.7) for water. Negative v_z (red shaded) is pointing into COPS. The integral over the red-shaded part of the distribution makes it inside the ram gauge and leads to a bulk speed of around -220 m/s. The gas that COPS measures is systematically overestimated 20 m/s compared to the actual bulk flow in $-z$ direction.

The lower the gas temperatures are and the higher the gas bulk velocities are, the smaller the systematic biases are. Coma gas velocity is usually higher than 200 m/s; COPS is most of the time measuring the gas in 67P's coma at distances < 100 km where gas temperature is typically less than 100 K (cf. Section 1.5.2). Therefore, the overestimation of the gas bulk velocities will be much less than 10%.

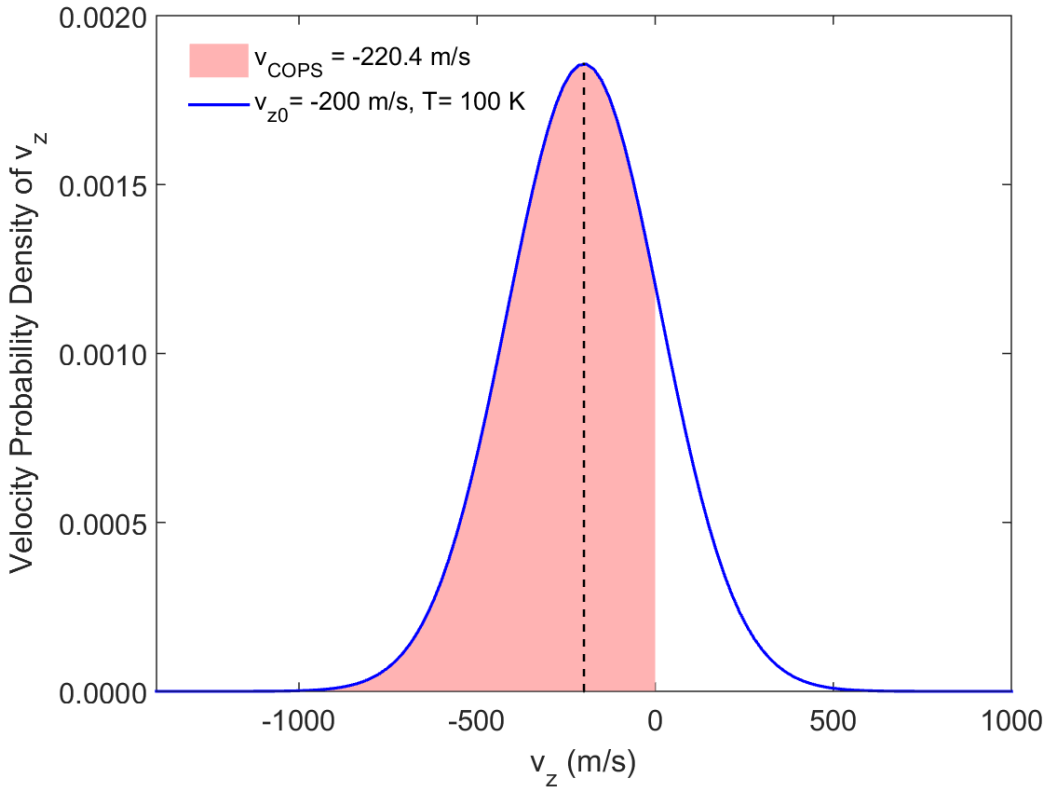

Figure 3.3: 1D Maxwell-Boltzmann velocity distribution (blue curve) with a bulk velocity of v_{z0} = -200 m/s (dashed line) and a temperature of 100 K for water. Gas molecules with negative v_z is pointing into COPS which the integration (red area) gives a velocity around -220 m/s as seen by COPS.

3.4 Main Error Sources of COPS

3.4.1 Systematic Error

Although COPS is capable of measuring neutral gas pressures down to 10^{-11} mbar, the spacecraft itself is outgassing and has a background (Graf et al., 2008) that should be considered as a systematic error during data analysis. As time goes on, quite some dust/gas could have settled or been absorbed on the spacecraft and contributed to its own dust/gas cloud. The spacecraft background could well be changing, especially during attitude changes when previously cold surfaces of the spacecraft come into sunlight and begin to outgas. But the background can only be characterized when the spacecraft is far from the comet. For COPS we use the measured pressure from the beginning of August 2014 before COPS detected the faint cometary atmosphere. For this study the background of the nude gauge is set to $5 \cdot 10^{-11}$ mbar and the one of the ram gauge is set to $1 \cdot 10^{-9}$ mbar.

3.4.2 Statistic Error

Calculating the statistical error of the COPS nude gauge and the ram gauge in the lab measuring stable chamber background pressures gives typically less than 1%.

3.4.3 Offset of Ion-Current

COPS obtains densities/pressures from the ion-current measured by the electrometers with different sensitivities and the corresponding calibration factors (Section 2.1). The ion-currents can be affected by temperature and probably the surrounding plasma. Thus offset measurements of the electrometers for both gauges are measured roughly every 24 hours for automatic correction.

The 24-hour change in the ion-current offsets is not important when the pressure is high, but may lead to obvious differences when the pressure is low as shown in Figure 3.4. In Figure 3.4 the low-ion range (high sensitivity electrometer) is used for the whole time. Offset measurements were performed on 2016 June 17 07:37, June 18 07:48, and June 19 05:54. For the offset measurements on June 17 and June 18 there was an obvious drop and rise at COPS pressure respectively. The error may be reduced when time interpolating the measured offsets if needed.

Furthermore, it is also possible that the ambient plasma have contributed partly to the variation of the offsets. The influence of plasma on COPS measurements is discussed in Section 4.3 and shown in Section 5.7.

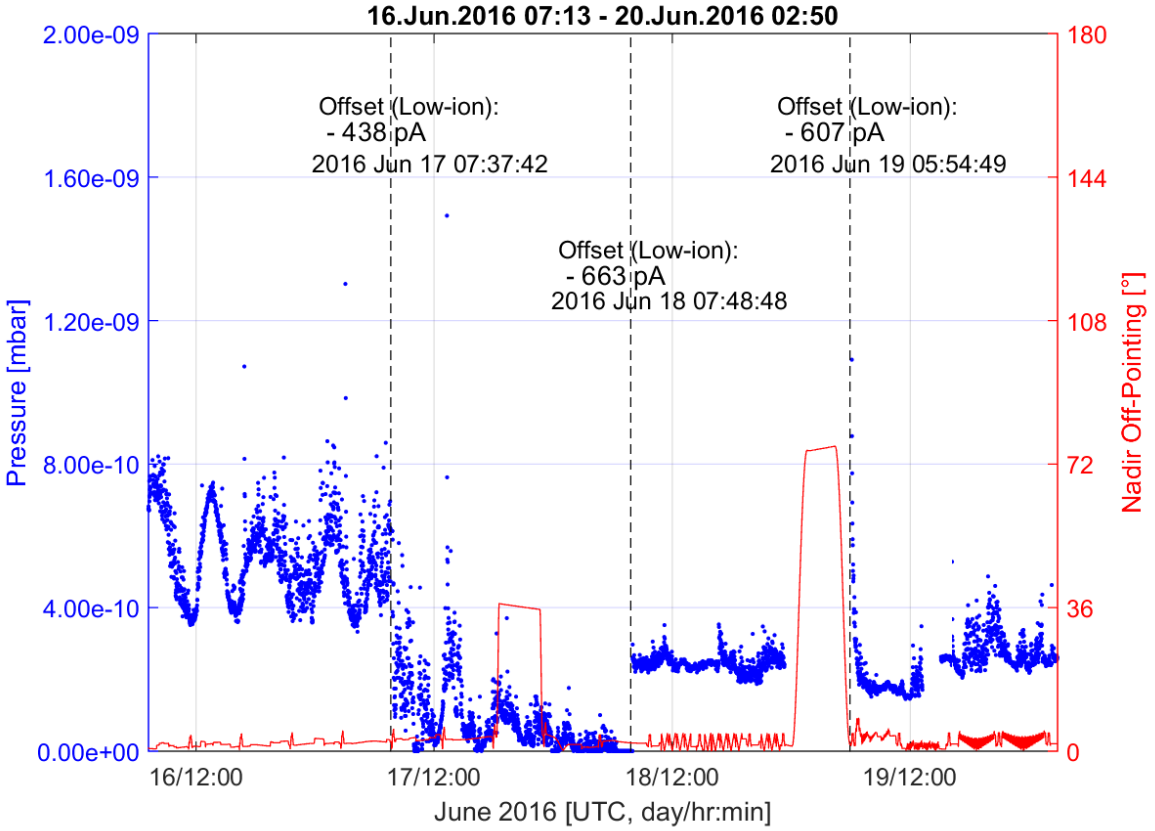
16.Jun.2016 07:13 - 20.Jun.2016 02:50
Offset (Low-ion):
- 438 pA
2016 Jun 17 07:37:42
Offset (Low-ion):
- 607 pA
2016 Jun 19 05:54:49
Offset (Low-ion):
- 663 pA
2016 Jun 18 07:48:48
Pressure [mbar]
2.00e-09
1.60e-09
1.20e-09
8.00e-10
4.00e-10
0.00e+00
Nadir Off-Pointing [°]
180
144
108
72
36
0
16/12:00
17/12:00
18/12:00
19/12:00
June 2016 [UTC, day/hr:min]

Figure 3.4

4. COPS Calibration

4.1 Static Gas Measurements

4.1.1 The CASYMIR Facility

Calibration measurements were performed in the CAlibration SYstem for the Mass spectrometer Instrument ROSINA (CASYMIR) at the Physics Institute of the University of Bern (Westermann et al., 2001). CASYMIR is capable of simulating different neutral gas environments for testing and calibration of space instruments.

The hardware of CASYMIR is composed of two main parts: the vacuum chambers (V0 to V3) with an instrument positioning system and the Gas Mixing Unit (GMU) (Figure 4.1). The chambers can be pumped to ultra-high vacuum pressures ($<10^{-9}$ mbar). Gas mixtures can be provided with the GMU and fed into the chamber by different gas lines controlled by a series of valves and mass flow controllers.

CASYMIR can be operated in two different modes. One is the static mode and the other is the dynamic mode. The static mode is suitable for measuring sensitivity factors for the instruments; the dynamic mode provides neutral gas beams of different velocities simulating the gas flow in the coma.

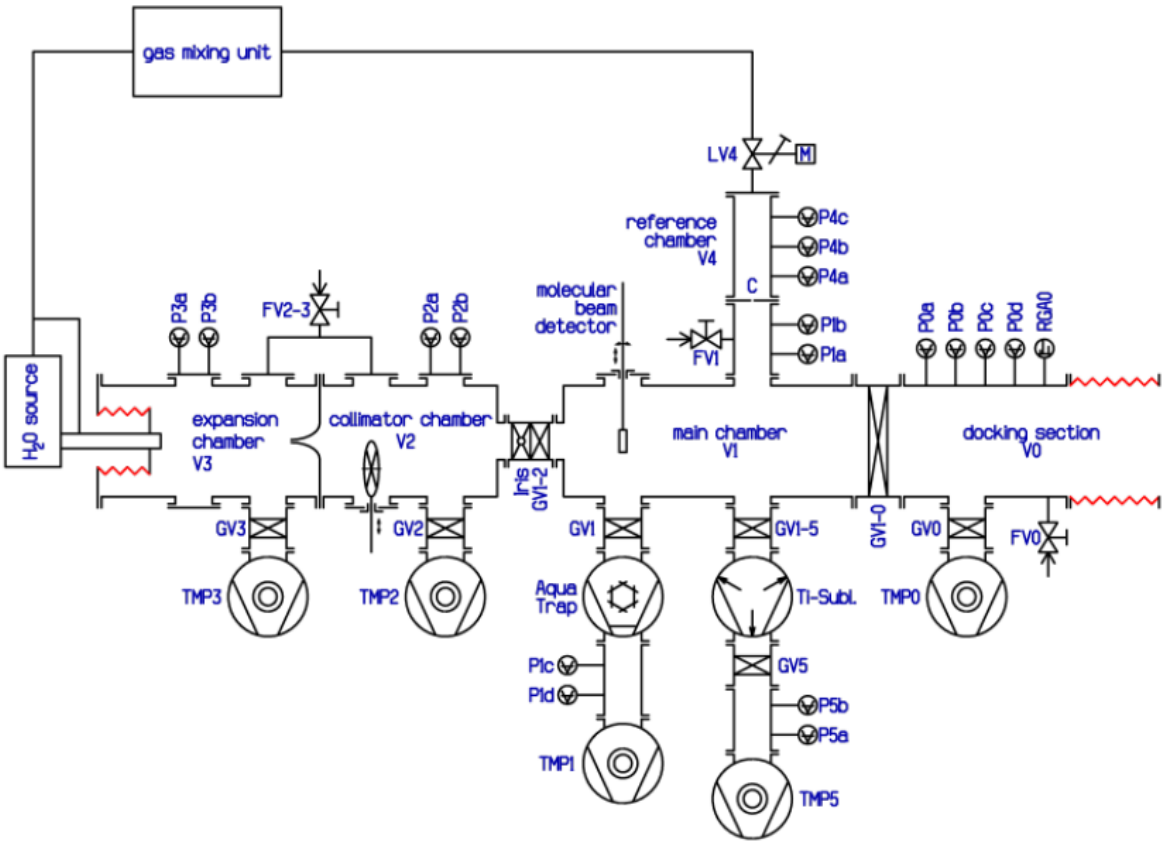

Figure 4.1: Schematic of the CAlibration SYstem for the Mass spectrometer Instrument ROSINA (CASYMIR).

For the static measurements, the gas mixture is introduced into the main chamber (V1) through a thermally regulated leak valve (LV4) which keeps the pressure stable, and is then measured by the instrument attached to the docking section (V0). The leak valve is regulating based on a pressure sensor in the chamber closest to LV4.

For the dynamic measurements the gas mixture is fed through the source on the left side of Figure 4.1 through the nozzle to form a jet into the expansion chamber (V3); when the gas is passing through the collimator chamber (V2) between the expansion chamber (V3) and the main chamber (V1) the size of the gas beam can be adjusted by an iris diaphragm.

Moreover, where the instruments are docked with CASYMIR is also a five degrees positioning system where the instruments are supported and fixed. The positioning system is partly seen in Figure 4.2 below the 6-way cross where COPS is fixed.

Further details on CASYMIR may be found in the thesis and papers of Westermann (2000), Westermann et al. (2001), and Graf et al. (2004).

4.1.2 Sensitivity Measurements

Motivation

The sensitivity of both gauges of COPS was determined during the calibration phase and implemented to the ROSINA-DPU software in order to output the correct density/pressure values. After so many years of operation it is worth verifying if the sensitivity factors evolved over time.

In this section we show some laboratory calibration measurements of the COPS-FS obtained in 2014 using similar methods like Graf et al. (2004) and determine the corresponding sensitivity factors for COPS.

Experiment Setup

The whole COPS instrument as shown in Figure 2.1 does not fit inside the vacuum chamber of CASYMIR. Both gauges were therefore removed from the electronic box and installed into a 6-way cross then connected to the docking section (V0) of CASYMIR as in Figure 4.2.

At the top flange the nude gauge is mounted vertically; at the right flange the ram gauge is mounted horizontally with its aperture pointing to the inflow direction of the gas from CASYMIR on the left side; at the back flange the Granville-Phillips Stabil-Ion pressure gauge (G.P.) monitors the pressure close to COPS; at the front is a transparent glass window.

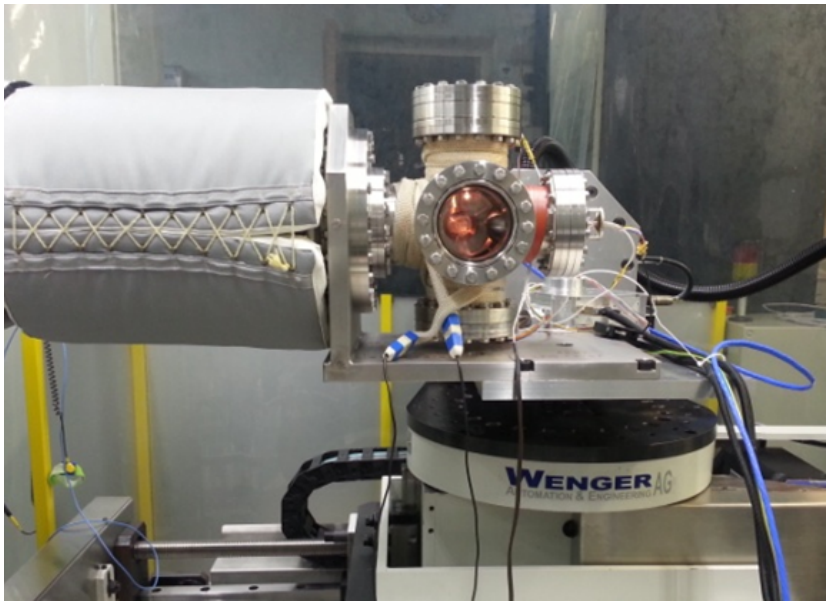

Figure 4.2: COPS mounted on the 6-way cross connected to CASYMIR for static and dynamic calibrations.

Measurement Procedures

The pressure of G.P. and its background, the COPS ion and electron immission currents and the ion current background/offsets are needed to determine the sensitivity factor. To determine the sensitivity factors, the pressure readings of COPS and G.P. are needed, as well as the ion and electron immission currents during operations, along with their backgrounds/offsets. Therefore, during the sensitivity test period at CASYMIR, both gauges of COPS and G.P. were kept running 24-hours, continuously recording data. On one hand, the background pressures and the 24-hour automatic electrometer ion-current offset measurements of each gauge are obtained (see Section 3.4.3). On the other hand, the instruments are kept warm to degass COPS after the switch on. The typical background for measurements is in the range of 10^{-10} mbar. Pressure ranges of $1 \cdot 10^{-9}$ to $5 \cdot 10^{-7}$ mbar are covered during the measurements. The measurement procedure is as described below:

1. COPS is already operating in low emission mode for both gauges.
2. The gas from the GMU is fed through the thermally regulated leak valve into the chamber to be at $1 \cdot 10^{-9}$ mbar according to the G.P.
3. Each gauge is switched through the different ion-ranges. The preferred sequence is high-medium-low because switching ion-ranges from low to high sometimes introduces overshoots in the ion-current that may trigger the self protection of COPS which leads to a switch off. In between each measurement is at least one minute waiting time for verification of stable pressures.
4. Switch the nude gauge to high emission mode and again switch through all three ion-ranges. More information on the ion-ranges are described in Section 2.4.
5. Adjust the inlet gas pressure to the next range and repeat the above procedure. The different pressures are measured from low to high, i.e., $1 \cdot 10^{-9}$, $1 \cdot 10^{-8}$,

$5 \cdot 10^{-8}$, and $5 \cdot 10^{-7}$ mbar to reduce waiting time for the chamber pressure to be pumped down to lower pressures.

The nude gauge was operated with the left filament all the time; at low emission mode it had an immission current of around 15μA and at high emission mode around 100μA. The ram gauge was operated with microtip groups 1, 2, and 3 running together in low emission mode with an immission around 15μA. For the COPS-FS on ground the ram gauge high emission mode was limited to below 30μA instead of 100μA for protection reasons since the microtips are not produced any more.

The gas species Ar, CO_2, N_2, and H_2O were measured. In this study we show the nitrogen measurements as an example since COPS and the G.P. were both calibrated to N_2.

Data Treatment and Results

To convert the COPS detected current signal to pressure, the following relation is used by the DPU:

$$\frac{I_{ion} - I_{off}}{I_{immi}} = P(N_2) \cdot S \tag{4.1}$$

with I_{ion} the ion current measured by the electrometer of either the nude gauge or the ram gauge with the background removed; I_{immi} the electron immission currents detected on the anode grids of both gauges; I_{off} the electrometer offset current measured automatically every 24 hours with the electron emission switched off; $P(N_2)$ the pressure of nitrogen in mbar measured with G.P after background subtraction; S the sensitivity factor in mbar^{-1}.

Each calibration point in Figure 4.3 represents the mean value over 20 single measurements taken within 40 s. The four panels are shown in log scale for better visualization. The top panels show the nude gauge low emission mode measurements with the low ion-range on the left and medium ion-range on the right; the bottom panels show on the left side the nude gauge high emission measurements with low ion-range, and on the right side the ram gauge in low emission with low ion-range. The current term $(I_{ion} - I_{off})/I_{immi}$ in Equation (4.1) is plotted on the y-axis and the pressure term $P(N_2)$ on the x-axis of each panel.

The uncertainty on the pressures measured with G.P. are 6% the higher limit while the variation on COPS current measurements are typically less than 1%. Using the common error propagation approach the error of sensitivity S using Equation (4.1) would be around 6%. Considering that there might be other possible systematic errors a conservative uncertainty of 10% is assumed. The error bars are not plotted since they are too small to be seen. Linear fits for each panel in the form of Equation (4.1) is shown in dashed lines. The fit results of the sensitivity factor (S) and the coefficient of determination (R^2) are listed in Table 4.1.

Table 4.1: Nitrogen calibration of the nude gauge and the ram gauge sensitivity of the COPS-FS. Sensitivity factor S is in mbar^{-1}, R^2 is the coefficient of determination for the linear fits to the data points.

Emission Type	**Ion-Range**	**Sensitivity** S	$\mathbf{R^2}$
	Nude Gauge		
Low, 15 µA	Low	16.7	0.9987
Low, 15 µA	Medium	21.2	0.9999
High, 100 µA	Low	17.8	0.9999
	Ram Gauge		
Low, 15 µA	Low	5.0	0.9990

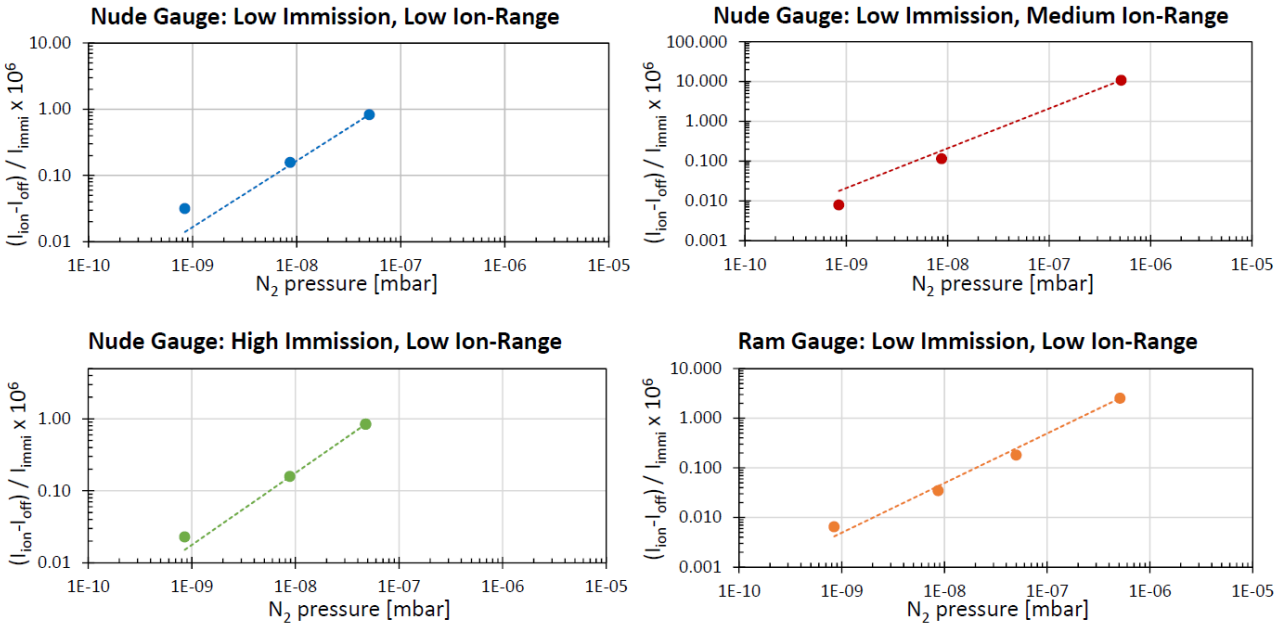

Figure 4.3: Nitrogen calibration of the nude gauge and the ram gauge sensitivity of the COPS-FS.

In the paper of Graf et al. (2004) the sensitivity factors in this paper are derived using argon measurements. To compare these argon sensitivity with the ones in this study we should consider the species correction factor (Section 3.1; Equation (3.1)) of the G.P. pressure measurements using argon but not nitrogen. This can be achieved by multiplying the sensitivity factors in Graf et al. (2004) by the correction factor 0.775 for argon. The Graf et al. (2004) sensitivities for the nude gauge then become 20.09 for low emission mode with low ion range; 18.62 for low emission mode with medium ion range; 21.51 for high emission mode with low ion range. Similarly, the ram gauge the sensitivity factor for low emission mode with low ion range becomes 4.96 and for the high emission mode with low ion range it is 5.08.

It is worth mentioning that in Graf et al. (2004) the listed sensitivities are derived fitting an equation similar to this study but with an offset r added:

$$\frac{I_{ion} - I_{off}}{I_{immi}} = P(Ar) \cdot S + r. \tag{4.2}$$

Graf et al. (2004) showed that using Equation (4.1) like the DPU software does not introduce significant loss of accuracy to the pressure readouts compared to Equation (4.2) and gives similar sensitivity factors. In addition, the nude gauge left filament was used with 100 μA electron emission current for high emission mode, whereas the low emission mode was at 5 and 15 μA; the ram gauge was operated with all eight microtip groups running at 100 μA for high emission mode, and 5 and 15 μA for the low emission mode. The uncertainties of the pressure measurements and sensitivity factors in Graf et al. (2004) were not specifically mentioned. However, since the same instruments as in this study were used (G.P and COPS), a 10% uncertainty is also assumed for comparison of the sensitivity factors.

Comparing Graf et al. (2004) with this work, it shows that the derived sensitivities from both COPS and Graf et al. (2004) have an overlap within the 10% uncertainties of one another. Moreover, as mentioned by Graf et al. (2004) the ram gauge sensitivity is roughly four times lower compared to the nude gauge due to the smaller anode grid.

4.1.3 Species Correction Factor Measurements

Motivation

When measuring either with COPS or G.P., the pressure/density has to be corrected since the ionization efficiency of electrons are different when ionizing different gas species (see Section 3.1). Both COPS and G.P. are calibrated to nitrogen so that when measuring pure N_2 the correction factor is equal to one. COPS space data has to be calibrated using the corresponding correction/scaling factors for each individual gas species as listed in Table 3.1.

The lab experiment was performed in 2016 to verify that COPS has similar correction factors as the G.P. In addition, a gas mixture is measured to acknowledge the theoretical method used for calculating the correction factor for mixed gas (cf. Section 3.1).

Experiment Setup

For the correction factor measurements, COPS was mounted in the 6-way cross similar to Figure 4.2 although not attached to CASYMIR (stand alone). The operation pressure was in the range of 10^{-10} to 10^{-9} mbar. The glass window at the front flange in Figure 4.2 is now replaced by a leak valve such that the gas bottles of different gas species can be connected. The leak valve is thermally regulated by the pressure read outs of G.P. to control the amount of gas inside the 6-way cross. During these correction factor measurements only the nude gauge of the COPS-FS was operated using the default left filament.

Measurement Procedures

COPS was kept running all the time to keep the instrument warm and avoid high pressures due to degassing after a switch on; this also reduced the waiting time for stable chamber pressures. Single gas species He, Ne, N_2, CO, Ar, CO_2, Kr, and Xe,

similar to the ones listed in Table 3.1, are measured except for O_2 and H_2O which are not suitable with this setup. A prepared gas mixture of He, Xe, and Ar of one-third each is also measured. The measurement procedure was as follows:

1. The nude gauge was already operating in high emission mode with low ion-range. Background pressures at COPS and G.P. are both recorded.
2. A selected gas species or mixture was fed into the 6-way cross to a pressure of about $1 \cdot 10^{-8}$ mbar. The pressure was regulated by the G.P pressure reading. Once the pressure was stable the COPS measurements were recorded. The same was done for $5 \cdot 10^{-8}$ and $1 \cdot 10^{-7}$ mbar. The pressures were measured in low to high sequence to reduce the waiting time for pressure to decrease.
3. COPS was set to low emission mode with low ion-range and was let to pump down for around 2 hours to a stable pressure. Measurements for the same pressure ranges as above for the high emission mode is repeated.
4. All gas inlets are closed. COPS set back to high emission mode with low ion range pumping down for next set of measurements with a different gas species.

In addition, it is suggested to start with the light species since in general it is harder to pump the heavy ones.

Data Treatment and Results

Assuming that there is a certain gas pressure P_{real} inside the measurement chamber. And that the gas sensitivity factor for species pressure correction as mentioned in Section 3.1 is β_c for the COPS nude gauge and β_g for G.P., respectively. Then the relation between the real gas pressure, P_{real}, and P_g the pressure measured with G.P. is

$$P_{real} = P_g \cdot \beta_g \tag{4.3}$$

and the relation between the real gas pressure P_{real} and P_c the pressure measured with the COPS nude gauge is

$$P_{real} = P_c \cdot \beta_c \tag{4.4}$$

Since COPS and G.P. are measuring the same amount of gas, Equation (4.3) equals to Equation (4.4). This gives $P_c \cdot \beta_c = P_g \cdot \beta_g$ and thus the correction factor of COPS β_c can be calculated as

$$\beta_c = \frac{P_g}{P_c} \cdot \beta_g \tag{4.5}$$

The relative error of β_c is

$$\left(\frac{\Delta\beta_c}{\beta_c}\right) = \sqrt{\left(\frac{\Delta P_c}{P_c}\right)^2 + \left(\frac{\Delta P_g}{P_g}\right)^2} \tag{4.6}$$

With 6% taken for the term $\Delta P_g/P_g$ since the given error in Granville-Phillips (2007) is 4% to 6%. $\Delta P_c/P_c$ is the COPS pressure with a variation (standard deviation) at stable pressures typically less than 1% gives the total uncertainty on β_c around 6%.

β_g is the correction factor for single species in Table 3.1 given by the Granville-Phillips (2007) user manual. The theoretical correction factor for the gas mixture is derived using Equation (3.4). The results of COPS β_c are shown compared to the G.P. correction factors β_g in Table 4.2 with the difference $|\beta_g - \beta_c| / \beta_g$.

The COPS derived correction factor for nitrogen is the closest to the theoretical one which makes sense since COPS is calibrated to N_2. Surprisingly, the COPS derived correction factor for the gas mixture is also quite close to the theoretically calculated one, which verifies the method used for calculating the correction factor as in Equation (3.4). The larger uncertainties might be due to systematic errors such as the diurnal pressure variations or due to temperature changes in the laboratory. Another possibility is the setup with the pump very close to COPS and G.P. which can affect the gas distribution in the 6-way cross.

Table 4.2: COPS derived species correction factor for densities compared with the G.P. β_g is the correction factor of the G.P. and β_c is the correction factor derived from COPS measurements.

Gas Species		β_g	β_c	Difference [%]
Helium	He	5.56	4.68	15.9
Neon	Ne	3.33	2.72	18.5
Nitrogen	N_2	1.00	1.01	1.2
Oxygen	O_2	$9.90 \cdot 10^{-1}$	not measured	
Carbon monoxide	CO	$9.52 \cdot 10^{-1}$	1.07	11.9
Water	H_2O	$8.93 \cdot 10^{-1}$	not measured	
Argon	Ar	$7.75 \cdot 10^{-1}$	$8.30 \cdot 10^{-1}$	7.1
Carbon dioxide	CO_2	$7.04 \cdot 10^{-1}$	$6.79 \cdot 10^{-1}$	3.6
Krypton	Kr	$5.15 \cdot 10^{-1}$	$5.87 \cdot 10^{-1}$	13.9
Xenon	Xe	$3.48 \cdot 10^{-1}$	$3.96 \cdot 10^{-1}$	13.7
Gas mixture	He, Xe, Ar	$6.91 \cdot 10^{-1}$	$6.66 \cdot 10^{-1}$	3.6

4.2 Dynamic Gas Measurements

4.2.1 Motivation

When the pressure/density is high enough COPS is also capable of deriving the gas velocity in the coma of 67P using both gauges (Section 3.2). Here we show an experiment performed in 2014 comparing the COPS, CASYMIR, and theoretically derived neutral gas beam velocities for different species.

4.2.2 Experiment Setup

The gas velocity measurements are carried out at CASYMIR using the dynamic mode of the system. Shown in Figure 4.4 is the illustration of CASYMIR with a photo of the COPS-FS in the 6-way cross docked to the vacuum chamber similar to the static test in Section 4.1.2. The gas mixing unit provides the selected gas. Molecules and atoms

are injected through a nozzle into the vacuum chamber. The nozzle can be heated to increase the beam's velocity. The gas beam then passes through the chamber where the beam size may be adjusted by an iris diaphragm and is then measured with the both gauges of COPS.

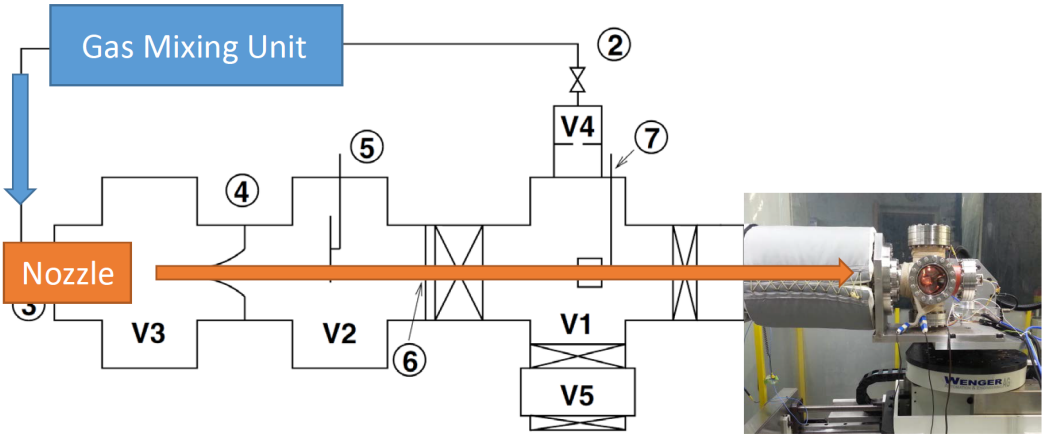

Figure 4.4: Flow diagram showing neutral gas beam measurement at CASYMIR with a photo of the COPS-FS in the 6-way cross docked to the vacuum chamber neutral gas beam. V0 is the bellow chamber, V1 is the main chamber, V2 is the collimator chamber, V3 is the expansion chamber, V4 is the reference chamber, and V5 one of the pumps. The other parts are 1, the gas mixing unit; 2, the leak valve used for static measurements; 3, the nozzle used for the dynamic measurements; 4, the skimmer; 5, the chopper mechanism; 6, the iris diaphragm; 7, the molecular beam analyser; and 8, the docking plate for the instruments. CASYMIR illustration extracted from Westermann et al. (2001)

4.2.3 Measurement Procedures

During the dynamic measurements both gauges of COPS were running in low emission with low ion-range. COPS is always on to stay warm and thermally stable throughout the measurements. Neutral gas beam of the species H_2, He, CH_4, Ar, and Xe are each measured with nozzle temperatures around 40°C, 250°C, and 550°C. Typical pressures in the CASYMIR chamber with a gas beam are in the range of 10^{-9} to 10^{-8} mbar where the background with no beam is 10^{-10} mbar. The measurement procedure follows below:

1. Set the nozzle temperature (40°C, 250°C, or 550°C).
2. A selected gas species is injected through the nozzle creating a gas beam.
3. Set the iris diaphragm (6 in Figure 4.4) opening.
4. A 2D beam scan with the CASYMIR beam detector (7 in Figure 4.4) is performed to make sure the beam is focused and centered at COPS. Otherwise, the nozzle position can be slightly adjusted to center the beam.
5. The chopper wheel (5 in Figure 4.4) is inserted in the beam path to measure the beam velocity with the beam detector. After the beam velocity measurement the chopper wheel and the beam detector is moved out of the beam path.

6. The positioning system is used to shift the 6-way cross horizontally such that the ram gauge scans across the beam; the same is done for the nude gauge by scanning vertically across the beam. By scanning across and outside the beam the background pressures of both gauges can be obtained.

4.2.4 Data Treatment and Results

Theoretical Gas Velocity

Westermann (2000) discussed the free molecular beam expansion from the nozzle. Considering the expanding gas from the nozzle to be ideal and the viscous and heat conduction effects to be neglectable are good approximations for a high-speed flows when the propagation time is short compared to the diffusion time scales. With these approximations the gas is considered to expand isentropically, i.e. reversible and adiabatic. In addition, the collision frequency between the gas molecules inside the heated nozzle are taken as sufficiently high for the gas expansion to be treated as a continuum flow. This yields the terminal bulk velocity u from the First Law of Thermodynamics:

$$u = \sqrt{2\frac{\gamma}{\gamma - 1}\frac{kT_0}{m}} \tag{4.7}$$

where γ is the adiabatic index, k the Boltzmann constant, T_0 the nozzle temperature, and m the mass of the molecules in the flow.

CASYMIR Beam Detection

CASYMIR has a movable detector located at 7 in Figure 4.4 for 2D scans across the neutral gas beam. If the beam is not centered, the nozzle position can be slightly adjusted to move the beam in the appropriate position.

The left panel in Figure 4.5 shows an example of a 2D scan of a centered Ar beam at 550°C nozzle temperature with the intensity. Red color shows the beam and dark blue shows the background outside the beam.

To measure the velocity of the beam with CASYMIR, the chopper wheel (5 in Figure 4.4) is inserted in between the nozzle and the beam detector. The chopper is a disc with two shutter holes in it to pulse the beam. It is operated at fast rotation speeds and the two gas signals are recorded with the molecular beam detector. Then the velocity distribution of the molecular beam is determined by dividing the distance between the shutter wheel and the beam scanner by the time difference between the shutter openings and the beam's arrival time at the scanner.

The right panel in Figure 4.5 shows the detected beam scanner signal (the velocity distribution of the molecular beam) of the beam on the left. On the x-axis is time, y-axis is the intensity. The 930 µs is the time between the chopper trigger and the manually selected peak center that indicates the time of flight between the chopper wheel and the beam detector which are seperated by 0.665 m. Thus the gas beam

velocity in m/s can be derived as

$$v = \frac{0.665}{(t - 0.0002)} \tag{4.8}$$

with t in seconds the time between the peak and trigger as the 930 µs marked in Figure 4.5; the 0.665 in meters is the distance between the chopper wheel and the detector; the 0.0002 in seconds is the correction for a read out time delay for the beam detector pre-amplification gain that was set at 10^{10} during the velocity measurements in this study.

This procedure was repeated for different chopper wheel rotation speeds yielding an error of about 10% relative to Equation (4.7).

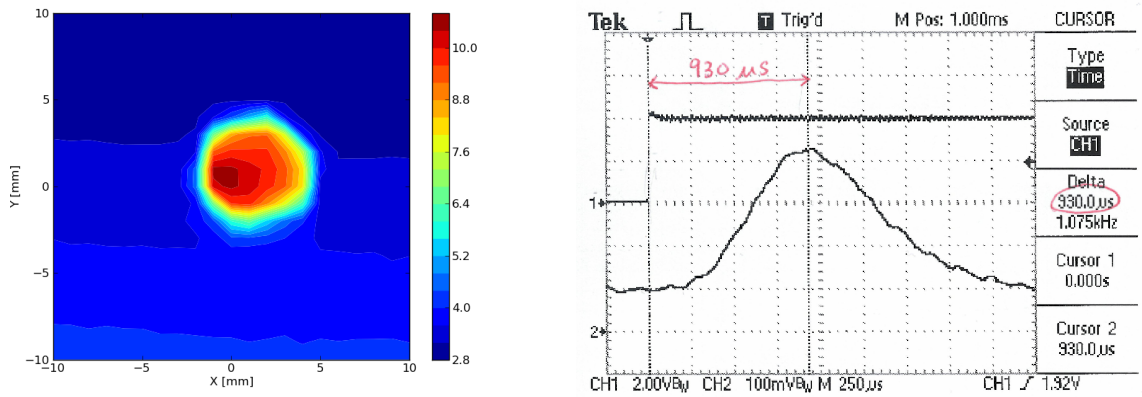

Figure 4.5: 2D scan and detected chopped beam of Ar with a nozzle temperature of 550°C. Left: the 2D beam scan. Right: the beam signal delayed by 930 µs detected with the chopper mechanism operating. The detected velocity was 910 m/s. The chopper wheel rotation speed was 1022 U/min, the Iris opening was 12%.

COPS Beam Scan

To derive the beam velocity with COPS pressure/density measurements COPS is scanned across the beam. The size of the beam is limited so both gauges of COPS can't measure the beam at the same time (explained in the following section). As an alternative, the scan makes it possible that both gauges can measure the same beam and the background. This can be done by operating the positioning system that supports the 6-way cross. For a clearer view, Figure 4.6 shows the configuration of the ram gauge and the nude gauge for measuring the neutral gas beam.

The ram gauge is first positioned at the beam center. Then COPS is shifted so that the ram gauge scans vertically in the z-direction by a 2 mm shift per step. COPS rests at each location taking measurements for at least 1 minute to make sure that the gas inside the ram gauge equilibrium sphere is stabilized. The ram gauge scan gives the beam profile as shown in the left panel of Figure 4.7 for an argon beam with nozzle temperature of 550°C, iris opening 13%, and mass flow of 1.7 sccm. Sccm is the flow measurement term "standard cubic centimeters per minute".

After the ram gauge scan, COPS is then placed so that the nude gauge is in the beam while the ram gauge aperture is outside. Following is a scan by shifting COPS in the horizontal x-direction by 2 mm shift per step similar to the ram gauge scan. An example beam profile of the nude gauge scan is shown in Figure 4.7.

In the beam scan profiles of both gauges, the flat ends - where the pressure is low and stable outside the beam - is taken as background for the measurements. Furthermore, the ratio of the highest densities in both profiles is used to derive the beam velocity using Equation (3.11) from Section 3.2.

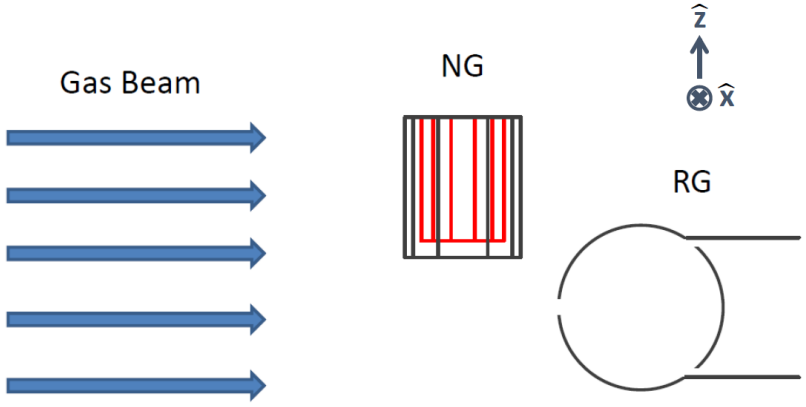

Figure 4.6: Illustration of COPS gauge configuration measuring neutral gas beam in CASYMIR. The ionization zone surrounded by the inner grid of the nude gauge is shown in red, whereas the outer grid is in black.

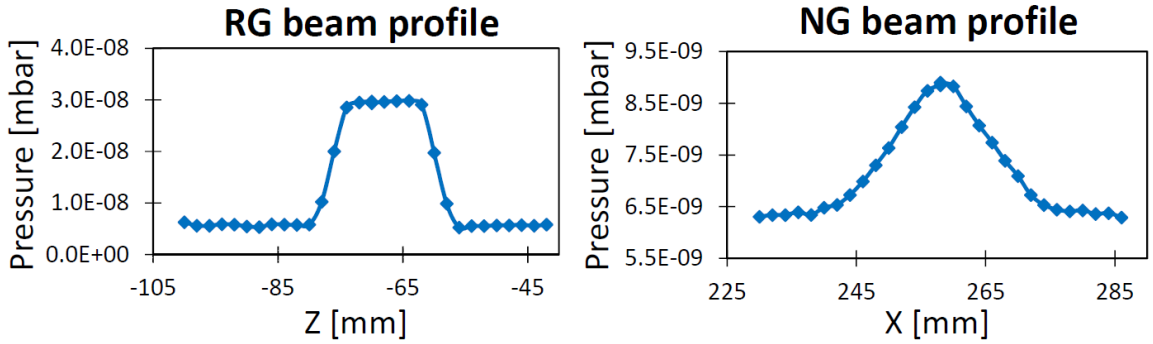

Figure 4.7: Ar gas beam profile as measured by a COPS scan in CASYMIR. The argon beam was generated with nozzle temperature of 550°C, iris opening of 13%, and a mass flow of 1.7 sccm.

Iris Opening Test

The iris diaphragm can be adjusted to control the beam size. Measuring in a size limited chamber, one would prefer that the gas beam is not too wide so that there are less reflections of gas on the chamber walls; measuring with COPS, one would also prefer that the beam size is at least as wide as the nude gauge ionization region illustrated surrounded by the red inner grid in Figure 4.6 for uniform conditions as expected in the coma of the comet.

One way to check how much the iris should be opened is to perform the nude gauge scan in x-direction as discussed in the previous section for different iris openings. The other way is to observe the relation between the iris opening and the corresponding COPS derived velocities.

Figure 4.8 shows the COPS derived gas velocity on the y-axis and the iris opening on the x-axis for argon and helium at 550°C nozzle temperature. Helium measurements (blue empty and filled diamonds) are done for two different mass flows which show similar trends. This confirms that the velocity measurements are more or less independent of the mass flow. Argon measurements are shown in green triangles. The theoretical velocities for both gases at 550°C are shown with dashed lines.

The results show that iris openings around 12% to 17% fit best to the theoretical values. An iris opening of 13% is used in this study.

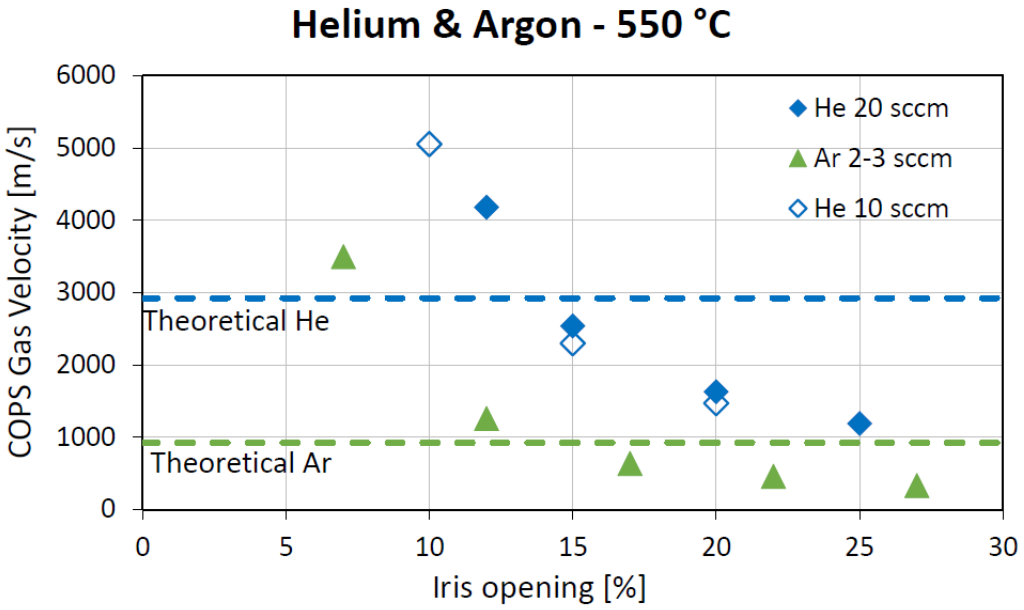

Figure 4.8: Iris diaphragm opening test results with He and Ar at 550 °C.

Combined Gas Velocity Results

In Figure 4.9 the theoretical velocities of H_2, He, CH_4, Ar, and Xe at different temperatures are plotted in colored curves. The gas beam velocity measurements with the chopper mechanism and beam detection system of CASYMIR are shown by the squares. The corresponding COPS gas velocity measurements are shown in filled circles.

The uncertainty of the chopper wheel based velocity is around 10%. Considering the variations (standard deviation) of the nude and ram gauge measurements at a stable pressure which are both below 1% (both set to 1% in the analysis), and the sensor temperature of the ram gauge which is even smaller compared to the pressures, the COPS derived gas beam velocity yields an error of 2%; the actual error may be larger due to other systematic uncertainties; here taking the 2% error, COPS gas velocity error bars are left out in Figure 4.9 since they will be too small to be well visualized.

The measurements for 250°C nozzle temperature were performed first in the sequence of He, CH_4, Ar, H_2, and Xe on five separate days. Then the measurements for 40°C and 550 °C nozzle temperature were done in the order of H_2, He, CH_4, Ar, and Xe; the 40°C and 550°C measurements for one species were executed within one single day. It can be seen that the velocities in squares (chopper mechanism) for 40°C and 550°C tend to be slower than the circles (COPS), whereas for the 250°C velocities it is not. Somehow there is a systematic bias on the measurements for 40°C and 550°C done on the same day compared to the 250°C ones performed alone on a separate day.

In Figure 4.9 most of the COPS and chopper wheel based velocities are close to the theoretical curve. Few measurements with high nozzle temperature (550°C) tend to be slower, i.e. H_2 and CH_4. For H_2 the time interval t in Equation (4.8) is small because of its light weight and high velocity at high temperature, thus manually selecting the peak center of the chopped beam signal (Figure 4.5 right panel) might give a larger error. Furthermore, COPS and chopper velocities for Xe are all higher than the theoretical values.

It is worth mentioning that COPS measures the bulk velocity, whereas with the chopper mechanism, the manually selected peak position in the chopped beam signal (right panel in Figure 4.5) gives the most probable velocity of the Maxwell-Boltzmann distribution, but not necessarily the bulk velocity if the shape of the distribution is not symmetric. This is also a possible element contributing to cause the discrepancy within the data.

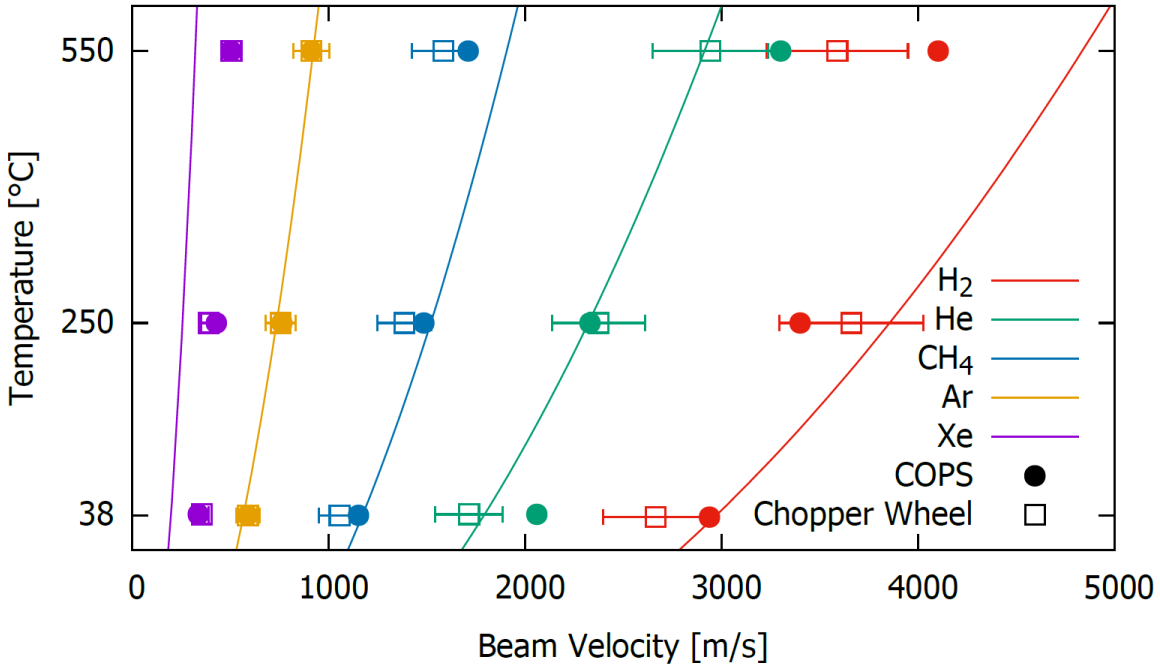

Figure 4.9: COPS dynamic gas velocity measurements in CASYMIR. The uncertainty of the chopper wheel based velocity is around 10%; the statistical uncertainty of COPS derived velocity is small so is not shown in this plot.

4.3 Measurements in a Plasma Environment

4.3.1 Motivation

COPS is designed to measure neutral gas but at times enhanced noise is observed in the measured COPS neutral gas density. Interestingly, this is correlated with plasma signals measured by the RPC instrument package on Rosetta (Section 5.7); COPS-FM in flight had observed obvious ion-current offset variations (Section 3.4.3) which is most probably also a plasma effect. Therefore, an extra set of calibration measurements were carried out with COPS-FS exposed to varying plasma conditions to investigate the instrument response.

4.3.2 Experiment Facility and Setup

The plasma test took place at ONERA (the acronym of "The French Aerospace Lab" in French) in Toulouse in 2015. The COPS nude gauge and its electronic box, the DPU, the ROSINA EGSE computer system (Electronic Ground Support Equipment), and other hardware components were shipped in protected boxes to Toulouse for a one week test.

The chamber that was used for the plasma test is JONAS (Ionospheric Ambience Simulator for the Study of Spacecraft/Plasmas Interactions). COPS was sharing the chamber with the Radio and Plasma Wave Instrument (RPWI) which is in development for the JUpiter ICy moons Explorer (JUICE) mission. A photo of the ONERA/JONAS facility is shown in Figure 4.10.

Figure 4.10: Photograph of the ONERA/JONAS facility used for the COPS plasma test. From Inguimbert and Murat (2015).

To test RPWI, twelve Langmuir probes with different materials were mounted on a carousel and placed in the chamber to test their characteristics when impacted by plasma. RPWI doesn't induce additional plasma or neutrals that affect the chamber environment. COPS and RPWI were measuring inside JONAS simultaneously. Figure 4.11 shows the setup inside the chamber. The COPS nude gauge was fixed on a flange that was mounted on a plate at the lower left. The electronic box was also placed in the chamber covered with kapton such that the electronics are not affected by plasma. The electrical feedthrough close to COPS was used.

The chamber volume is around 10 m^3. During the tests argon is used to create plasma with densities typically in the range of 10^4 to 10^6 cm^{-3} depending on the locations inside the chamber and the settings of the source. The argon beam ions had energies around 20 eV (velocity around 10 km/s) with thermalized cold ions assumed having a temperature of 300 K similar to the gas. The best match found by RPWI is 90% of beam ions and 10% of thermalized ions in the chamber. The chamber neutral pressure was in the order of 10^{-7} to 10^{-6} mbar.

An additional set of four grid plates was built and installed around the original grids of the nude gauge as shown in Figure 4.12. The grid plates opposite to one another are considered a pair. One pair has a fine mesh size compared to the nude gauge outer grid; the other pair has a course mesh size comparable to the nude gauge outer grid. Voltages may be applied to the four grids individually. They will act as a filter/shield to the charged particles when needed. During the test a kapton foil is added on the top of the set of additional grids and kapton tape is placed on the gap between the additonal grids to provide insulation from plasma (Figure 4.12).

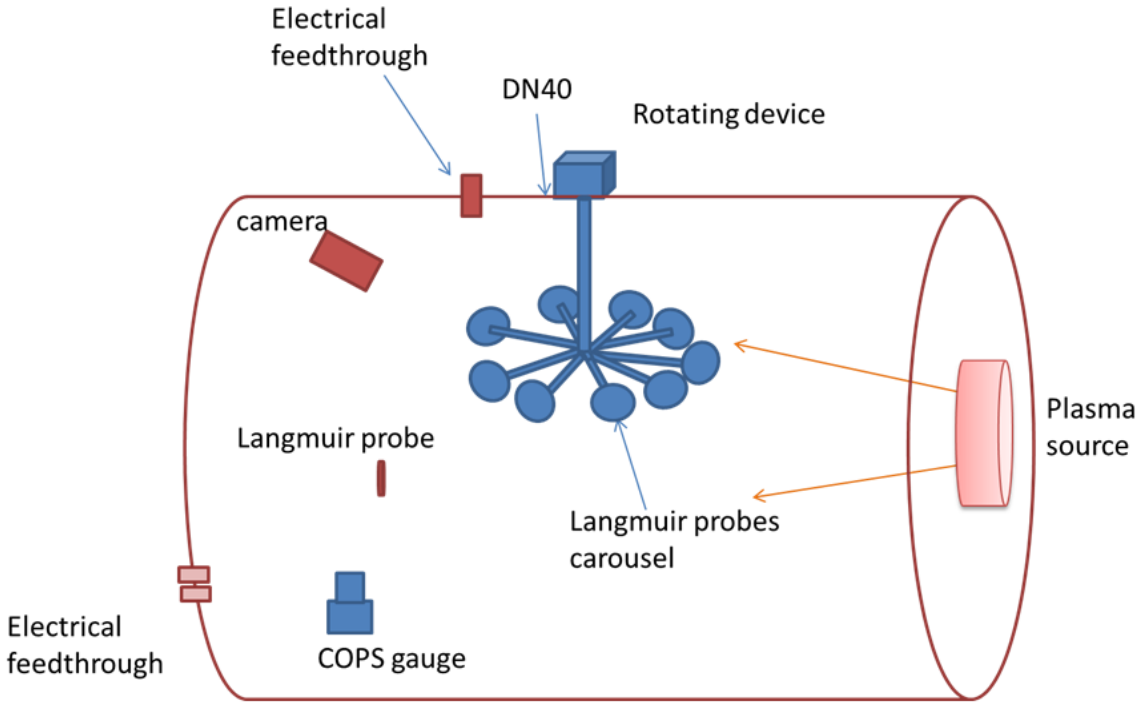

Figure 4.11: Illustration of the plasma test setup inside ONERA/JONAS chamber. From Inguimbert and Murat (2015).

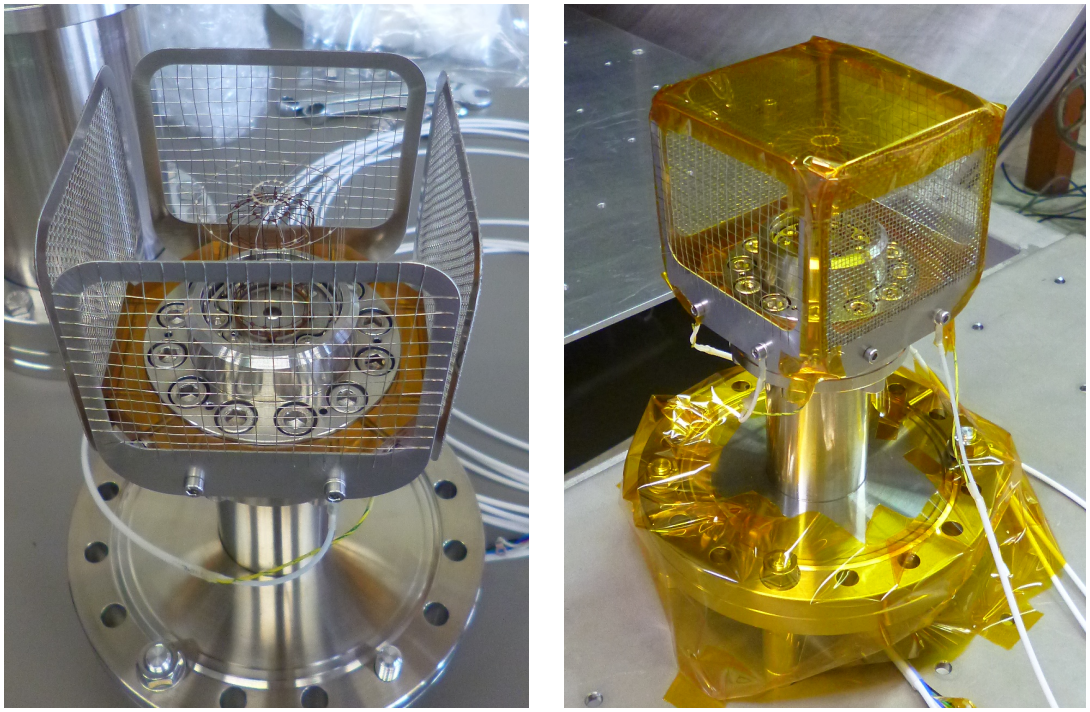

Figure 4.12: Left: COPS nude gauge with the additional grids mounted for the plasma test. Right: Kapton foil and tape added to the setup to insulate plasma.

4.3.3 Test 1 - with and without plasma

Measurement Procedures

A test was performed to check whether COPS pressure/density measurements are different when operating in an environment with only neutral particles and when in an environment with both neutrals and plasma. The following steps were executed:

1. COPS is switched on in the chamber with the plasma source off in a measurement mode so that only neutrals are measured.
2. The chamber pressure might be high when switching on the plasma source thus COPS is switched off for safety.
3. The argon plasma source is switched on and regulated.
4. COPS is again switched to a measurement mode while neutrals and plasma are both present in the chamber.

Data and Results

The two plots in Figure 4.13 have the same time scale on the x-axis and pressure scale on the y-axis. The time interval is always 10 min. On both plots no extra voltages were applied to the additional grids. On the left side are measurements with only neutrals and on the right are measurements with argon plasma. The neutral gas density inside JONAS chamber was stable during the measurements either with or without plasma.

However, it can be seen that COPS pressure measurements with plasma (right panel) is much more noisy than without plasma. A possibility is that the additional plasma might have contributed to COPS signal.

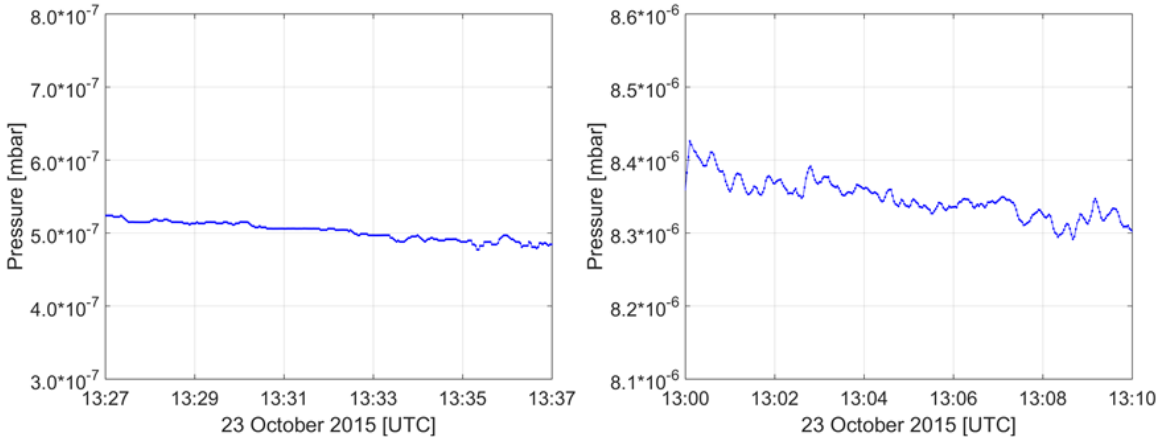

Figure 4.13: COPS nude gauge measurements with (right) and without (left) plasma. Both plots are plotted for 10 min on the x-axis and same pressure scale on the y-axis.

Having a closer look, we checked COPS pressure together with other electronic parameters for the case when plasma was present. Shown in Figure 4.14 the left plot is pressure relative to the immission current. The immission current is flat and does not go together with the pressure since the immission current is regulated to a set value, in this case to ≈ 15 µA, in a fixed emission mode. The only electronic parameter found to follow the trend of the pressure is the ion current shown on the right side. It makes sense since COPS pressure is derived by the DPU using the ratio of ion current to immission current Equation (4.1).

This suggests that plasma indeed has an extra influence on the ion current of COPS resulting in noisy pressure measurements. In the next test we try to figure out how and why COPS is affected.

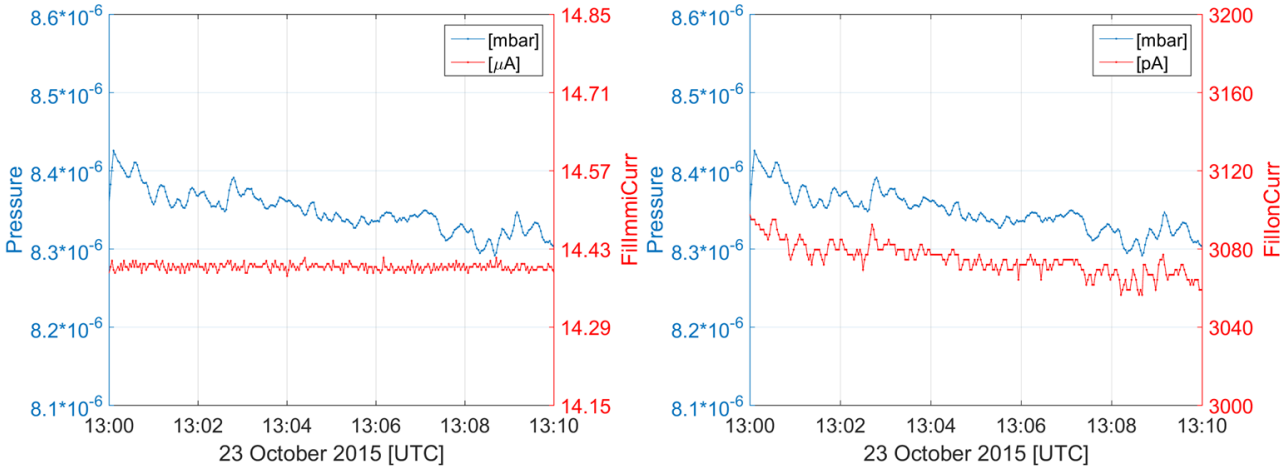

Figure 4.14: Nude gauge pressure compared with immission current and ion-current in plasma environment.

4.3.4 Test 2 - different voltages applied to the additional grids

Measurement Procedures

The current applied on the filament (i.e. the filament current) to emit electrons is regulated on the immission current (i.e. the current of the filament emitted electrons detected on the nude gauge inner/anode grid) to be stable around 15μA. Usually in a neutral gas only environment, the immission current at the start of a mode is zero since there is no filament current applied and thus no electrons emitted from the filament; then the regulation will start vary the filament current until a stable immission around 15μA is reached.

It was observed that in this plasma environment, the nude gauge wasn't able to be set to operation in low emission mode. The cause was that with this setup, at the start of a mode the immission current is already at close to 20 μA without any filament current applied, i.e. no electron emission at all from the filament. So the regulation was confused by the "fake" immission current and couldn't set the nude gauge to operate. By applying -10 to -50 volts to all four of the additional grids helped to reduce the initial fake immission current and the nude gauge was then successfully set to operation as usual.

The purpose of this test was to observe how applying different voltages to the additional grids added around the nude gauge influence the COPS measurements in a plasma environment. The measurement procedure is as below:

1. Set all four additional grids to -50 V.
2. Switch COPS to operation in a low emission mode.
3. Decrease the voltage settings of the additional grids step by step slowly from -50 V to -210 V.
4. Additional grid voltages are set back to -50 V.
5. Increase of the voltages of the additional grids step by step slowly from -50 V to +1 V.
6. Voltage on the additional grids set to -30 V.

Data and Results

There was no obvious change in COPS behavior during the decrease of the grid voltages. Surprisingly, the filament current was observed to drop dramatically when the additional grid voltages are set to more positive values indicating that external electrons provided a significant contribution to the measured immission current.

A zoom on when the additional grid voltages were increased is shown in Figure 4.15. The x-axis shows the time, and on the y-axis the four panels from top to bottom show pressure, ion-current, filament current, and immission current, respectively. The red vertical lines indicate the time when a voltage change is applied to the additional grids. The applied voltages are marked with red numbers above each red line.

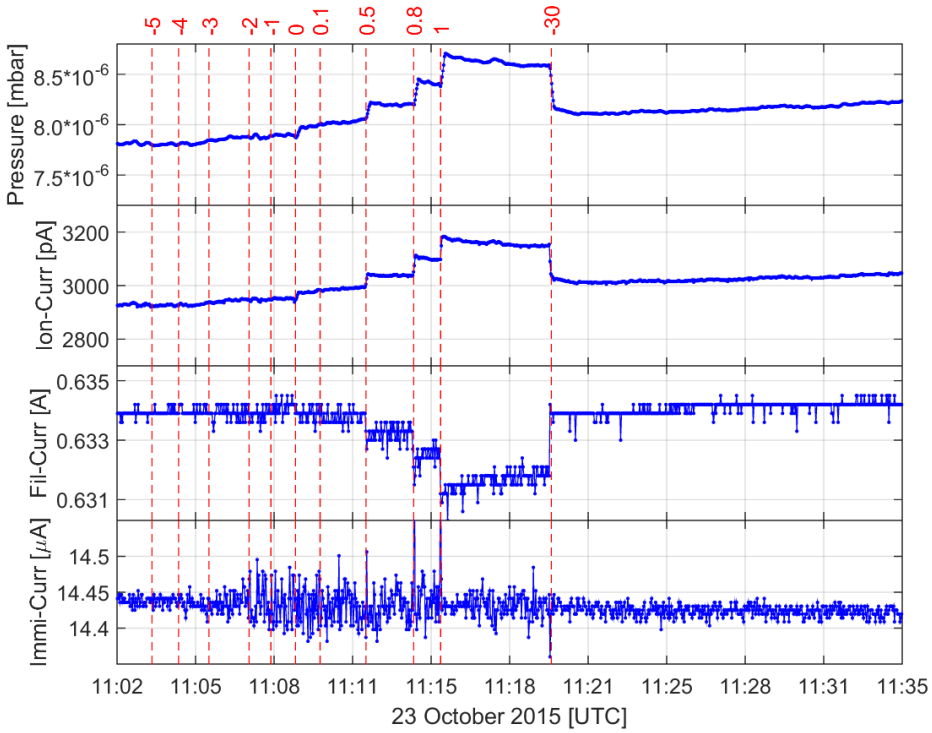

Figure 4.15: COPS nude gauge data while adjusting the additional grid voltages in plasma environment.

It can be seen that when the applied voltages are > 0 V, there is a change in all parameters except the immission current. In this case more external electrons are attracted and reach the anode grid of the nude gauge contributing additionally to the original immission-current. Then the regulation determines that the immission is too high and reduces the filament current (3^{rd} panel in Figure 4.15) to regulate back to $\approx$ 15 µA immission current (4^{th} panel). The external electrons therefore contributed to the ionization of the neutrals, and this results in a higher ion-current (2^{nd} panel), thus a higher density/pressure (1^{st} panel).

5. COPS Observations at Comet 67P

In this Chapter the used COPS density data was calibrated for the spacecraft background and the different gas species as mentioned in Section 3.1 except for Section 5.1 and 5.6 where raw data was used. Data at times when spacecraft events (during or/and after maneuvers and wheel off-loadings) might affect the densities are removed when required for the studies.

5.1 A Multipurpose Instrument

Besides the coma neutral gas density COPS also measures gas released in thruster firings during wheel off-loadings, slews of the spacecraft, and cometary dust impacting the instrument/spacecraft. In the following some examples are shown with non-calibrated raw density data measured with the nude gauge.

In Figure 5.1 in addition to the regular coma density pattern there are some sharp large peaks due to thruster firings during the time periods shaded in blue. These blue shaded maintenance slots are the spacecraft wheel off-loading periods defined by the ESA spacecraft operation team. Normally the actual wheel off-loadings are much shorter than the allocated time periods.

Since the wheel off-loadings affect the density measurements of COPS, quite often data during the defined wheel off-loading periods are ignored. There are also orbital

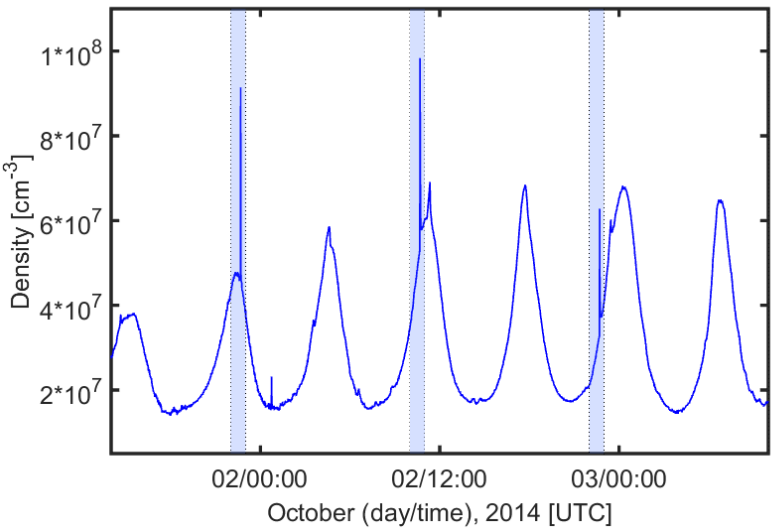

Figure 5.1: COPS density measurements affected by spacecraft wheel off-loading process. The blue shaded periods are the official wheel off-loading periods where a sharp peak may be seen in the COPS measured neutral density above the regular coma smooth periodical pattern.

correction maneuvers which increase the density even more. COPS is usually switched off during the defined maneuver periods. When COPS is switched on again there is often a large density peak due to degassing of the contamination that settled on the cold instrument during maneuvers. It takes some time to degas, hence data within approximately 60 min after maneuver periods are to be removed if required.

Surprisingly, although not designed to detect grains, COPS appears to be able to sense grain signals as well. Figure 5.2 shows two different days in February 2015 where grain signals are either present or not. In the lower panel the coma density is smooth with regular variation patterns, whereas the upper panel shows that besides the usual coma density pattern there is additionally a large amount of small spiky signals.

We suggest that this is caused by grains heating up near or at COPS and the volatile part of the grain is released and contributes to the observed density. Grains with only a small volatile content are expected to create smaller dust signals, thus are harder to be seen if the cometary gas density is relatively high, and vice versa.

COPS density measurements are also affected by attitude changes of Rosetta. Figure 5.3 shows an example obtained in February 2015 with the changes in COPS measured densities corresponding to the changes in off-nadir pointing of the spacecraft.

These are slews back and forth past the nadir direction, thus every second peak in the off-nadir angle corresponds to a more or less same attitude again; therefore, every second peak in the off-nadir pointing corresponds to a peak in the density. The increase in density signal might be the sublimation of ice/dust which settled down and froze on the cold parts of the spacecraft.

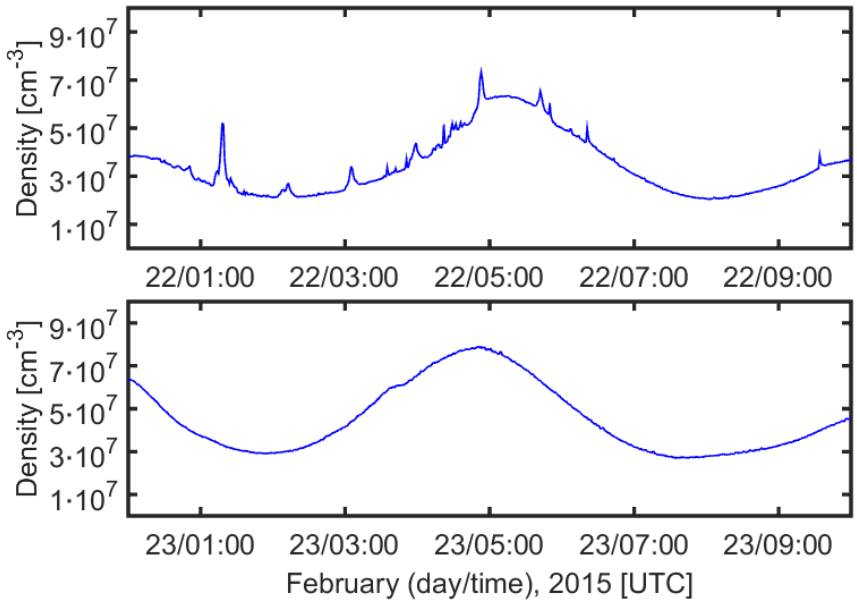

Figure 5.2: COPS coma density measurements with and without dust signal. Lower panel shows the regular smooth neutral gas density pattern of the coma. Upper panel shows the spiky dust signals in addition to the usual coma density pattern.

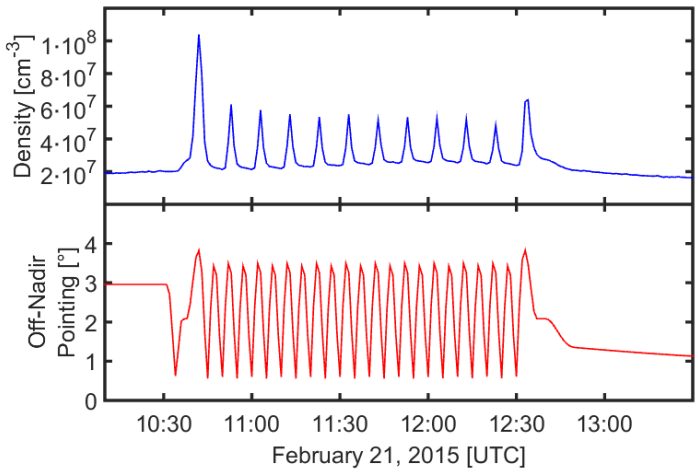

Figure 5.3: COPS neutral density measurements affected by spacecraft attitude when changing the off-nadir pointing. Every second peak in the nadir off-pointing angle (red) corresponds to a peak in density (blue).

5.2 Diurnal and Seasonal Variation

At the beginning of August 2014 when Rosetta came to as close as 100 km to the comet ROSINA started to see strong density variations in the coma correlated to the rotation of the nucleus of 67P. COPS neutral density observations show not only diurnal variations, but also seasonal variations. Diurnal variations refer to change of sub-spacecraft longitude of the coordinate frame attached to the nucleus, whereas seasonal variations refer to change in sub-spacecraft latitude. Table 5.1 shows the list of dates of the seasonal change on 67P during the mission. Here Figure 5.4 and Figure 5.5 demonstrate the seasonal variation and the diurnal variation of the comet with COPS absolute density after spaccraft background subtraction and correction for composition-dependent sensitivities as derived from DFMS (cf. Section 3.1).

Figure 5.4 shows neutral number density and the corresponding sub-spacecraft longitude and latitude for several days in September 2014 when the sub-solar point is on the northern hemisphere of 67P. During this time the northern/summer hemisphere of 67P is more active than the southern/winter hemisphere. The diurnal variation due to the comet's rotation period of 12.4 hour at that time is also illustrated in the figure by the sub-spacecraft longitude. In contrast, Figure 5.5 shows the same parameters but for several days from mid December 2015 to mid January 2016 when the sub-solar point is on the southern hemisphere. The northern hemisphere is in fall/winter and the southern is rather spring/summer just opposite to the situation in Figure 5.4.

Table 5.1: Dates of seasonal change at 67P

Date	**Seasonal parameters**
2015 May 5	Equinox (Southern hemisphere spring)
2015 September 4	Southern hemisphere summer solstice
2016 Mar 21	Equinox (Southern hemisphere autumn)

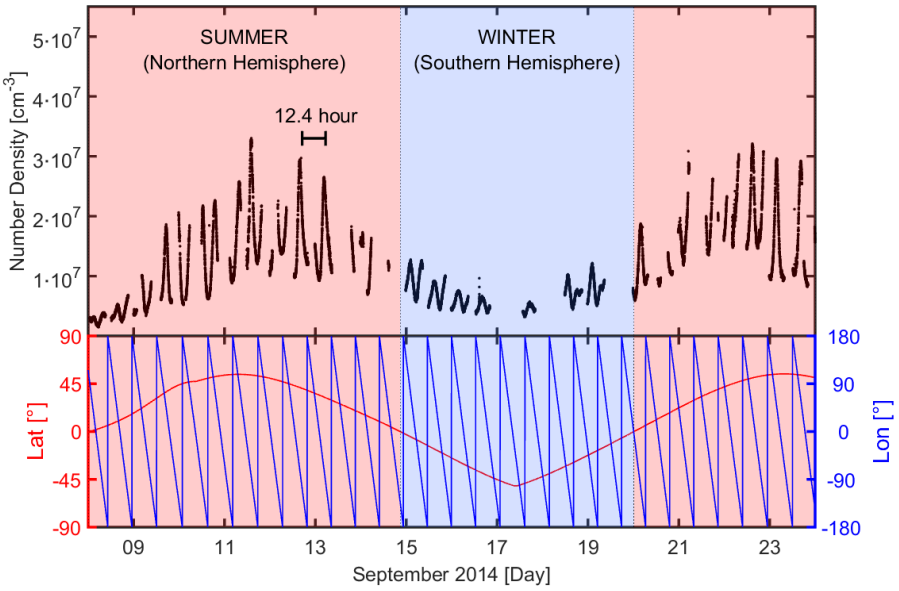

Figure 5.4: Seasonal and diurnal variation of the coma during summer on the northern hemisphere in September 2014. The 12.4 hour diurnal variation is also shown. The upper panel shows calibrated neutral density measurements from COPS with composition-dependent corrections based on DFMS data. Lower panel shows the corresponding latitude (red) and longitude (blue). Where the latitude is positive the neutral density is higher, and vice versa. The first half of the data was measured when the phase angle was around 60° to 120°, and the second half of the data was measured during near terminator orbits.

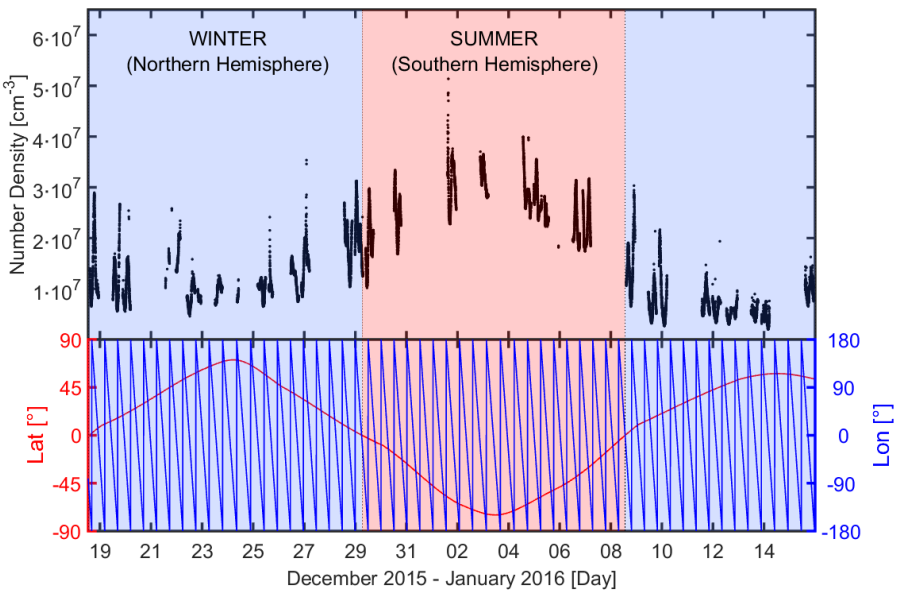

Figure 5.5: Similar to Figure 5.4, but shows the seasonal variation of the coma during summer on the southern hemisphere in December 2015 to January 2016. The neutral density is higher where the latitude is more negative, and vice versa. These data were measured when the spacecraft orbits were near terminator.

5.3 Density Evolution

Throughout more than 2 years of comet escort and extended mission at 67P COPS has been running continuously except during orbital correction maneuvers when the densities might have been high enough to damage the instrument, during times when the densities are below the detection limit, or during some ROSINA software updates.

Dates of the scientific phases during the mission are listed in Table 5.2 and Figure 5.6 shows the neutral density evolution measured in situ by COPS with the corresponding distance between the spacecraft and the comet. It shows that the measured density is anti-correlated to the distance of the spacecraft to the comet.

Table 5.2: List of main scientific phases of Rosetta.

Time	Phase	Distance [km]
2014 Oct 15 - 28	Close bound terminator orbits	around 10
2015 Feb 14	Close flyby	as close as 8
2015 Mar 28	Close flyby	as close as 15
2015 Sep 23 - Oct 17	Bow shock excursion	up to 1500
2016 Mar 23 - Apr 9	Tail excursion	up to 1000

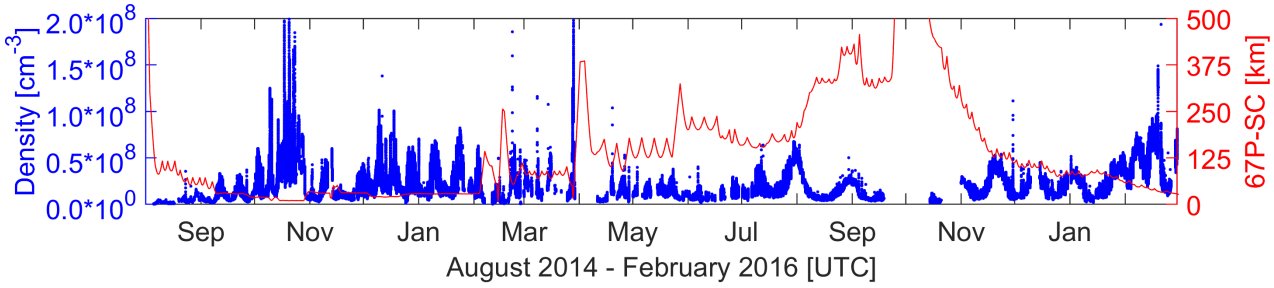

Figure 5.6: The calibrated coma total neutral gas density evolution of 67P from August 2014 to February 2016 shown with the distance of Rosetta to the comet.

5.4 Total Production Rate

In the coma of 67P the local total neutral gas density was measured in situ by ROSINA-COPS. Bieler et al. (2015b) estimated with 3D coma models the total production rate of 67P between August and November 2014 to be about $1 \cdot 10^{26}$ molecules/s. The study shows that illumination driven models were able to reproduce the overall features of the local neutral number densities measured by COPS.

With the neutral number density measurements from COPS one can estimate the total production rate using the simple Haser model as in Equation (1.3). The total production rate calculated with an assumption of 700 m/s for gas velocity gives a peak of approximately $4 \cdot 10^{28}$ molecules/s around 18 days after perihelion. The peak is also due to the orbits of Rosetta, i.e. the variation in the sub-spacecraft positive/negative latitudes.

In the study of Hansen et al. (2016) the water production evolution of 67P during the mission is examined based on Rosetta in situ and remote sensing measurements, ground-based observations. An empirical method is developed using Direct Simulation Monte Carlo (DSMC) modelled (Fougere et al., 2016a) density outputs constrained by ROSINA data. The developed empirical model is then also applied to detrending spacecraft position effects from ROSINA data. Though using a different method, the peak water production rate was also found by Hansen et al. (2016) to occur 18-22 days after perihelion similar to our study using the simple Haser model.

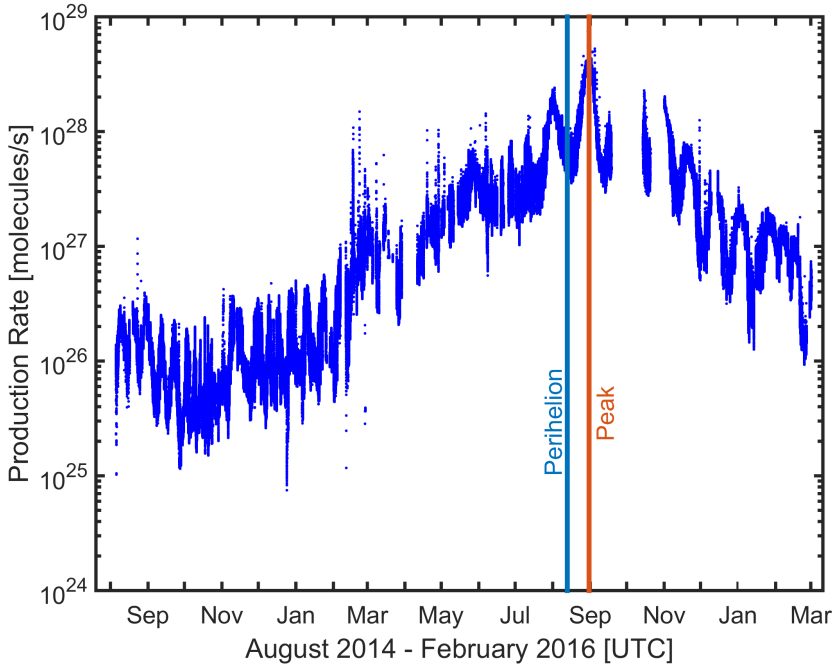

Figure 5.7: Production rate of the total neutral gas molecules derived using the simple Haser model as in Equation (1.3) with an assumption of gas expansion velocity of 700 m/s. The peak production rate is around 18 days after perihelion similar to the peak H_2O production in Hansen et al. (2016).

5.5 Gas Bulk Velocity

The expansion velocity of the neutral gas in the coma of 67P was derived with 3D coma models in the study of Bieler et al. (2015b) giving estimated values around 400 - 800 km/s. The velocities were obtained from a DSMC model using surface boundary temperatures defined by the model of Davidsson et al. (2007). The velocities were roughly in agreement with the measured water expansion velocity of 680 m/s reported by Gulkis et al. (2015).

The gas velocity of the neutral gas coming from the comet can be calculated with COPS neutral gas observations when the calibrated neutral densities are higher than the background of both nude and ram gauge. The procedure of how the gas velocity is calculated is as follows:

1. Calibrate nude gauge and ram gauge densities for the background and gas species using DFMS relative abundances for the main gas species using the method mentioned in Section 3.1:

(a) Background subtraction: nude gauge $1.2 \cdot 10^6\,\mathrm{cm}^{-3}$, ram gauge $2.5 \cdot 10^7\,\mathrm{cm}^{-3}$.

(b) Species correction for main gas species: H_2O, CO_2, CO, O_2.

(c) DFMS measures one integer mass line after the other, so the time-resolution is much lower than COPS. For instance, in th nominal high-resolution mode a DFMS mass scan from 13 Da to 100 Da lasts approximately 45 minutes. Thus COPS data can only be calibrated when there are DFMS measured relative abundances available within a short time period of the COPS individual measurements. For this work here we require DFMS measurements of the major species within 1 hour of the corresponding COPS measurement and perform a linear interpolation in time between the individual DFMS measurements.

2. Ram gauge is pointing in the +z direction of Rosetta spacecraft frame and measures the gas flux coming in the spacecraft -z direction from the comet. So only COPS data obtained while the off-nadir pointing (θ_n) is smaller than $10\,^\circ$ are used for the velocity analysis. The ram gauge density is then multiplied by $1/cos(\theta_n)$ to estimate the actual projected cross section of the nude gauge entry exposed to the incoming gas flux (cf. Figure 3.1).

3. The gas velocity is then calculated using Equation (3.11) in Section 3.2. The mean gas mass is calculated using the relative abundances of the main species measured by DFMS.

5.5.1 Longitude-Latitude Map

In Equation (3.11) used to calculate the velocity the parameters are: the mean gas mass (which is in the square root), the other is the density ratio of ram gauge to nude gauge. Both are shown in Figure 5.8 for October 2014. The left panel shows the sub-spacecraft point longitude-latitude map of the mean gas mass considering the four main gas species with the color scale showing the mass in atomic mass units; The right panel shows the longitude-latitude map of the ram gauge to nude gauge density ratio. It is important to note that the longitude-latitude map mentioned here does not show the gas velocity on the nucleus, but the velocity of the gas derived from COPS in situ above the corresponding sub-spacecraft longitude and latitude.

Looking at Figure 5.8 the mean gas mass in the square root can vary maximum up to a factor of ≈ 2.4 due to the range of molar mass of the major species (from 18 amu for H_2O to 44 amu for CO_2), whereas the density ratio of ram gauge to nude gauge can go up to a factor of 7. Hence, the calculated velocity will be affected more by the density ratio than the mean gas mass.

The calculated COPS gas velocity is shown in the longitude-latitude map in Figure 5.9 with the main parts of 67P marked in black and white text. It can be seen that the pattern in the COPS derived gas velocity map is more similar to the density ratio of ram gauge to nude gauge in the right panel of Figure 5.8 than to the one of mean gas mass to the left. This is as expected as the relative variation in the density/pressure ratio is much bigger than the variation in average mass. Also, as discussed above the average mass goes in only with the square root.

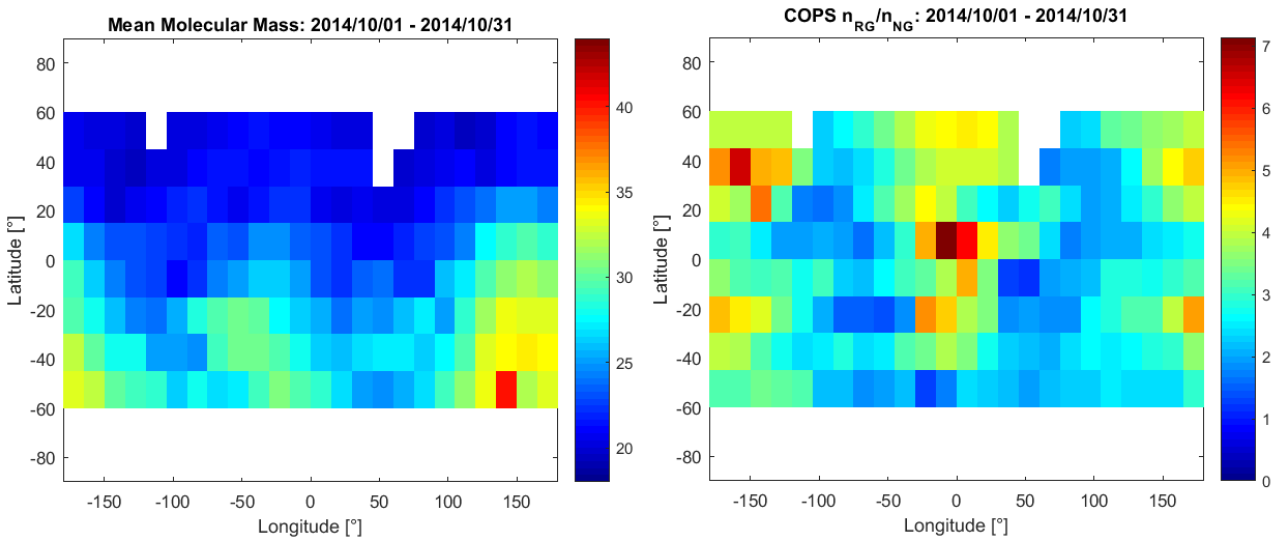

Figure 5.8: Left: sub-spacecraft longitude-latitude map of the mean gas mass for October 2014. Right: sub-spacecraft point longitude-latitude map of the ram gauge to nude gauge density ratio for October 2014.

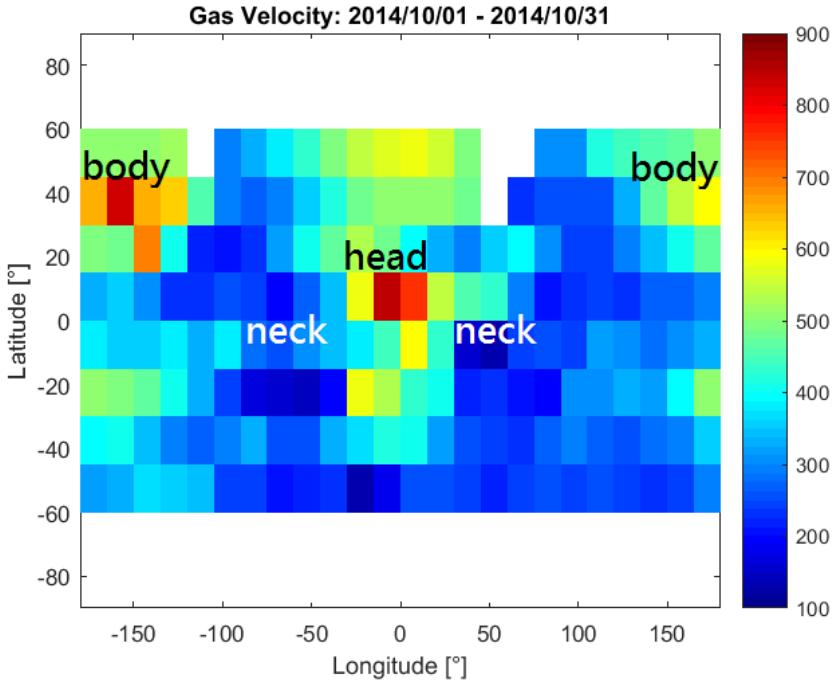

Figure 5.9: Sub-spacecraft longitude-latitude map of the calculated coma gas velocity in October 2014 in m/s. The approximate locations of the main parts of 67P is marked in black and white text.

Mentioning velocities of gas in the coma, one would think it might be linked to the activity on the surface of the nucleus through the temperature/illumination. Since the cometary ices require certain temperatures to be sublimated, it is very likely that the gas velocity is somehow linked to the temperature below the surface of the nucleus.

The Microwave Instrument for the Rosetta Orbiter (MIRO) offers a view below the

surface of 67P. Figure 5.10 is a temperature map at a depth of approximately 2 cm below the surface of 67P of the diurnal maximum temperature predicted by a thermal model based on Rosetta MIRO observations (Schloerb et al., 2015) for September 2014. The body longitudes and latitudes are similar to the sub-spacecraft ones in Figure 5.9 except that the longitude range of 180° to 360° in this plot corresponds to -180° to 0° in Figure 5.9. The main parts of the comet are also denoted on this temperature plot. Schloerb et al. (2015) pointed out that in this plot the temperatures in the high latitude regions are probably over-estimated.

In Figure 5.9 when the sub-spacecraft location is on the head and body regions of 67P, the measured neutral gas seems to have higher velocities than when pointing to the neck. Comparing the COPS gas velocity map with the MIRO temperature map (Figure 5.10) it makes sense that the gas velocity is higher in locations where the temperatures are higher; at the neck region it is also quite warm, but the velocity is rather low. Note that the temperature map shows the diurnal maximum of the whole month; also the September 2014 temperature map corresponds to a period when the phase angle (the spacecraft-comet-Sun angle) varies from around 40° to 120° whereas for the October 2014 gas velocity map the phase angle was always around 90° (terminator orbits).

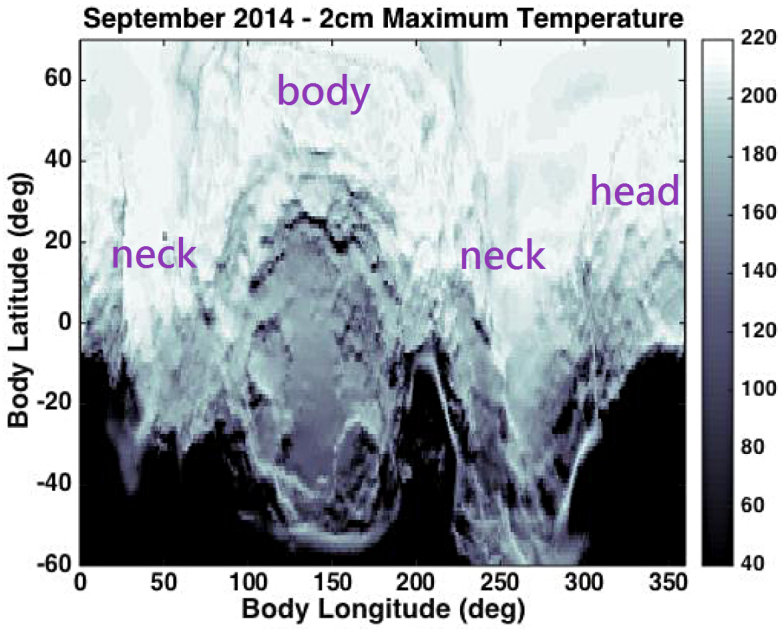

Figure 5.10: Thermal model map of the expected diurnal maximum temperature at a depth of 2 cm below surface of 67P for September 2014 based on Rosetta MIRO observations. The thermal model does not include effects of water ice sublimation and probably over estimates the temperatures in high latitude regions. The longitudes and latitudes are similar to Figure 5.9 except that the longitude of 180° to 360° in this plot corresponds to -180° to 0° in Figure 5.9. The rough locations of the main parts of 67P are added to the original plot in purple text. Modified from Schloerb et al. (2015).

Shape models of the nucleus of 67P are derived from the images taken with the OSIRIS (Optical, Spectroscopic, and Infrared Remote Imaging System) camera on Rosetta. Then the energy input on the nucleus can be obtained from the shape models. Theo-

retically the more energy input the nucleus has, the higher the nucleus temperature is; the higher the nucleus temperature is, the higher gas activity it can have.

Figure 5.11 shows on the left a total energy input map of 67P per comet rotation on 6 August 2014 viewing from the north pole; the total energy includes the energy received from the Sun and self heating (especially at the neck) from the thermal illumination by the comet's own surface. In contrast, the right figure shows the total energy received over an entire orbital period (around 12 days) where the neck gains less energy input on average.

Thus the energy input averaged over a longer period might explain partly the lower gas velocity obtained with COPS when the neck region is facing the spacecraft. Considering also that when gas leaves the nucleus the velocity is in general perpendicular to the surface, it is not surprising that the COPS derived gas velocity is low when the sub-spacecraft point is viewing the neck; after all, when the COPS ram gauge is facing the neck quite a large portion of the nucleus surface is not perpendicular to the nadir direction, so the gas flow that comes into the ram gauge is less.

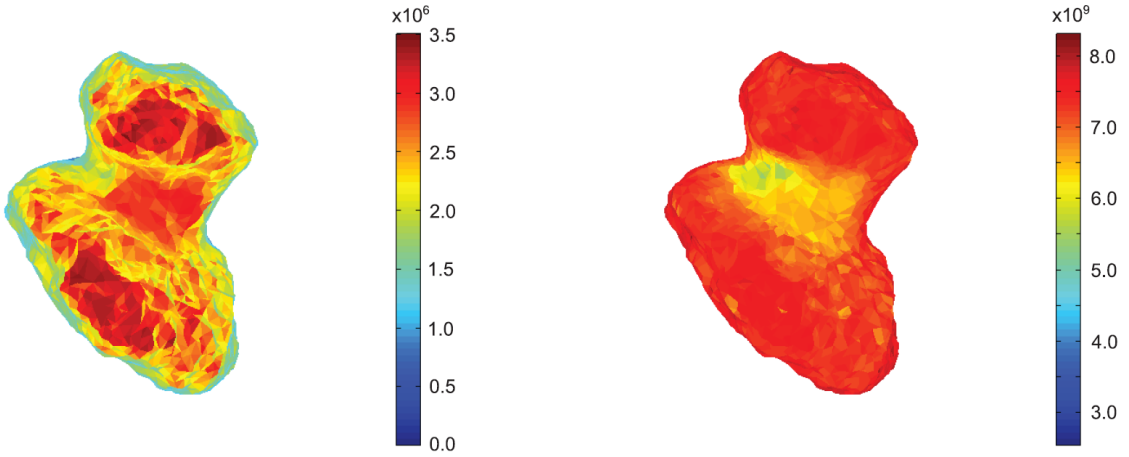

Figure 5.11: Energy input map of 67P derived from OSIRIS shape model. Left figure shows a map of the total energy in Jm^{-2} received from the Sun and self heating from the thermal illumination by 67P's own surface per rotation on 6 August 2014 from the north pole. Right figure is similar to the left one showing total energy received over an entire orbital period. Extracted from Sierks et al. (2015).

5.5.2 Time Evolution

In Figure 5.12 and Figure 5.13 the COPS nude and ram gauge densities, the density ratio ram/nude, the mean gas mass from DFMS, and the COPS derived gas velocity (red) together with the same parameters extracted from the DSMC model (blue) like the one in Bieler et al. (2015b) for October 2014 and 1 to 5 October 2014, respectively, are shown.

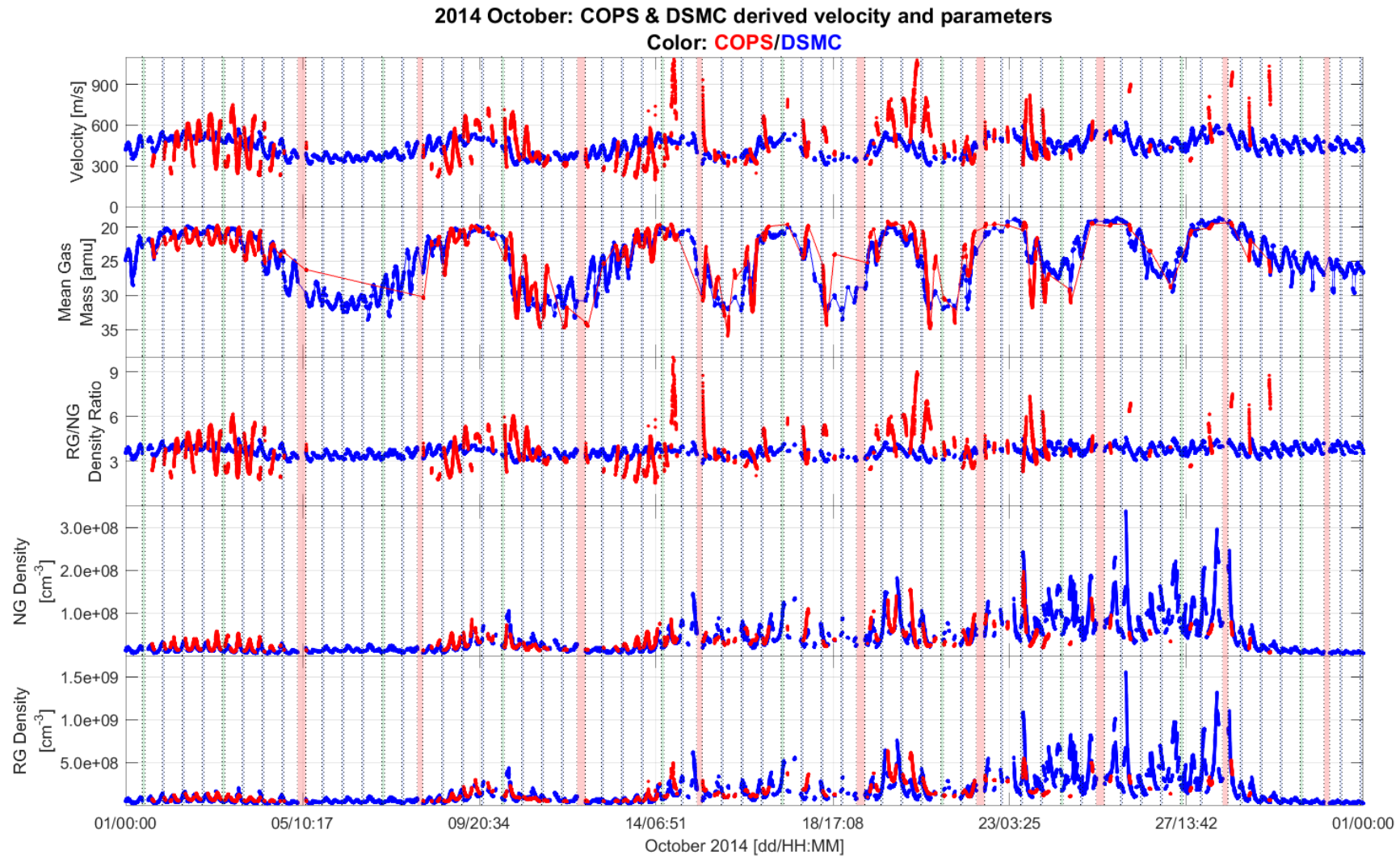

Figure 5.12: Time evolution of coma gas velocity derived from COPS observations in October 2014 (red) and DSMC modeling (blue; Bieler et al. (2015b)). Uppermost panel: COPS derived velocity in m/s. Second panel: mean gas mass in atomic mass units. Third panel: COPS density ratio of ram gauge to nude gauge. Fourth panel: nude gauge density in cm^{-3}. Bottom panel: ram gauge density in cm^{-3}.

The DSMC model is described in detail by Fougere et al. (2016a). The most important aspects are described as follows: the relative response of the nucleus surface to solar illumination was represented by an activity map of the surface; the activity map was then used as input for the DSMC model; for a set of heliocentric distances, 12 simulations were ran, spaced one hour apart, that together model a single rotation of 67P.

In this study, the real spacecraft trajectory for October 2014 is used, and the physical parameters in Figure 5.12 and Figure 5.13 are extracted from the simulation closest in time out of the 12 individual runs. Therefore, when the trajectory crosses from one rotation state to the next, there might be some discontinuity in the physical properties. The extracted model data were displayed without any smoothing, hence the discontinuities are clearly seen.

It can be seen in Figure 5.12 that in this one-month time scale the overall features are similar for both COPS and DSMC. It seems that on the long time scale when the neutral density (activity) is higher, corresponding to the H_2O dominated northern/summer hemisphere in this case, the expansion gas velocity is higher as well.

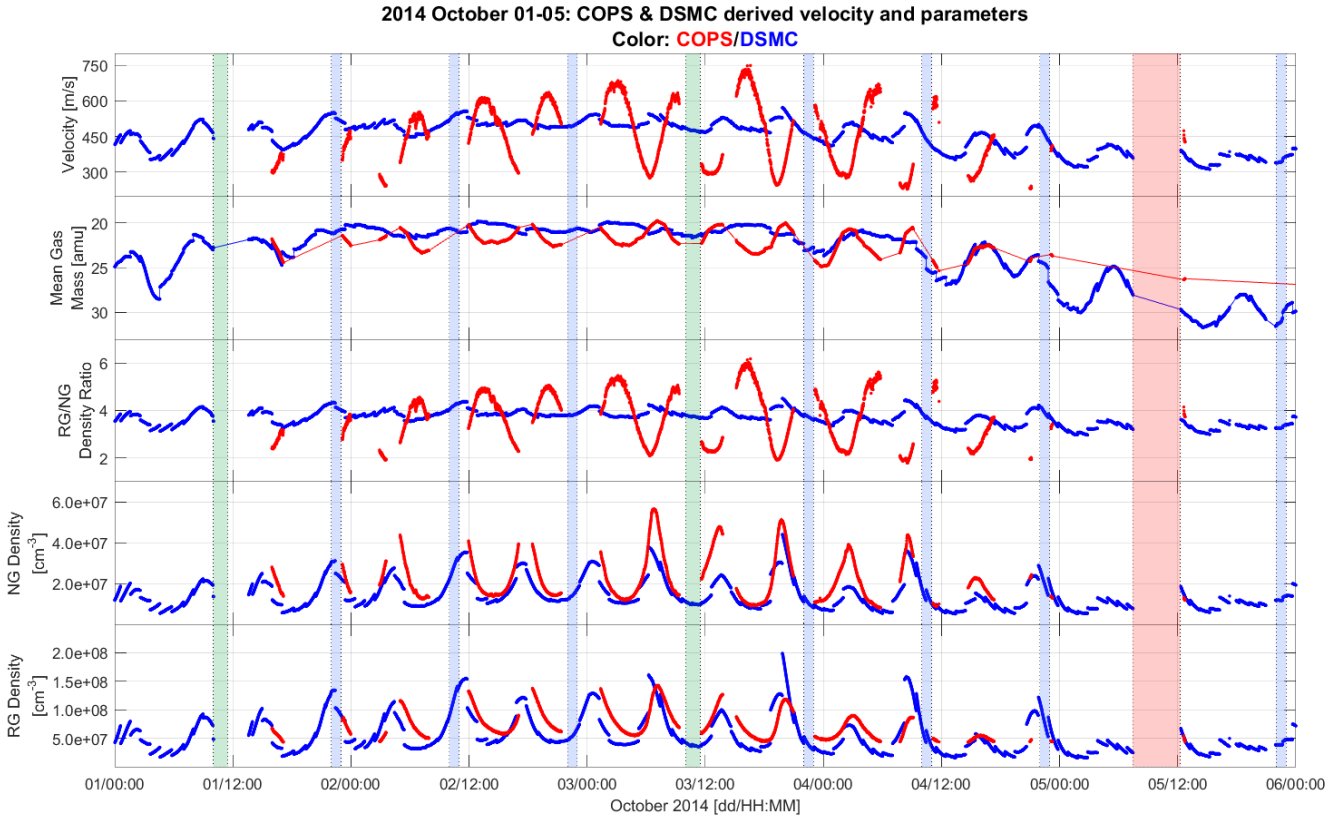

Figure 5.13: Time evolution of coma gas velocity derived from COPS observations (red) and DSMC modeling (blue; Bieler et al. (2015b)) for 1 to 5 October 2014. Top panel: COPS derived velocity in m/s. Second panel: mean gas mass in atomic mass unit. Third panel: COPS density ratio of ram gauge to nude gauge. Fourth panel: nude gauge density in cm^{-3}. Bottom panel: ram gauge density in cm^{-3}.

However, when zoomed to a shorter five-day time scale as in Figure 5.13 for 1 to 5 October 2014 the highest neutral densities (fourth panel from top) do not correspond to high gas velocities (first panel from top) any more, but to low gas velocities.

As previously mentioned, the role of the mean gas mass in the velocity calculation is not as critical as the density ratio of the two gauges. Taking a closer look at the curve of the density ratio (third panel from top) of the ram gauge to the nude gauge it is expected that the velocity curve follows the same variation.

Yet instrument-wise, the ram pressure measured by the ram gauge should be high when the total pressure measured by the nude gauge is high, and vice versa. But we find that the peaks in the nude gauge (fourth panel from top) and ram gauge (bottommost panel) are not always aligned in time. The ram gauge density peaks roughly 14 min later compared to the nude gauge; the density troughs of both gauges have even a larger shift; this means that even if the nude and ram gauge density peaks would be at the same time the troughs wouldn't.

Gas entering the ram gauge sphere should reach equilibrium within not more than 200 ms seconds and the time resolution is ≈ 10 s (Balsiger et al., 2007). This kind of long delay/shift was not noticed during the dynamic measurements of neutral gas beams with the COPS flight spare instrument in the laboratory (Section 4.2). Coincidentally, MIRO observations for water shows that the highest velocities do not correspond to times when the column densities or the continuum temperatures (which is linked to the surface and subsurface temperatures of the nucleus) are highest, but are also shifted from one another in time.

Figure 5.14 (Gulkis et al., 2015) shows the water column density and expansion velocity measured by MIRO from 7 to 9 August 2014 by using nadir $H_2^{18}O$ spectra. The upper panel shows the column density of water in blue, and the nucleus submillimeter continuum temperatures in red; large drops in the continuum temperature are observed when the MIRO line of sight crosses the limb of 67P; the peaks labelled with blue-boxed 1,3, and 5 are when MIRO beam is positioned on the neck region of the comet, where 2, 4, and 6 are rather on the body.

To the surprise of Gulkis et al. (2015), the highest water column densities are often observed above shadowed neck regions (blue-boxed 1,3, and 5) where the nucleus thermal continuum temperature (consequently the surface and subsurface temperatures) is low. They also suggest that observed gases are originating from nearby insolated regions. The lower panel shows the mean water expansion velocity. It is similar for the water velocity that the pattern is also shifted compared to either the water column density or the nucleus surface temperature.

So far we cannot fully interpret what happened while COPS was measuring the coma of 67P during flight. It is probably a combined effect of the instruments/spacecraft while hovering in the coma around the complicate-shaped 67P.

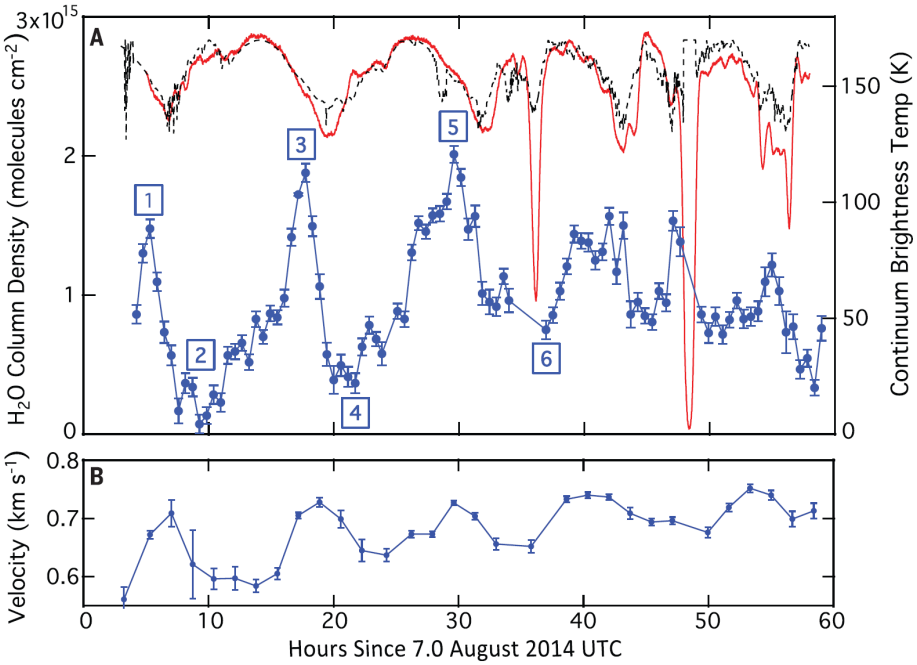

Figure 5.14: Water column density and expansion velocity measured by MIRO from 7 to 9 August 2014 UTC by using nadir H_2O spectra. Upper panel shows water column density (blue), nucleus submillimeter continuum temperatures (red); large drops in the continuum temperature are observed when the MIRO line of sight crosses the limb; the peaks labelled with 1,3, and 5 are when MIRO beam is positioned on the neck region of 67P, where 2, 4, and 6 are rather on the body. The lower panel shows mean water expansion velocities given by the spectra. Details are described in the paper of Gulkis et al. (2015).

5.5.3 Error Estimation - Density and Velocity

Calibrated Neutral Gas Density

Previously in Section 3.1 the calibration for the COPS nude gauge and ram gauge densities is described. As detected by DFMS in the coma of 67P the major neutral gas species are H_2O, CO_2, CO, and O_2. So the formula for COPS neutral gas density correction for either the nude gauge or the ram gauge is as follows:

$$\begin{aligned} n_{corr} &= (n_{raw} - n_{bg}) \cdot \beta_{C,total} \\ &= (n_{raw} - n_{bg}) \cdot \frac{1}{\frac{R_{H_2O}}{\beta_{H_2O}} + \frac{R_{CO_2}}{\beta_{CO_2}} + \frac{R_{CO}}{\beta_{CO}} + \frac{R_{O_2}}{\beta_{O_2}}} \end{aligned} \tag{5.1}$$

with $\beta_{C,total}$ the combined correction factor for the total density, n_{corr} the calibrated (background removed and gas species corrected) density, n_{raw} the uncorrected raw density measured by COPS, n_{bg} the spacecraft background density which is roughly $1.2 \cdot 10^6\,\mathrm{cm}^{-3}$ for nude gauge and $2.5 \cdot 10^7\,\mathrm{cm}^{-3}$ for ram gauge, R_i the ratio of the

main species' densities n_i, to the total density n_{total}, obtained with DFMS, and β_i the correction factor of each individual species as in Table 3.1.

The calculated error propagation assuming independent variables for Equation (5.1) using the common error propagation approach will then give the relative error of the species corrected density:

$$\frac{\Delta n_{corr}}{n_{corr}} = \sqrt{\frac{{\Delta n_{raw}}^2 + {\Delta n_{bg}}^2}{(n_{raw} - n_{bg})^2} + \frac{\left(\frac{\Delta R_{H_2O}}{\beta_{H_2O}}\right)^2 + \left(\frac{\Delta R_{CO_2}}{\beta_{CO_2}}\right)^2 + \left(\frac{\Delta R_{CO}}{\beta_{CO}}\right)^2 + \left(\frac{\Delta R_{O_2}}{\beta_{O_2}}\right)^2}{\left(\frac{R_{H_2O}}{\beta_{H_2O}} + \frac{R_{CO_2}}{\beta_{CO_2}} + \frac{R_{CO}}{\beta_{CO}} + \frac{R_{O_2}}{\beta_{O_2}}\right)^2}} \tag{5.2}$$

with Δn_{raw} and Δn_{bg} the statistical uncertainties of COPS measured densities n_{raw} and n_{bg}, respectively. The statistical uncertainty of both gauges were estimated with laboratory data where the pressure is stable; the uncertainties are found to be typically less than one percent, so an upper limit of 1% is used in this study; ΔR_{CO_2}, ΔR_{CO}, ΔR_{O_2} the absolute errors of the density ratios R_i. Since $R_i = n_i/n_{total}$ the relative error on the density ratios are written as:

$$\frac{\Delta R_i}{R_i} = \sqrt{\left(\frac{\Delta n_i}{n_i}\right)^2 + \left(\frac{\Delta n_{total}}{n_{total}}\right)^2} \tag{5.3}$$

where $\Delta n_{total}/n_{total}$ is taken as the statistic error of either nude or ram gauge; the relative error of the individual species densities $\Delta n_i/n_i$ is dominated by the relative error of the DFMS sensitivities $\Delta S_i/S_i$ for the corresponding species.

The sensitivity error for H_2O and CO_2 are both known from laboratory calibrations (Hässig, 2013) and is 16%. For CO and O_2 we introduce an educated guess. The DFMS sensitivity for individual species a is multiplication of a few factors: 1. the ionization efficiency given by the electron-impact ionization cross section with a 10% uncertainty is assumed; 2. the particle mass and energy dependent transmission efficiency with an error of 20% assumed; 3. the detection efficiency that depends on the particle energy and composition assuming a 20% uncertainty. The multiplication of the three factors gives an uncertainty of 30% on CO and O_2 sensitivity and is used in this study. However, it is worth mentioning that the factors 2 and 3 are not totally independent of one another. Calibration approaches for error estimation were performed and discussed by Schläppi (2011), Hässig (2013), and Calmonte (2015). We do not preclude the possibility that future calibration measurements may lead to new interpretations of the uncertainties.

Thus, in Equation (5.3) the total density uncertainty term can be neglected since it is much smaller compared to the DFMS sensitivity uncertainties. The errors ΔR_{H_2O}, ΔR_{CO_2}, ΔR_{CO}, and ΔR_{O_2} then become as follows:

$$\begin{aligned} \Delta R_{H_2O} &= \sqrt{\left[\left(\frac{\Delta n_{H_2O}}{n_{H_2O}}\right)^2 + \cancel{\left(\frac{\Delta n_{total}}{n_{total}}\right)^2}\right]} \cdot R_{H_2O} \\ &= 0.16 \cdot R_{H_2O} \end{aligned} \tag{5.4}$$

$$\Delta R_{CO_2} = \sqrt{\left[\left(\frac{\Delta n_{CO_2}}{n_{CO_2}}\right)^2 + \cancel{\left(\frac{\Delta n_{total}}{n_{total}}\right)^2}\right]} \cdot R_{CO_2}$$
$$= 0.16 \cdot R_{CO_2} \tag{5.5}$$

$$\Delta R_{CO} = \sqrt{\left[\left(\frac{\Delta n_{CO}}{n_{CO}}\right)^2 + \cancel{\left(\frac{\Delta n_{total}}{n_{total}}\right)^2}\right]} \cdot R_{CO}$$
$$= 0.30 \cdot R_{CO} \tag{5.6}$$

$$\Delta R_{O_2} = \sqrt{\left[\left(\frac{\Delta n_{O_2}}{n_{O_2}}\right)^2 + \cancel{\left(\frac{\Delta n_{total}}{n_{total}}\right)^2}\right]} \cdot R_{O_2}$$
$$= 0.30 \cdot R_{O_2} \tag{5.7}$$

For October 2014 the species combined correction factor $\beta_{C,total}$ is calculated to be in the range of 0.81 to 0.89 with an error less than 15%. The relative error on the background and species corrected density n_{corr} using Equation (5.2) results in maximum relative errors of around 15% for the nude gauge and 17% for the ram gauge.

Coma Velocity

In Section 3.2 it is discussed that the coma gas velocity can be derived with Equation (3.11). Using the common error propagation assuming all variables are independent to calculate error propagation gives the following uncertainty for the estimated velocity:

$$\left(\frac{\Delta v_{n,z}}{v_{n,z}}\right)^2 = \left(\frac{\Delta n_r}{n_r}\right)^2 + \left(\frac{\Delta n_n}{n_n}\right)^2 + \frac{1}{4}\left[\left(\frac{\Delta T_r}{T_r}\right)^2 + \left(\frac{\Delta m_g}{m_g}\right)^2\right] \tag{5.8}$$

$v_{n,z}$ is the estimated gas velocity, n_r the species corrected ram gauge density, n_n the species corrected nude gauge density, T_r the ram gauge sensor temperature, and m_g the mean mass of the gas which can be derived from DFMS data. The mean mass can be written with R_i, the ratio of the individual species to the total density (volume mixing ratio) or with r_i the ratio of the individual species to water:

$$m_g = m_{H_2O} \cdot R_{H_2O} + m_{CO_2} \cdot R_{CO_2} + m_{CO} \cdot R_{CO} + m_{O_2} \cdot R_{O_2} \tag{5.9a}$$

$$= \frac{m_{H_2O} + m_{CO_2} \cdot r_{CO_2} + m_{CO} \cdot r_{CO} + m_{O_2} \cdot r_{O_2}}{1 + r_{CO_2} + r_{CO} + r_{O_2}} \tag{5.9b}$$

The volume mixing ratio, R_i, was used to derive the uncertainties of COPS density. So deriving the error of the mean mass where R_i is used (Equation (5.9a)) gives:

$$\left(\frac{\Delta m_g}{m_g}\right) = \sqrt{\frac{m_{H_2O}^2 \Delta R_{H_2O}^2 + m_{CO_2}^2 \Delta R_{CO_2}^2 + m_{CO}^2 \Delta R_{CO}^2 + m_{O_2}^2 \Delta R_{O_2}^2}{(m_{H_2O} \cdot R_{H_2O} + m_{CO_2} \cdot R_{CO_2} + m_{CO} \cdot R_{CO} + m_{O_2} \cdot R_{O_2})^2}}$$

The mass m_i of the individual species are extracted from the "Handbook of Chemistry and Physics" with a neglectable errors. To derive the uncertainty of the COPS gas velocity as in Equation (5.8) the ram gauge sensor temperature term $\Delta T_r/T_r$ can be ignored because it is found to be small compared to the term $\Delta m_g/m_g$. The error on the calibrated density of the nude gauge and ram gauge are estimated as Equation (5.2).

The uncertainty on the mean gas mass for October 2014 yields a maximum of 15% and the gas velocity error derived from Equation (5.8) for COPS measurements has a maximum of 23% relative error.

5.6 Dust Observation

As mentioned in Section 5.1, additional to the coma neutral gas diurnal and seasonal variation patterns in the density, COPS occasionally observed small spikes in the total neutral density. These signals are believed to be a result of cometary dust releasing semi-volatiles while heated up near COPS and/or the spacecraft. In this study we extract dust signals found in the time period of January to June 2015.

5.6.1 Dust Signal Selection

As COPS density measurements are affected by spacecraft maneuvers (5.1), wheel off-loadings, and when the spacecraft changes orientation, data used for dust signal selection are ignored (1) during a maneuver and in the following 75 min, (2) during a wheel offloading and in the following 30 min, and (3) when the spacecraft off-nadir pointing is greater than 5°.

Typically each dust signal is apparent within three COPS data points, i.e., three minutes. Therefore, when a density value is higher than the mean of the two data points before and after with a height of $8 \cdot 10^5 - 2 \cdot 10^7\,\mathrm{cm}^{-3}$, this density peak is selected as dust signal.

An example of the dust selection is shown in Figure 5.15. The x-axis is time on 25 March 2015. The top panel shows the nude gauge density with the selected dust signals marked by red dots; the second panel shows the nadir off-pointing angle (orange) and phase angle (blue); the third panel shows the sub-spacecraft longitude (blue) and latitude (orange); the bottom panel shows the Rosetta-67P distance (orange) and the Sun-Rosetta distance (blue).

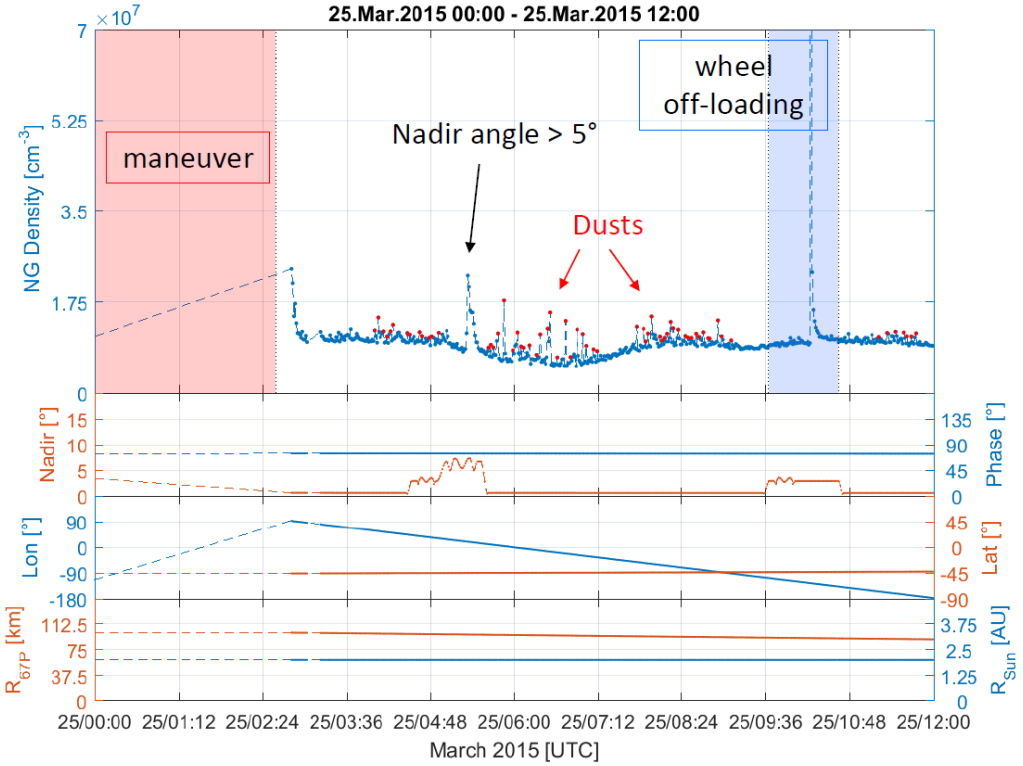

Figure 5.15: An example of the dust signal selection strategy on 25 March 2015. Uppermost panel: nude gauge density with the selected dust signals marked by red dots; second panel: nadir angle (orange) and phase angle (blue); third panel: sub-spacecraft longitude (blue) and latitude (orange); bottommost panel: Rosetta-67P distance (orange) and the Sun-Rosetta distance (blue).

5.6.2 Statistics

In this section some statistics of the selected dust signals are discussed. Figure 5.16 shows the raw counts of each month from January to June 2015. The dust signals were acquired while many parameters underwent significant changes including time, sub-spacecraft longitude, sub-spacecraft latitude, local time of the sub-spacecraft point, nadir off-pointing, and distance.

Each dust sample is obtained at different observation conditions which may bias the interpretation of the data. It may be rather complicated, but one may normalize or weight the obtained distributions to disentangle the bias from the spatial coverage of Rosetta.

For example, in Figure 5.17 the distribution of dust at different distances between the spacecraft and the comet is shown. The distance distribution is weighted by the time spent at each distance interval to reduce the bias depending on the frequency of the spacecraft flying at a certain distance more often than others; it is also filtered for showing only near terminator phase angles (Sun-67P-Rosetta angle) of 70°to 110°. The amount of dust is expected to decrease as the spacecraft goes further from the comet, but in the plot we see that there is more dust counted around 250 km than 70 km. This is due to the fact that the larger distances were sampled closer to perihelion when the comet was more active.

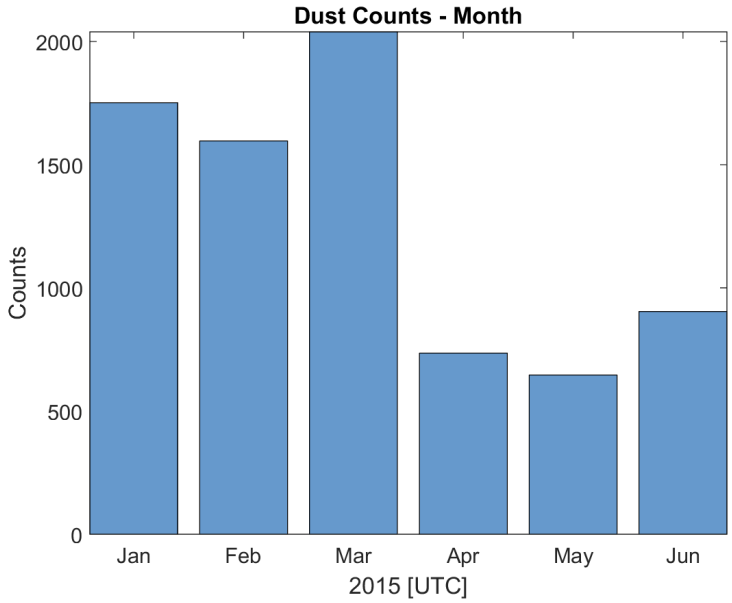

Figure 5.16: Monthly raw counts of the COPS observed dust signals from January to June 2015.

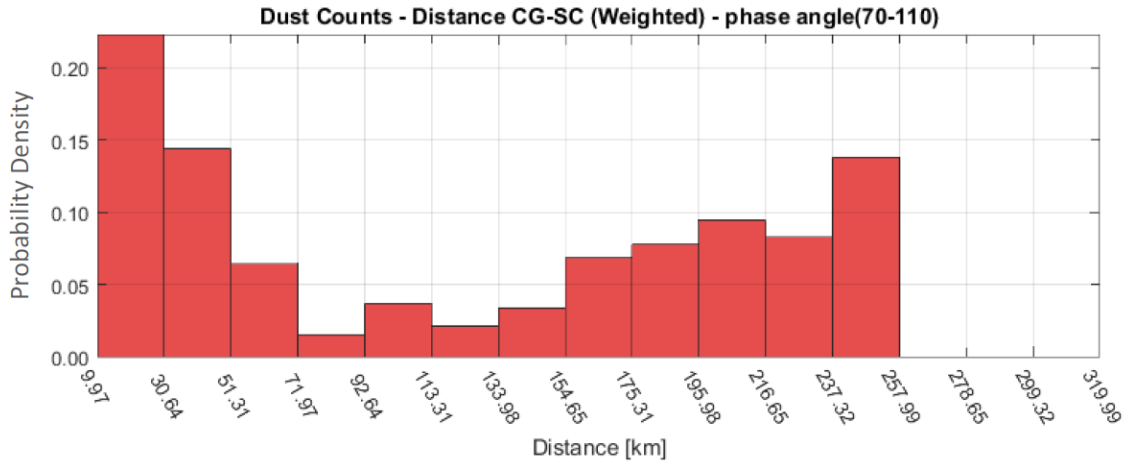

Figure 5.17: Distance distribution of dust signals from January to June 2015 weighted by the time spent at each distance and also filtered for observations obtained near the terminator plane, i.e. phase angles of 70°to 110°.

5.7 Plasma Effect

The Rosetta Plasma Consortium (RPC) is designed to characterize the plasma environment around 67P and the comet's interaction with the solar wind. It consists of five different sensors to measure the ion and electron densities and fluxes and the magnetic properties of the plasma.

While comparing COPS neutral gas density with plasma data measured by RPC-IES (Ion and Electron Sensor) one can sometimes observe increased intensity of high energy electrons (such as 200 eV)correlated to increased noise in the COPS density measurements as shown in Figure 5.18. This phenomenon became the motivation for

carrying out the laboratory plasma test to observe the impact of high energy plasma on COPS measurements as discussed in Section 4.3.

Besides, the evident jumps in COPS neutral gas densities due to ion-current offset measurements at low densities as discussed in Section 3.4.3 is probably also caused by increased plasma fluxes. an effect of plasma.

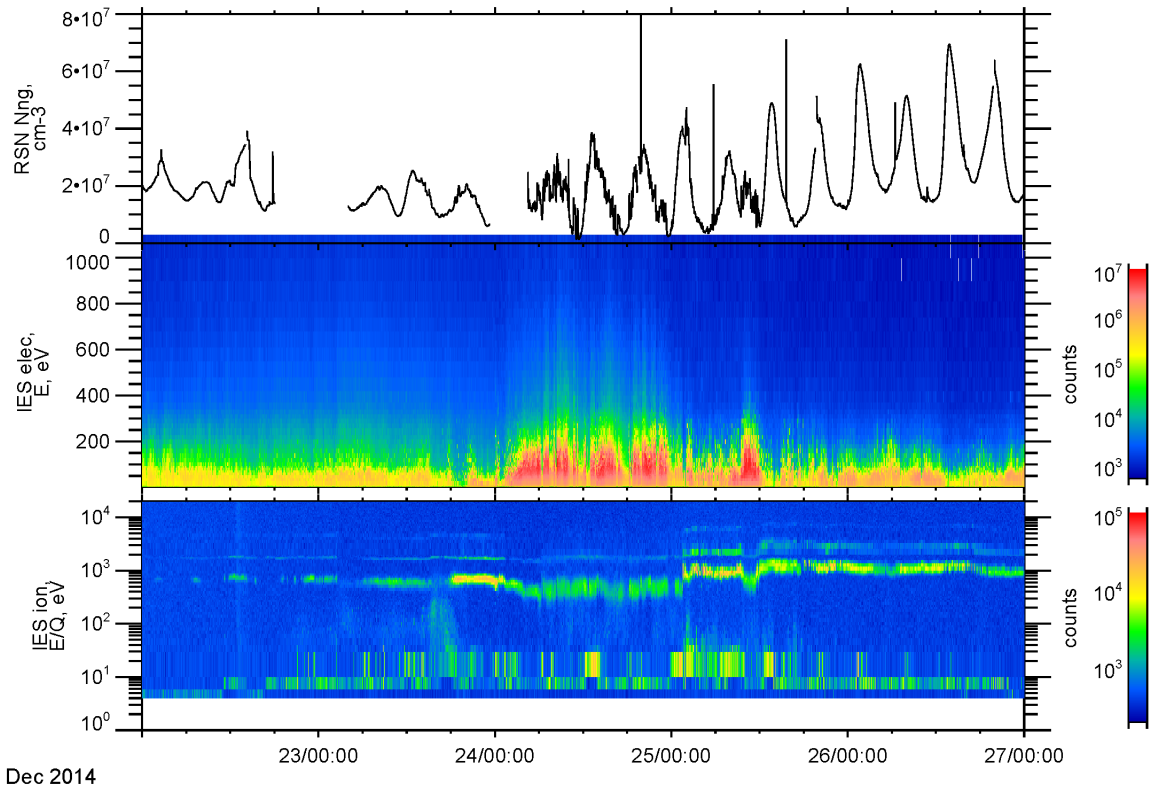

Figure 5.18: COPS density showing noise during increased high energy plasma fluxes observed with RPC-IES in flight from 22 to 26 December 2014. Upper panel: COPS nude gauge neutral gas density data; middle panel: RPC-IES electron spectra; bottom panel: RPC-IES ion spectra. Data analysis was performed with the AMDA science analysis system provided by the Centre de Données de la Physique des Plasmas (CDPP) supported by CNRS, CNES, Observatoire de Paris and Université Paul Sabatier, Toulouse.

5.8 Gas Temperature

COPS is also designed to measure the temperature of the neutral gas flow. In order to derive the gas temperature, it is necessary to obtain measurements at different flow angles, especially around 80° to 110°, with respect to the inflow direction (cf. Section 3.3).

Hence, in flight five spacecraft slews were performed, to contain nadir off-pointing in the range of 80° to 110°where the temperature effect is expected to be most pronounced, specifically for COPS in 2014. Two of them were performed early in the mission on 31 August and 3 September where the ram gauge densities were in the range of the

spacecraft background, thus are not suitable for deriving temperatures; the slew on 26 and 28 September were measured above the equator and southern/winter hemisphere, respectively, where the ram gauge density was only slightly above nominal background and consequently the data analysis is not that straight forward; the slew on 24 September was above the northern/summer hemisphere and had adequate gas density for both gauges. Therefore, the 24 September 2014 slew was selected for a first analysis as shown in Figure 5.19.

The uppermost panel of Figure 5.19 shows the nude gauge (blue) and ram gauge (green) raw density; the second panel shows the off-nadir angle (blue) and the phase angle (green); the third panel shows the sub-spacecraft longitude (blue) and latitude (green); the bottommost panel shows the spacecraft-comet distance (blue) and the Sun-comet distance (green). The nude gauge density from 03:05 to 04:20 UTC shows an additional density to the regular smooth comet density pattern (cf. Section 5.1) during the slew similar to the effect discussed in Figure 5.3. Thus, a linear fit of the nude gauge density during the slew is performed to simulate the nominal comet density pattern. The linearly fitted nude gauge density will be used in this analysis and is represented with a red dashed-line in Figure 5.19.

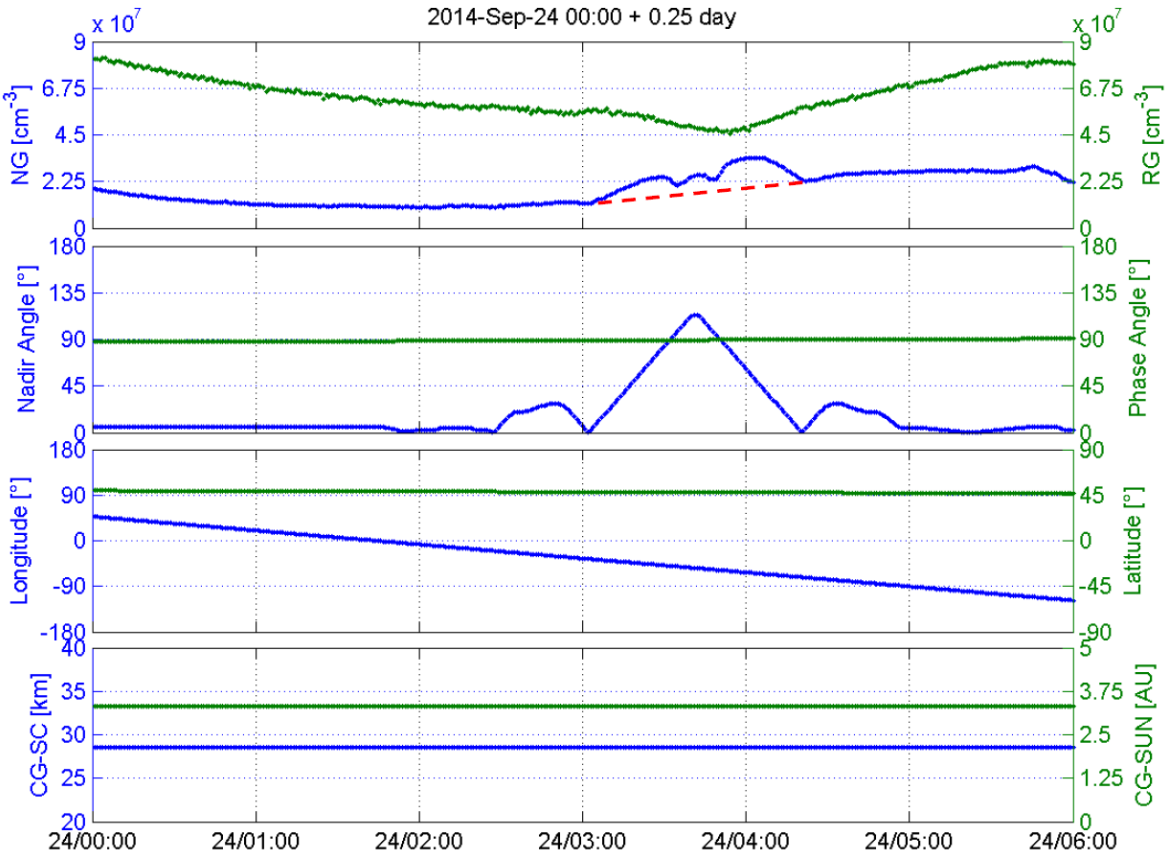

Figure 5.19: Dynamic slew including the range of 80° to 110 degree off-nadir angle on 24 September 2014. Top panel: the nude gauge and ram gauge densities; second panel: nadir and phase angles; third panel: sub-spacecraft longitude and latitude; bottom panel shows the spacecraft-comet and the Sun-comet distance.

In Figure 5.20 a 3D view of the same dynamic slew as in Figure 5.19 is shown with a focus on 24 September 2014 from 03:05 to 04:20 UTC.

The plot is shown in a CSO frame with comet 67P as center where +x is pointing towards the Sun; the component of the inertially referenced velocity of the sun relative to 67P orthogonal to the x-axis is the +y direction; and +z completed by the right-hand rule.

The spacecraft is moving from lower right to the upper left with the three thin green long arrows pointing to the center of mass of 67P. The pointing of the colored arrows show the pointing of the ram gauge. The color of the arrows represent the ram gauge raw density in cm^{-3} with the rainbow color scale; the color of the dots at the pointy end of the arrows show the off-nadir angle during this time which shows that the slew was around 1°to 114°off the nadir direction with the color scale to the far right.

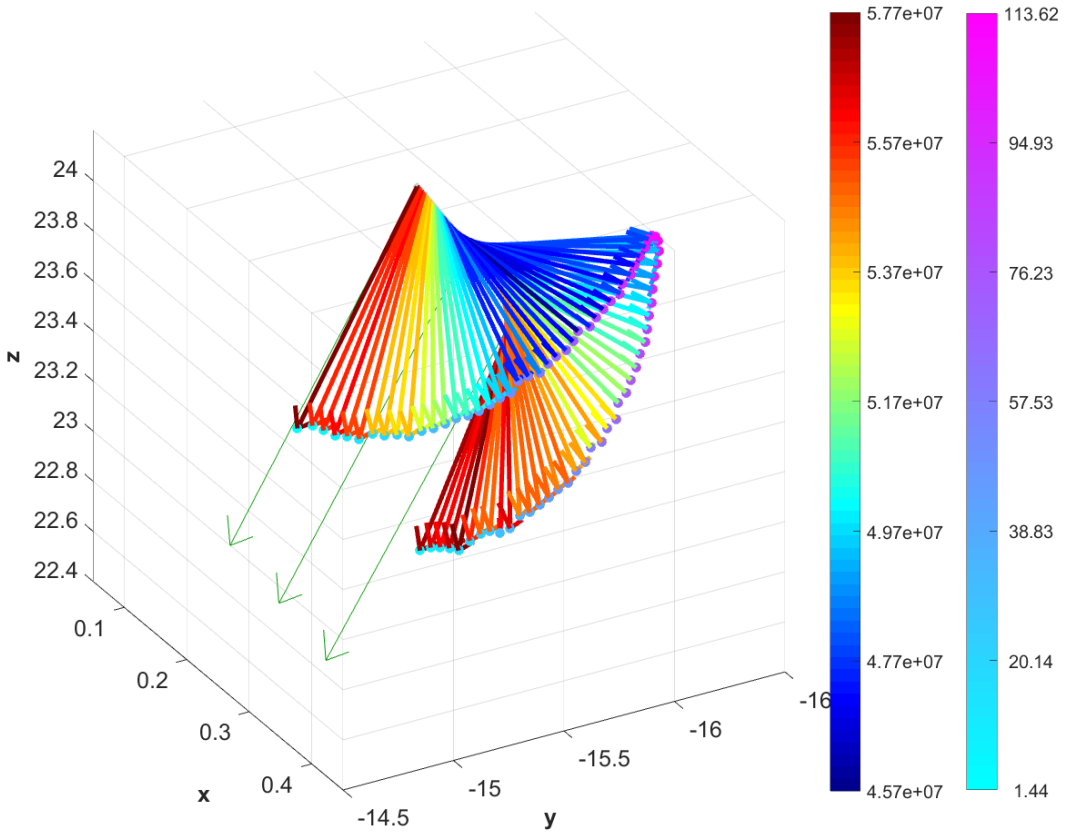

Figure 5.20: Dynamic slew with ram gauge density and pointing information on 24 September 2014 from 03:05 to 04:20 UTC. This figure is in a 67P centered CSO-coordinate system. Colored arrows show the spacecraft z-direction using the rainbow color scale to show the ram gauge raw density in cm^{-3}; colored dots at the pointy end of the arrows refer to the off-nadir angle of the ram gauge pointing in degrees (right color scale). Green thin arrows point to 67P's center of mass.

We assume that the angle with the highest ram gauge to nude gauge density ratio corresponds to the undisturbed inflow direction. Due to the fact that the slew only occurs in one plane this is only an approximation. Since for this measurement the whole spacecraft has to be slewed it is not possible to cover the full solid angle within a time scale short enough to maintain constant conditions in the surrounding coma. It is then possible to obtain the angle between the gas flow and the nadir direction. With the dynamic slews the velocity measured by COPS can be plotted with respect to the flow-nadir angle as in Figure 5.21.

The neutral gas velocity is shown in Figure 5.21 (red points) with respect to the angle between the approximate undisturbed inflow direction and the spacecraft pointing. The red points with low angles of the upper curve were measured first when slewing from nadir to larger angles; the red points with low angles of the lower curve were measured last when slewing back from larger angles to nadir. The rainbow theoretical curves shown in this plot are examples derived assuming a gas bulk velocity of 350 m/s with different gas temperatures.

During a dynamic slew background is changing and DFMS gas species are not measured at the same time. As a consequence, the mean gas mass during the slew is not known. Thus, a fixed mean mass of 21 amu obtained at times nearby with similar longitude-latitude location is used for calculating the COPS velocity and the theoretical curves. This slew was performed when the spacecraft was above the comet's neck region close to the head, where the calculated bulk velocities (angle around 0°) are lower and consistent with the October 2014 values in Figure 5.9.

Ideally, by adjusting the inputs for theoretical fits like in Figure 3.2, one should be able to gain the temperature and bulk velocity of the neutral gas. Many attempts of fitting the two slew curves formed by the red circles were done individually. However, none of the theoretical curves are found to fit so far. The derived COPS velocity at larger angles should become close to 0 m/s like the theoretical curves, but it is not. It might be due to the changes in spacecraft background during a slew which is most likely more pronounced in the nude gauge than in the ram gauge.

In addition, one would expect that during a slew the lowest ram gauge density should correspond to the largest off-nadir pointing, but instead, as shown in Figure 5.19, the lowest density appears later than the largest angle similar to the time delay in nude gauge and ram gauge density as discussed in Section 5.5.2. Moreover, the gas conditions might also have changed over the slew as in Figure 5.21 the v_z at the beginning and at the end of the slew is different.

At the moment, the results are not very conclusive. Nevertheless, other spacecraft slews which cover large angles, similar to the COPS dynamic slews, will be further investigated to resolve the difficulties to derive the gas temperature.

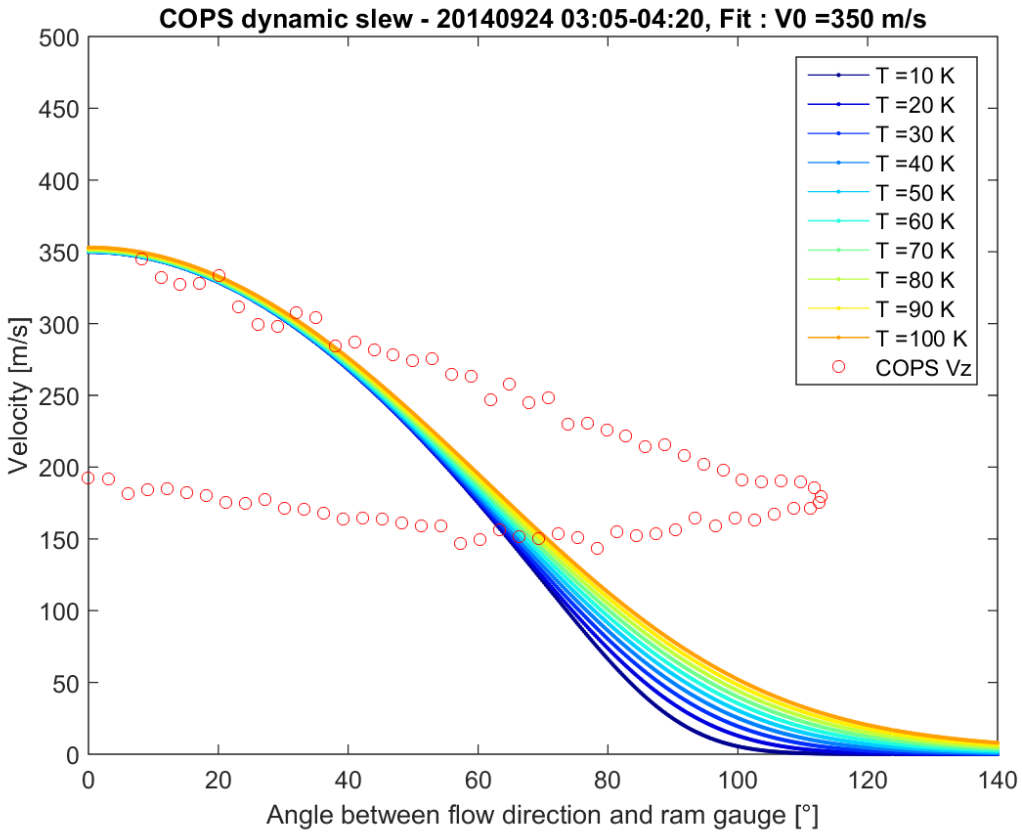

Figure 5.21: Velocity-Angle plot demonstrating gas temperature fit method for the 24 September 2014 from 03:05 to 04:20 UTC dynamic slew.

6. Conclusions and Perspectives

The Rosetta space mission achieved many firsts in the study of comets. It was the first space mission using solar panels as main power source at such far distances from the Sun, the first spacecraft to orbit a comet for a period of more than two years, and the first mission to soft land on a comet.

Out of the instruments onboard of the spacecraft, ROSINA with its COPS, RTOF, and DFMS had the task to derive the composition and abundance of volatiles in the coma of the Jupiter-family comet 67P/Churyumov-Gerasimenko's coma via in situ measurements.

COPS was responsible for monitoring the neutral coma pressure/density during the active phase of Rosetta. On one hand, COPS played the role of Rosetta's security guard to alert other instruments automatically in case the gas density rises too high; on the other hand, with COPS measurements the total neutral gas production rate, gas expansion velocities, dust signals, plasma signals, and eventually gas temperatures were estimated or observed. These observations will provide clues to answer some of the scientific questions. Such as, how active was the comet? How did the neutral coma behave and how did it vary? How much mass did the comet lose during the passage into the Solar System? How long would the comet eventually live with similar mass loss during each passage?

In this study we have presented the first analysis of the COPS flight model (COPS-FM) observations at comet 67P regarding the previously mentioned scientific questions, and also the calibration of the COPS flight spare (COPS-FS) in the laboratory to verify the characteristics of COPS and the analysis methods applied to the space data.

All flight model (FM) and flight spare (FS) instruments of the three sensors of ROSINA were calibrated. COPS sensitivity factors for converting the measured ion currents to pressure were implemented in the DPU software for FM and FS. The sensitivity calibration measurements in this study showed that the sensitivity results are comparable to a previous study performed more than ten years ago before arriving at the comet (Graf et al., 2004); this implies that the sensitivity factors used in the DPU software during the Rosetta mission were applicable and that COPS is indeed providing reliable and stable long term measurements.

COPS measured the neutral gas using electron-impact ionization. This means that when COPS measured different types of gas it had different sensitivities due to the different electron-impact ionization cross-sections of the individual species. Thus correction factors are needed when different gas species are measured by COPS. The correction factors obtained through static calibration measurements in this work were confirmed to be in agreement with the reference correction factors that were used for analyzing the ROSINA data. The reference correction factors were only given for individual gas species; in addition, the calibrations in this work also verified the method used for deriving a gas mixture correction factor that was applied to space observations where the gases in the coma were always a mixture of several components, mainly H_2O, CO_2, CO, and O_2.

Dynamic gas measurements were also performed with COPS-FS in the lab and showed that COPS was capable to derive gas velocities in an environment similar to the comet's gas coma. The velocity measurements were performed for different gas species starting from H_2 to the much heavier noble gas Xe at different outflow velocities. Most of the measured velocities were close to the expected values from theory.

Although built for measuring neutral gas, the COPS-FM occasionally observed increased noise while the Rosetta Plasma Consortium (RPC) onboard of the spacecraft measured high energy plasma with high intensity. In the course of this work the COPS-FS was then tested in a plasma chamber and it was demonstrated that plasma indeed influences the pressure/density measurements as external cometary electrons and ions were able to reach the ionization volume of the sensor. Additional investigation and collaboration with the plasma instrument teams will be required to quantify the plasma effects on COPS and the possibility to use COPS as a high energy plasma sensor.

In August 2014 Rosetta rendezvoused with comet 67P after a ten year journey. COPS soon noticed the seasonal and diurnal variations in the density of 67P's neutral coma; this was seen while orbiting the comet at different sub-spacecraft longitudes and latitudes. The change from summer in the northern hemisphere to summer in the southern hemisphere was also observed before and after the two equinoxes.

COPS was operating the majority of the time throughout the two-year Rosetta mission. Therefore, the in situ coma density evolution was monitored and showed an anti-correlation to the distance between the spacecraft and the comet. Furthermore, the total neutral gas production rate of 67P was estimated with the simple Haser model (Haser, 1957) giving approximately $4 \cdot 10^{28}$ molecules/s at the peak around 18 days after perihelion similar to the results of Hansen et al. (2016).

In October 2014 Rosetta was all the time within 20 km from the comet. The conditions were good to simultaneously observe the total neutral gas density as well as the dynamic pressure of the volatiles emanating from the comet. From these measurements the neutral gas velocity was derived. The velocities showed a variation from about 300 to 1200 m/s with generally higher velocities when the sub-spacecraft position was above the head and body regions while lower above the neck region.

Interestingly, the COPS-FM occasionally observed grain impact signals. The interpretation is that the volatile content of a grain evaporated upon impact near COPS and/or the spacecraft. The released semi-volatiles were then measured by COPS. Estimations of the magnitude of the volatile part in dust would be possible with further studies. In addition, experiments with the COPS-FS to measure icy dust particles are planned to gain better knowledge on the COPS response to such grains and therefore the dust observations in the coma of the comet.

It is worthwhile to mention that COPS performed quite well throughout the Rosetta mission. It assisted the Rosetta flight dynamics team to plan favorable spacecraft orbits during the orbiting and landing phase. Moreover, the total pressure/density measurements were necessary for obtaining the absolute abundances of the different gas species from the relative abundances derived with the ROSINA mass spectrometers DFMS and RTOF. COPS indicates that this type of pressure gauge is a promising and indispensable candidate for future space missions.

Bibliography

K. Altwegg, H. Balsiger, A. Bar-Nun, J. J. Berthelier, A. Bieler, P. Bochsler, C. Briois, U. Calmonte, M. Combi, J. De Keyser, P. Eberhardt, B. Fiethe, S. Fuselier, S. Gasc, T. I. Gombosi, K. C. Hansen, M. Hässig, A. Jäckel, E. Kopp, A. Korth, L. Le Roy, U. Mall, B. Marty, O. Mousis, E. Neefs, T. Owen, H. Rème, M. Rubin, T. Sémon, C.-Y. Tzou, H. Waite, and P. Wurz. 67P/Churyumov-Gerasimenko, a Jupiter family comet with a high D/H ratio. *Science*, 347(27):1261952, January 2015. doi: 10.1126/science.1261952.

K. Altwegg, H. Balsiger, A. Bar-Nun, J.-J. Berthelier, A. Bieler, P. Bochsler, C. Briois, U. Calmonte, M. R. Combi, H. Cottin, J. De Keyser, F. Dhooghe, B. Fiethe, S. A. Fuselier, S. Gasc, T. I. Gombosi, K. C. Hansen, M. Haessig, A. Ja ckel, E. Kopp, A. Korth, L. Le Roy, U. Mall, B. Marty, O. Mousis, T. Owen, H. Reme, M. Rubin, T. Semon, C.-Y. Tzou, J. H. Waite, and P. Wurz. Prebiotic chemicals–amino acid and phosphorus–in the coma of comet 67P/Churyumov-Gerasimenko. *Science Advances*, 2:e1600285–e1600285, May 2016. doi: 10.1126/sciadv.1600285.

H. Balsiger, K. Altwegg, P. Bochsler, P. Eberhardt, J. Fischer, S. Graf, A. Jäckel, E. Kopp, U. Langer, M. Mildner, J. Müller, T. Riesen, M. Rubin, S. Scherer, P. Wurz, S. Wüthrich, E. Arijs, S. Delanoye, J. de Keyser, E. Neefs, D. Nevejans, H. Rème, C. Aoustin, C. Mazelle, J.-L. Médale, J. A. Sauvaud, J.-J. Berthelier, J.-L. Bertaux, L. Duvet, J.-M. Illiano, S. A. Fuselier, A. G. Ghielmetti, T. Magoncelli, E. G. Shelley, A. Korth, K. Heerlein, H. Lauche, S. Livi, A. Loose, U. Mall, B. Wilken, F. Gliem, B. Fiethe, T. I. Gombosi, B. Block, G. R. Carignan, L. A. Fisk, J. H. Waite, D. T. Young, and H. Wollnik. Rosina Rosetta Orbiter Spectrometer for Ion and Neutral Analysis. *Space Science Reviews*, 128:745–801, February 2007. doi: 10.1007/s11214-006-8335-3.

Hans Balsiger, Kathrin Altwegg, Akiva Bar-Nun, Jean-Jacques Berthelier, Andre Bieler, Peter Bochsler, Christelle Briois, Ursina Calmonte, Michael Combi, Johan De Keyser, Peter Eberhardt, Björn Fiethe, Stephen A. Fuselier, Sébastien Gasc, Tamas I. Gombosi, Kenneth C. Hansen, Myrtha Hässig, Annette Jäckel, Ernest Kopp, Axel Korth, Lena Le Roy, Urs Mall, Bernard Marty, Olivier Mousis, Tobias Owen, Henri Rème, Martin Rubin, Thierry Sémon, Chia-Yu Tzou, J. Hunter Waite, and Peter Wurz. Detection of argon in the coma of comet 67p/churyumov-gerasimenko. *Science Advances*, 1(8), 2015. doi: 10.1126/sciadv.1500377. URL `http://advances.sciencemag.org/content/1/8/e1500377`.

K. R. Bell, P. M. Cassen, H. H. Klahr, and T. Henning. The Structure and Appearance of Protostellar Accretion Disks: Limits on Disk Flaring. *Astrophysical Journal*, 486: 372–387, September 1997. doi: 10.1086/304514.

J.-L. Bertaux. Estimate of the erosion rate from H_2O mass-loss measurements from SWAN/SOHO in previous perihelions of comet 67P/Churyumov-Gerasimenko and connection with observed rotation rate variations. *Astronomy and Astrophysics*, 583: A38, November 2015. doi: 10.1051/0004-6361/201525992.

A. Bieler, K. Altwegg, H. Balsiger, A. Bar-Nun, J.-J. Berthelier, P. Bochsler, C. Briois,

U. Calmonte, M. Combi, J. De Keyser, E. F. van Dishoeck, B. Fiethe, S. A. Fuselier, S. Gasc, T. I. Gombosi, K. C. Hansen, M. Hässig, A. Jäckel, E. Kopp, A. Korth, L. Le Roy, U. Mall, R. Maggiolo, B. Marty, O. Mousis, T. Owen, H. Rème, M. Rubin, T. Sémon, C.-Y. Tzou, J. H. Waite, , and P. Walsh, C. Wurz. Abundant molecular oxygen in the coma of comet 67P/Churyumov–Gerasimenko. *Nature*, 526:678–681, October 2015a. doi: 10.1038/nature15707.

A. Bieler, K. Altwegg, H. Balsiger, J.-J. Berthelier, U. Calmonte, M. Combi, J. De Keyser, B. Fiethe, N. Fougere, S. Fuselier, S. Gasc, T. Gombosi, K. Hansen, M. Hässig, Z. Huang, A. Jäckel, X. Jia, L. Le Roy, U. A. Mall, H. Rème, M. Rubin, V. Tenishev, G. Tóth, C.-Y. Tzou, and P. Wurz. Comparison of 3D kinetic and hydrodynamic models to ROSINA-COPS measurements of the neutral coma of 67P/Churyumov-Gerasimenko. *Astronomy and Astrophysics*, 583:A7, November 2015b. doi: 10.1051/0004-6361/201526178.

N. Biver, M. Hofstadter, S. Gulkis, D. Bockelée-Morvan, M. Choukroun, E. Lellouch, F. P. Schloerb, L. Rezac, W. H. Ip, C. Jarchow, P. Hartogh, S. Lee, P. von Allmen, J. Crovisier, C. Leyrat, and P. Encrenaz. Distribution of water around the nucleus of comet 67P/Churyumov-Gerasimenko at 3.4 AU from the Sun as seen by the MIRO instrument on Rosetta. *Astronomy and Astrophysics*, 583:A3, November 2015. doi: 10.1051/0004-6361/201526094.

N. Biver, R. Moreno, D. Bockelée-Morvan, A. Sandqvist, P. Colom, J. Crovisier, D. C. Lis, J. Boissier, V. Debout, G. Paubert, S. Milam, A. Hjalmarson, S. Lundin, T. Karlsson, M. Battelino, U. Frisk, D. Murtagh, and Odin Team. Isotopic ratios of H, C, N, O, and S in comets C/2012 F6 (Lemmon) and C/2014 Q2 (Lovejoy). *Astronomy and Astrophysics*, 589:A78, May 2016. doi: 10.1051/0004-6361/201528041.

D. Bockelée-Morvan, V. Debout, S. Erard, C. Leyrat, F. Capaccioni, G. Filacchione, N. Fougere, P. Drossart, G. Arnold, M. Combi, B. Schmitt, J. Crovisier, M.-C. de Sanctis, T. Encrenaz, E. Kührt, E. Palomba, F. W. Taylor, F. Tosi, G. Piccioni, U. Fink, G. Tozzi, A. Barucci, N. Biver, M.-T. Capria, M. Combes, W. Ip, M. Blecka, F. Henry, S. Jacquinod, J.-M. Reess, A. Semery, and D. Tiphene. First observations of H_2O and CO_2 vapor in comet 67P/Churyumov-Gerasimenko made by VIRTIS onboard Rosetta. *Astronomy and Astrophysics*, 583:A6, November 2015. doi: 10.1051/0004-6361/201526303.

D. E. Brownlee. *Comets*, pages 335–363. 2014.

U. Calmonte. *Sulfur Isotopic Ratios at 67P/Churyumov-Gerasimenko and Characterization of ROSINA-DFMS FM & FS*. PhD thesis, University of Bern, 2015.

M. R. Combi, W. M. Harris, and W. H. Smyth. *Gas dynamics and kinetics in the cometary coma: theory and observations*, pages 523–552. 2004.

COPS-Manual. *Rosetta ROSINA-COPS Instrument Mode*, 2011.

B. J. R. Davidsson, P. J. Gutiérrez, and H. Rickman. Nucleus properties of Comet 9P/Tempel 1 estimated from non-gravitational force modeling. *Icarus*, 187:306–320, March 2007. doi: 10.1016/j.icarus.2006.07.022.

B. J. R. Davidsson, S. Gulkis, C. Alexander, P. v. Allmen, L. Kamp, S. Lee, and

J. Warell. Gas kinetics and dust dynamics in low-density comet comae. *Icarus*, 210: 455–471, November 2010. doi: 10.1016/j.icarus.2010.06.022.

B. J. R. Davidsson, P. J. Gutiérrez, H. Sierks, C. Barbieri, P. L. Lamy, R. Rodrigo, D. Koschny, H. Rickman, H. U. Keller, J. Agarwal, M. F. A'Hearn, M. A. Barucci, J.-L. Bertaux, I. Bertini, D. Bodewits, G. Cremonese, V. Da Deppo, S. Debei, M. De Cecco, S. Fornasier, M. Fulle, O. Groussin, C. Güttler, S. F. Hviid, W.-H. Ip, L. Jorda, J. Knollenberg, G. Kovacs, J.-R. Kramm, E. Kührt, M. Küppers, F. La Forgia, L. M. Lara, M. Lazzarin, J. J. Lopez Moreno, S. Lowry, S. Magrin, F. Marzari, H. Michalik, R. Moissl-Fraund, G. Naletto, N. Oklay, M. Pajola, C. Snodgrass, N. Thomas, C. Tubiana, and J.-B. Vincent. Orbital elements of the material surrounding comet 67P/Churyumov-Gerasimenko. *Astronomy and Astrophysics*, 583:A16, November 2015. doi: 10.1051/0004-6361/201525841.

L. M. Feaga, S. Protopapa, E. Schindhelm, S. A. Stern, M. F. A'Hearn, J.-L. Bertaux, P. D. Feldman, J. W. Parker, A. J. Steffl, and H. A. Weaver. Far-UV phase dependence and surface characteristics of comet 67P/Churyumov-Gerasimenko as observed with Rosetta Alice. *Astronomy and Astrophysics*, 583:A27, November 2015. doi: 10.1051/0004-6361/201526671.

J. A. Fernandez. On the existence of a comet belt beyond Neptune. *Monthly Notices of the RAS*, 192:481–491, August 1980. doi: 10.1093/mnras/192.3.481.

U. Fink, L. Doose, G. Rinaldi, A. Bieler, F. Capaccioni, D. Bockelée-Morvan, G. Filacchione, S. Erard, C. Leyrat, M. Blecka, M. T. Capria, M. Combi, J. Crovisier, M. C. De Sanctis, N. Fougere, F. Taylor, A. Migliorini, and G. Piccioni. Investigation into the disparate origin of CO_2 and H_2O outgassing for Comet 67/P. *Icarus*, 277:78–97, October 2016. doi: 10.1016/j.icarus.2016.04.040.

N. Fougere, K. Altwegg, J.-J. Berthelier, A. Bieler, D. Bockelée-Morvan, U. Calmonte, F. Capaccioni, M. R. Combi, J. De Keyser, V. Debout, S. Erard, B. Fiethe, G. Filacchione, U. Fink, S. A. Fuselier, T. I. Gombosi, K. C. Hansen, M. Hässig, Z. Huang, L. Le Roy, C. Leyrat, A. Migliorini, G. Piccioni, G. Rinaldi, M. Rubin, Y. Shou, V. Tenishev, G. Toth, and C.-Y. Tzou. Three-dimensional direct simulation Monte-Carlo modeling of the coma of comet 67P/Churyumov-Gerasimenko observed by the VIRTIS and ROSINA instruments on board Rosetta. *Astronomy and Astrophysics*, 588:A134, April 2016a. doi: 10.1051/0004-6361/201527889.

N. Fougere, K. Altwegg, J.-J. Berthelier, A. Bieler, D. Bockelée-Morvan, U. Calmonte, F. Capaccioni, M. R. Combi, J. De Keyser, V. Debout, S. Erard, B. Fiethe, G. Filacchione, U. Fink, S. A. Fuselier, T. I. Gombosi, K. C. Hansen, M. Hässig, Z. Huang, L. Le Roy, C. Leyrat, A. Migliorini, G. Piccioni, G. Rinaldi, M. Rubin, Y. Shou, V. Tenishev, G. Toth, and C.-Y. Tzou. Direct Simulation Monte Carlo modelling of the major species in the coma of comet 67P/Churyumov-Gerasimenko. *Monthly Notices of the RAS*, 462:S156–S169, November 2016b. doi: 10.1093/mnras/stw2388.

K.-H. Glassmeier, H. Boehnhardt, D. Koschny, E. Kührt, and I. Richter. The Rosetta Mission: Flying Towards the Origin of the Solar System. *Space Science Reviews*, 128:1–21, February 2007. doi: 10.1007/s11214-006-9140-8.

S. Graf, K. Altwegg, H. Balsiger, A. Jäckel, E. Kopp, U. Langer, W. Luithardt, C. Westermann, and P. Wurz. A cometary neutral gas simulator for gas dynamic sensor

and mass spectrometer calibration. *Journal of Geophysical Research (Planets)*, 109: E07S08, May 2004. doi: 10.1029/2003JE002188.

S. Graf, K. Altwegg, H. Balsiger, P. Bochsler, B. Fiethe, E. Montagnon, L. Duvet, and S. Fuselier. Thruster Plumes: Sources for High Pressure and Contamination at the Payload Location. *Journal of Spacecraft and Rockets*, 45:57–64, January 2008. doi: 10.2514/1.30600.

Granville-Phillips. *Granville-Phillips Series 370 Stabil-Ion® Vacuum Measurement Controller Instruction Manual*, 2007.

S. Gulkis, M. Allen, P. von Allmen, G. Beaudin, N. Biver, D. Bockelée-Morvan, M. Choukroun, J. Crovisier, B. J. R. Davidsson, P. Encrenaz, T. Encrenaz, M. Frerking, P. Hartogh, M. Hofstadter, W.-H. Ip, M. Janssen, C. Jarchow, S. Keihm, S. Lee, E. Lellouch, C. Leyrat, L. Rezac, F. P. Schloerb, and T. Spilker. Subsurface properties and early activity of comet 67P/Churyumov-Gerasimenko. *Science*, 347 (1):aaa0709, January 2015. doi: 10.1126/science.aaa0709.

Kenneth C. Hansen, K. Altwegg, J.-J. Berthelier, A. Bieler, N. Biver, D. Bockelée-Morvan, U. Calmonte, F. Capaccioni, M. R. Combi, J. De Keyser, B. Fiethe, N. Fougere, S. A. Fuselier, S. Gasc, T. I. Gombosi, Z. Huang, L. Le Roy, S. Lee, H. Nilsson, M. Rubin, Y. Shou, C. Snodgrass, V. Tenishev, G. Toth, C.-Y. Tzou, C. Simon Wedlund, and the ROSINA team. Evolution of water production of 67p/churyumov-gerasimenko: An empirical model and a multi-instrument study. *Monthly Notices of the Royal Astronomical Society*, 2016. doi: 10.1093/mnras/stw2413. URL `http://mnras.oxfordjournals.org/content/early/2016/09/23/mnras.stw2413.abstract`.

L. Haser. Distribution d'intensité dans la tête d'une comète. *Bulletin de la Societe Royale des Sciences de Liege*, 43:740–750, 1957.

M. Hässig. *Sensitivity and fragmentation calibration of the ROSINA Double Focusing Mass Spectrometer*. PhD thesis, University of Bern, 2013.

M. Hässig, K. Altwegg, H. Balsiger, A. Bar-Nun, J. J. Berthelier, A. Bieler, P. Bochsler, C. Briois, U. Calmonte, M. Combi, J. De Keyser, P. Eberhardt, B. Fiethe, S. A. Fuselier, M. Galand, S. Gasc, T. I. Gombosi, K. C. Hansen, A. Jäckel, H. U. Keller, E. Kopp, A. Korth, E. Kührt, L. Le Roy, U. Mall, B. Marty, O. Mousis, E. Neefs, T. Owen, H. Rème, M. Rubin, T. Sémon, C. Tornow, C.-Y. Tzou, J. H. Waite, and P. Wurz. Time variability and heterogeneity in the coma of 67P/Churyumov-Gerasimenko. *Science*, 347(1):aaa0276, January 2015. doi: 10.1126/science.aaa0276.

V. Inguimbert and G. Murat. Tests of the COPS instrument and of the JUICE RPWI instrument in JONAS chamber. *ONERA, The French Aerospace Lab*, 2015. RF 1/25803-25818 DESP.

H. U. Keller and L. Jorda. *The morphology of cometary nuclei*, page 1235. Kluwer Academic Publishers, 2002.

V. A. Krasnopolsky, V. I. Moroz, A. A. Krysko, V. S. Jegulev, A. Y. Tkachuk, M. Gogoshev, T. Gogosheva, G. Moreels, J. Clairemidi, and J. P. Parisot. Near infrared spectroscopy of Comet Halley by the Vega-2 three channel spectrometer. In B. Bat-

trick, E. J. Rolfe, and R. Reinhard, editors, *ESLAB Symposium on the Exploration of Halley's Comet*, volume 250 of *ESA Special Publication*, December 1986.

P. Lammerzahl, D. Krankowsky, R. R. Hodges, U. Stubbemann, J. Woweries, I. Herrwerth, J. J. Berthelier, J. M. Illiano, P. Eberhardt, U. Dolder, W. Shulte, and J. H. Hoffman. Expansion Velocity and Temperatures of Gas and Ions Measured in the Coma of Comet p/ Halley. *Astronomy and Astrophysics*, 187:169, November 1987.

H. P. Larson, D. S. Davis, M. J. Mumma, and H. A. Weaver. Velocity-resolved observations of water in comet Halley. *Astrophysical Journal, Letters*, 309:L95–L99, October 1986. doi: 10.1086/184769.

L. Le Roy, K. Altwegg, H. Balsiger, J.-J. Berthelier, A. Bieler, C. Briois, U. Calmonte, M. R. Combi, J. De Keyser, F. Dhooghe, B. Fiethe, S. A. Fuselier, S. Gasc, T. I. Gombosi, M. Hässig, A. Jäckel, M. Rubin, and C.-Y. Tzou. Inventory of the volatiles on comet 67P/Churyumov-Gerasimenko from Rosetta/ROSINA. *Astronomy and Astrophysics*, 583:A1, November 2015. doi: 10.1051/0004-6361/201526450.

S. Lee, P. von Allmen, M. Allen, G. Beaudin, N. Biver, D. Bockelée-Morvan, M. Choukroun, J. Crovisier, P. Encrenaz, M. Frerking, S. Gulkis, P. Hartogh, M. Hofstadter, W.-H. Ip, M. Janssen, C. Jarchow, S. Keihm, E. Lellouch, C. Leyrat, L. Rezac, F. P. Schloerb, T. Spilker, B. Gaskell, L. Jorda, H. U. Keller, and H. Sierks. Spatial and diurnal variation of water outgassing on comet 67P/Churyumov-Gerasimenko observed from Rosetta/MIRO in August 2014. *Astronomy and Astrophysics*, 583:A5, November 2015. doi: 10.1051/0004-6361/201526155.

P. A. Redhead. New hot-filament ionization gauge with low residual current. *Journal of Vacuum Science and Technology*, 3:173–180, 1966. doi: 10.1116/1.1492470.

A. Rotundi, H. Sierks, V. Della Corte, M. Fulle, P. J. Gutierrez, L. Lara, C. Barbieri, P. L. Lamy, R. Rodrigo, D. Koschny, H. Rickman, H. U. Keller, J. J. López-Moreno, M. Accolla, J. Agarwal, M. F. A'Hearn, N. Altobelli, F. Angrilli, M. A. Barucci, J.-L. Bertaux, I. Bertini, D. Bodewits, E. Bussoletti, L. Colangeli, M. Cosi, G. Cremonese, J.-F. Crifo, V. Da Deppo, B. Davidsson, S. Debei, M. De Cecco, F. Esposito, M. Ferrari, S. Fornasier, F. Giovane, B. Gustafson, S. F. Green, O. Groussin, E. Grün, C. Güttler, M. L. Herranz, S. F. Hviid, W. Ip, S. Ivanovski, J. M. Jerónimo, L. Jorda, J. Knollenberg, R. Kramm, E. Kührt, M. Küppers, M. Lazzarin, M. R. Leese, A. C. López-Jiménez, F. Lucarelli, S. C. Lowry, F. Marzari, E. M. Epifani, J. A. M. McDonnell, V. Mennella, H. Michalik, A. Molina, R. Morales, F. Moreno, S. Mottola, G. Naletto, N. Oklay, J. L. Ortiz, E. Palomba, P. Palumbo, J.-M. Perrin, J. Rodríguez, L. Sabau, C. Snodgrass, R. Sordini, N. Thomas, C. Tubiana, J.-B. Vincent, P. Weissman, K.-P. Wenzel, V. Zakharov, and J. C. Zarnecki. Dust measurements in the coma of comet 67P/Churyumov-Gerasimenko inbound to the Sun. *Science*, 347(1):aaa3905, January 2015. doi: 10.1126/science.aaa3905.

M. Rubin, K. Altwegg, H. Balsiger, A. Bar-Nun, J.-J. Berthelier, A. Bieler, P. Bochsler, C. Briois, U. Calmonte, M. Combi, J. De Keyser, F. Dhooghe, P. Eberhardt, B. Fiethe, S. A. Fuselier, S. Gasc, T. I. Gombosi, K. C. Hansen, M. Hässig, A. Jäckel, E. Kopp, A. Korth, L. Le Roy, U. Mall, B. Marty, O. Mousis, T. Owen, H. Rème, T. Sémon, C.-Y. Tzou, J. H. Waite, and P. Wurz. Molecular nitrogen in comet 67P/Churyumov-Gerasimenko indicates a low formation temperature. *Science*, 348: 232–235, April 2015. doi: 10.1126/science.aaa6100.

B. Schläppi. *Characterization of the ROSINA Double Focusing Mass Spectrometer*. PhD thesis, University of Bern, 2011.

B. Schläppi, K. Altwegg, H. Balsiger, M. HäSsig, A. JäCkel, P. Wurz, B. Fiethe, M. Rubin, S. A. Fuselier, J. J. Berthelier, J. de Keyser, H. RèMe, and U. Mall. Influence of spacecraft outgassing on the exploration of tenuous atmospheres with in situ mass spectrometry. *Journal of Geophysical Research (Space Physics)*, 115: A12313, December 2010. doi: 10.1029/2010JA015734.

F. P. Schloerb, W. M. Kinzel, D. A. Swade, and W. M. Irvine. HCN production from comet Halley. *Astrophysical Journal, Letters*, 310:L55–L60, November 1986. doi: 10.1086/184781.

F. P. Schloerb, S. Keihm, P. von Allmen, M. Choukroun, E. Lellouch, C. Leyrat, G. Beaudin, N. Biver, D. Bockelée-Morvan, J. Crovisier, P. Encrenaz, R. Gaskell, S. Gulkis, P. Hartogh, M. Hofstadter, W.-H. Ip, M. Janssen, C. Jarchow, L. Jorda, H. U. Keller, S. Lee, L. Rezac, and H. Sierks. MIRO observations of subsurface temperatures of the nucleus of 67P/Churyumov-Gerasimenko. *Astronomy and Astrophysics*, 583:A29, November 2015. doi: 10.1051/0004-6361/201526152.

R. Schulz. The Rosetta Mission: Comet and Asteroid Exploration. In J. A. Fernandez, D. Lazzaro, D. Prialnik, and R. Schulz, editors, *Icy Bodies of the Solar System*, volume 263 of *IAU Symposium*, pages 312–316, 2010. doi: 10.1017/S1743921310001997.

G. Schwehm and R. Schulz. Rosetta Goes to Comet Wirtanen. *Space Science Reviews*, 90:313–319, October 1999. doi: 10.1023/A:1005231006010.

H. Sierks, C. Barbieri, P. L. Lamy, R. Rodrigo, D. Koschny, H. Rickman, H. U. Keller, J. Agarwal, M. F. A'Hearn, F. Angrilli, A.-T. Auger, M. A. Barucci, J.-L. Bertaux, I. Bertini, S. Besse, D. Bodewits, C. Capanna, G. Cremonese, V. Da Deppo, B. Davidsson, S. Debei, M. De Cecco, F. Ferri, S. Fornasier, M. Fulle, R. Gaskell, L. Giacomini, O. Groussin, P. Gutierrez-Marques, P. J. Gutiérrez, C. Güttler, N. Hoekzema, S. F. Hviid, W.-H. Ip, L. Jorda, J. Knollenberg, G. Kovacs, J. R. Kramm, E. Kührt, M. Küppers, F. La Forgia, L. M. Lara, M. Lazzarin, C. Leyrat, J. J. Lopez Moreno, S. Magrin, S. Marchi, F. Marzari, M. Massironi, H. Michalik, R. Moissl, S. Mottola, G. Naletto, N. Oklay, M. Pajola, M. Pertile, F. Preusker, L. Sabau, F. Scholten, C. Snodgrass, N. Thomas, C. Tubiana, J.-B. Vincent, K.-P. Wenzel, M. Zaccariotto, and M. Pätzold. On the nucleus structure and activity of comet 67P/Churyumov-Gerasimenko. *Science*, 347(1):aaa1044, January 2015. doi: 10.1126/science.aaa1044.

C. Simon Wedlund, E. Kallio, M. Alho, H. Nilsson, G. Stenberg Wieser, H. Gunell, E. Behar, J. Pusa, and G. Gronoff. The atmosphere of comet 67P/Churyumov-Gerasimenko diagnosed by charge-exchanged solar wind alpha particles. *Astronomy and Astrophysics*, 587:A154, March 2016. doi: 10.1051/0004-6361/201527532.

C. Snodgrass, C. Opitom, M. de Val-Borro, E. Jehin, J. Manfroid, T. Lister, J. Marchant, G. H. Jones, A. Fitzsimmons, I. A. Steele, R. J. Smith, H. Jermak, T. Granzer, K. J. Meech, P. Rousselot, and A.-C. Levasseur-Regourd. The perihelion activity of comet 67P/Churyumov-Gerasimenko as seen by robotic telescopes. *Monthly Notices of the RAS*, 462:S138–S145, November 2016. doi: 10.1093/mnras/stw2300.

V. Tenishev, M. Combi, and B. Davidsson. A Global Kinetic Model for Cometary Comae: The Evolution of the Coma of the Rosetta Target Comet Churyumov-Gerasimenko throughout the Mission. *Astrophysical Journal*, 685:659-677, September 2008. doi: 10.1086/590376.

N. Thomas, H. Sierks, C. Barbieri, P. L. Lamy, R. Rodrigo, H. Rickman, D. Koschny, H. U. Keller, J. Agarwal, M. F. A'Hearn, F. Angrilli, A.-T. Auger, M. A. Barucci, J.-L. Bertaux, I. Bertini, S. Besse, D. Bodewits, G. Cremonese, V. Da Deppo, B. Davidsson, M. De Cecco, S. Debei, M. R. El-Maarry, F. Ferri, S. Fornasier, M. Fulle, L. Giacomini, O. Groussin, P. J. Gutierrez, C. Güttler, S. F. Hviid, W.-H. Ip, L. Jorda, J. Knollenberg, J.-R. Kramm, E. Kührt, M. Küppers, F. La Forgia, L. M. Lara, M. Lazzarin, J. J. L. Moreno, S. Magrin, S. Marchi, F. Marzari, M. Massironi, H. Michalik, R. Moissl, S. Mottola, G. Naletto, N. Oklay, M. Pajola, A. Pommerol, F. Preusker, L. Sabau, F. Scholten, C. Snodgrass, C. Tubiana, J.-B. Vincent, and K.-P. Wenzel. The morphological diversity of comet 67P/Churyumov-Gerasimenko. *Science*, 347(1):aaa0440, January 2015. doi: 10.1126/science.aaa0440.

P. R. Weissman. The Oort Cloud. In T. Rettig and J. M. Hahn, editors, *Completing the Inventory of the Solar System*, volume 107 of *Astronomical Society of the Pacific Conference Series*, pages 265–288, 1996.

C. B. Westermann. *A Novel Calibration System for the Simulation of Cometary Atmospheres*. PhD thesis, University of Bern, 2000.

C. B. Westermann, W. Luithardt, E. Kopp, T. Koch, R. Liniger, H. Hofstetter, J. Fischer, K. Altwegg, and H. Balsiger. A high precision calibration system for the simulation of cometary gas environments. *Measurement Science and Technology*, 12: 1594–1603, September 2001. doi: 10.1088/0957-0233/12/9/327.

F. L. Whipple. A comet model. I. The acceleration of Comet Encke. *Astrophysical Journal*, 111:375–394, March 1950. doi: 10.1086/145272.

Acknowledgments

I would like to deeply thank my supervisor Prof. Dr. Kathrin Altwegg for offering me the unique opportunity to participate in such a wonderful space project. I'm especially grateful for her support, guidance, encouragement, and fruitful discussions. I also appreciate very much the possibilities of attending various meetings and conferences which enlarged my horizons in many aspects.

Special thanks go to Prof. Dr. Michael R. Combi from the Department of Climate and Space Sciences and Engineering at the University of Michigan for refereeing this work.

Many thanks go to Prof. Dr. Nicolas Thomas of the University of Bern for being my examiner and for chairing the defense.

The work in the laboratory would have been impossible without the support from the technical workshops. Many thanks to:

- Adrian Etter as a teacher for the technical training and his support of finding suitable solutions for different test setups.
- Harald Mischler with clever hands and the mechanical workshop concerning installation and mounting of the instruments.
- Jürg Jost and the electronics workshop for their support when needed.

Furthermore, I owe many thanks to:

- PD Dr. Martin Rubin for fruitful discussions, advices, and proofreading of the thesis which improved the completeness of the content.
- Dr. Anette Jäckel for the first introduction to COPS and always being there to share her valuable lab experiences.
- Dr. Björn Fiethe for his support on the DPU software modifications.
- My excellent officemates Dr. Ursina Calmonte and Dr. Sébastien Gasc for their helping hands in the laboratory, the constructive discussions, the casual atmosphere, and the endless supplies of chocolate and Ovomaltine power during the challenging times.
- Dr. Léna Le Roy, as a great teammate to work with, whom shared the task of writing command files every four weeks during the mission operation phase.
- Thierry Sémon for his support regarding checking and modifying the files for operating the instruments in flight and handling data.
- Dr. Urs Rohner for the consultation on technical functionality of COPS based on his in-depth understanding of COPS.
- Prof. Dr. Hans Balsiger, Prof. Dr. Peter Wurz, Prof. Dr. Ernest Kopp, Dr. André Bieler, and Dr. Myrtha Hässig for sharing their knowledge and experiences.
- Dr. Thomas Smith for reading parts of the thesis and providing practical suggestions.

- The actual and former ROSINA team members for the collaboration and support.
- Many people for their assistance concerning administrative and technical matters.

Moreover, I would like to express heartfelt thanks to my parents Shuh-Kang and Chuen-Mei for their unconditional support that they provided all the time. In addition, I thank my brothers I-Cheng and I-Ta for their continuous solicitude. Special thanks to James for being there during the ups and downs. I would have never made it this far without any of you.

This work was funded by the Swiss National Science Foundation, the Prodex Program of the European Space Agency, and the Kanton Bern.

Declaration of consent

on the basis of Article 28 para. 2 of the RSL05 phil.-nat.

Name/First Name: Tzou / Chia-Yu

Matriculation Number: 12-135-273

Study program: Doktorat Physik

Bachelor ☐ Master ☐ Dissertation ☑

Title of the thesis: Calibrations of ROSINA-COPS and Observations at Comet 67P/Churyumov-Gerasimenko

Supervisor: Prof. Dr. Kathrin Altwegg

I declare herewith that this thesis is my own work and that I have not used any sources other than those stated. I have indicated the adoption of quotations as well as thoughts taken from other authors as such in the thesis. I am aware that the Senate pursuant to Article 36 para. 1 lit. r of the University Act of 5 September, 1996 is authorised to revoke the title awarded on the basis of this thesis. I allow herewith inspection in this thesis.

Bern/28.02.2017

Place/Date

Signature

Curriculum Vitae

Chia-Yu (Helen) Tzou（鄒佳諭）

Family Name: Tzou

First Name: Chia-Yu (Helen)

Education ……..…….……

2013-2017	Physics Institute, Unversity of Bern, Bern, Switzerland Ph.D, Space Research and Planetary Sciences
2010-2012	National Central University, Taoyuan, Taiwan M. S., Space Science
2006-2010	National Central University, Taoyuan, Taiwan B. S., Atmospheric Science

Research Experience ……..…….

2013-2017	Physics Institute, Unversity of Bern, Switzerland Research Topic: Calibrations of ROSINA-COPS and Observations at Comet 67P/Churyumov-Gerasimenko Supervisor: Prof. Kathrin Altwegg
2010-2012	Graduate Institute of Space Science, National Central University, Taiwan Research Topic: A Statistical Study of the Source Regions of the Saturnian Injection Events from Cassini MIMI/LEMMS Measurements Supervisor: Prof. Wing-Huen Ip
2008-2009	Department of Atmospheric Physics, National Central University, Taiwan Reasearch Topic: Space Weather Observation with FORMOSAT-3 Supervisor: Prof. Jann-Yenq Liu

Professional Training ……..……...…….

2013 Feb - 2015 Jul	Teaching Assistant, Physiks Praktikum, University of Bern, Switzerland
2011 Spring	Teaching Assistant, Introduction to Space Physics, NCU, Taiwan
2010 Fall	Teaching Assistant, Introdution to Planetary Science I, NCU, Taiwan

Miscellaneous …..……...

2013 CSH Summer School: Cosmochemistry – Schwägalp, Switzerland

2015 CSH Summer School: From dust to planets & geology – Leukerbad, Switzerland